EFFECTS OF WATER CONTENT AND ALUMINO-SILICATE SOURCES ON THE STRUCTURE AND PROPERTIES OF GEOPOLYMERS

A Dissertation

by

MARICELA LIZCANO

Submitted to the Office of Graduate Studies of
Texas A&M University
in partial fulfillment of the requirements for the degree of

DOCTOR OF PHILOSOPHY

August 2011

Major Subject: Mechanical Engineering

Effects of Water Content and Alumino-Silicate Sources

on the Structure and Properties of Geopolymer

EFFECTS OF WATER CONTENT AND ALUMINO-SILICATE SOURCES ON THE STRUCTURE AND PROPERTIES OF GEOPOLYMERS

A Dissertation

by

MARICELA LIZCANO

Submitted to the Office of Graduate Studies of
Texas A&M University
in partial fulfillment of the requirements for the degree of

DOCTOR OF PHILOSOPHY

Approved by:

Chair of Committee,	Miladin Radovic
Committee Members,	Terry Creasy
	Hong Liang
	Victor Ugaz
	Karen Lozano
Head of Department,	Jerald A. Caton

August 2011

Major Subject: Mechanical Engineering

ABSTRACT

Effects of Water Content and Alumino-Silicate Sources on

The Structure and Properties of Geopolymers. (August 2011)

Maricela Lizcano, B.S., The University of Texas-Pan American

M.S., The University of Texas-Pan American

Chair of Advisory Committee: Dr. Miladin Radovic

Geopolymers (GPs) are a special class of inorganic polymers with unique properties. Their 3-D amorphous structure and properties are often attributed to SiO_2/Al_2O_3 molar ratios. However, contradictory results reported in literature on the structure and properties do not conclusively support these reported findings. Furthermore, alternative processing methods are necessary for synthesizing pure geopolymers without impurities, which are often found in precursor material. A rigorous study on chemical composition and processing parameters, as well as alternative processing methods, are necessary for advancing GPS in various engineering applications.

The effects of $H_2O/(SiO_2 + Al_2O_3)$ and SiO_2/Al_2O_3 molar ratios , as well as precursor material on the density, open porosity, microstructure and the thermal and mechanical properties in K and Na activated geopolymers, is investigated. X-ray diffraction, Nuclear Magnetic Resonance as well as alcohol immersion to determine

density and open porosity is utilized for structural characterization. Thermogravimetric Analysis and Thermomechanical Analysis are used to investigate thermal behavior. Thermal conductivities and mechanical properties were measured using Thermal Constant Analysis and compression testing respectively.

Conclusive results demonstrate that the amount of water used to process GPs is the governing factor affecting their structure while SiO_2/Al_2O_3 molar ratio plays no significant role. The K- and Na-activated samples have similar amounts of residual water after aging for 21 days at ambient conditions. In addition, the effects of the initial water content, SiO_2/Al_2O_3 ratio, and alkaline activator (Na or K) on the thermal and mechanical properties of GPs, indicate that the dominant factor controlling thermal conductivity is $H_2O/(SiO_2 + Al_2O_3)$ ratio used in processing, and to a lesser degree, the type of activation ion (Na or K). The SiO_2/Al_2O_3 ratio did not have an effect on thermal conductivity. However, GPs compressive strengths are strongly affected by $H_2O/(SiO_2 + Al_2O_3)$ ratio, especially at higher water ratio. At high and intermediate $H_2O/(SiO_2 + Al_2O_3)$ ratios, liquid/solid ratio is the most important factor controlling the strength of GPs. At low $H_2O/(SiO_2 + Al_2O_3)$ ratios, SiO_2/Al_2O_3 ratio also plays an important role. Finally, partial geopolymer synthesis was possible using pure SiO_2 and $Al(OH)_3$ precursors, providing a possible low temperature alternative to other aluminosilicate precursors.

DEDICATION

I would like to dedicate this work to my friends and family who have supported me tirelessly throughout my endeavor. In particularly, a special dedication is given to my mother, Alma Sirenia Lizcano de Ramos and to Dr. Miladin Radovic, Dr. Karen Lozano, Dr. Edwin LeMaster and Dr. Aracely Rocha. I would also like to dedicate this dissertation to the many mentors who have inspired me to pursue my dreams:

In loving memory of

Dr. Hector M. Lizcano

Dr. Joseph Wiener

Dr. Miguel Paredes

Dr. Hashim S. Mahdi

Dr. Roger Morgan

Greg Cypet

Alex Lizcano-Knittle

and

In loving memory of

Duke my feline friend

"I am not here to dwell on my obstacles; I am here to explore my potential."

Maricela Lizcano

ACKNOWLEDGEMENTS

I would like to acknowledge Texas Engineering Experimental Station, TEES, for providing funding for this research project. I am grateful to Dr. Vladimir Bakhmoutov from Texas A&M University for help with NMR characterization, Samantha Salinas and Richard Patlan from The University of Texas Pan American for their help with TGA and TMA. I would also like to thank Kwonguk Jeon, Andrea Adamzack, Hynsoo Kim, Sandip Basu from Texas A&M University for help with XRD and SEM characterization, and Patrick Klein from Texas A&M University for help with thermal conductivity measurements.

Thank you lord, I am done!

NOMENCLATURE

Al	Aluminum
E	Young's Modulus
GPs	Geopolymers
HV	Vickers Hardness Number
K	Potassium
K-GPs	Potassium Activated Geopolymers
K_{IC}	Fracture Toughness
KOH	Potassium Hydroxide
MAS-NMR	Magic-Angle Spinning Nuclear Magnetic Resonance
MK	Metakaolin
Na	Sodium
Na-GPs	Sodium Activated Geopolymers
NaOH	Sodium Hydroxide
NMR	Nuclear Magnetic Resonance Spectroscopy
ppm	Parts Per Million
S	Probability of Survival
Si	Silicon
SEM	Scanning Electron Microscopy
XRD	X-Ray Diffraction

TABLE OF CONTENTS

Page

Page

LIST OF FIGURES

Page

Page

Page

Page

LIST OF TABLES

Page

1. INTRODUCTION-GEOPOLYMERS: A REVIEW OF PROCESSING METHODS, STRUCTURE, PROPERTIES, APPLICATIONS AND CHALLENGES

Geopolymers, GPs, recently came to light as a new class of inorganic alkaline activated aluminosilicate polymeric ceramics that are synthesized by polycondensation of Al and Si species from different precursor at near ambient temperatures in alkaline aqueous solutions. This relatively new class of inorganic polymers has attracted much attention as low temperature processing material with potential of being used for various engineering applications even at temperatures as high as 1000-1400 ^{o}C. These polymeric ceramics can be historically traced back to the 1940's in work published by A. O. Purdon [1] and later in the 50's by Glukhovsky [2], However, only after Davidovits' [3] work in the early 1970's was the interest in these inorganic polymers renewed. The term Geopolymer was introduced for the first time also by Davotovits to denote their inorganic and mineral nature ("geo") and structural similarity to organic polymers ("polymers"), and is commonly used today.

1.1 Processing Methods and Structure of Geopolymers

GPs synthesis is based on Al and Si speciation and condensation polymerization. An alkali silicate aqueous solution is added to an aluminosilicate source such as clays

---

This dissertation follows the style of Materials Science and Engineering A.

(kaolin), metakaolin, (MK), and industrial waste (fly-ash or furnace slug) to activate the polymerization process. Two alkali metal hydroxides are commonly used as alkaline activators, namely sodium hydroxide (NaOH) and potassium (KOH) [1]. Other cations from group I and II of the periodic table may also be used for activation such as Ca^{++} and Cs^{+}, as well as NH_4^{+}, and H_3O^{+} [2, 3]. The silicon content in geopolymers can be additionally adjusted by the addition of SiO_2 to the alkaline aqueous solution. The silicate solutions are usually mixed for 24 hours under sealed conditions to ensure SiO_2 dissolution, obtain homogeneous solutions, and prevent reaction of SiO_2 with CO_2 from air. Once the silicate solutions are ready, they are mixed with aluminosilicate precursor until a homogenous mixture/paste is obtained. The mixtures are then cast into molds, placed in sealed containers and cured in oven at temperatures between 20 ^{o}C and 120 ^{o}C for different times [1, 4, 5].

The geopolymerization process begins when an alkali silicate solution (pH $\geq$ 13) is mixed with the precursor source initiating activation. Si and Al speciation starts by dissolution and hydrolysis of the aluminosilicate source in conjunction with the condensation polymerization process. The OH^{-} ions hydrolyze Si^{4+} and Al^{3+} constituents forming monomeric species, largely $[SiO(OH)_3]^{-}$, $[SiO_2(OH)_2]^{2-}$ and $[Al(OH)_4]^{-}$ and other oligomeric species [2]. The aluminosilicate dissolution and hydrolysis reaction and formation of common Si and Al monomeric speciation is given as:

$SiO_2 + 2OH^{-} \rightarrow [SiO_2(OH)_2]^{2}$ .....(1.1)

$SiO_2 + H_2O + OH^{-} \rightarrow [SiO(OH)$.....(1.2)

$$Al_2O_3 + 3H_2O + 2OH^- \rightarrow 2[Al(OH).....(1.3)$$

During this condensation process, $[SiO_2(OH)_2]^{2-}$, $[SiO(OH)_3]^-$ and $[Al(OH)_4]^-$ link together releasing water molecules according to following reactions [2]:

$$(Si_2O_5,Al_2O_2)_n + nH_2O \xrightarrow{KOH,\ NaOH} n(OH)_3 - Si - O - Al(OH)_3^{(-)}$$

$$n(OH)_3 - Si - O - Al - (OH)_3 \xrightarrow{(-)\ KOH,\ NaOH} (Na,K)(-Si - O - Al - O)n + 3nH_2O$$

orthosialate (Na,K)-poly(sialate)

.....(1.4)

$$(Si_2O_5,Al_2O_2)_n + nSiO_2 + nH_2O \xrightarrow{KOH,\ NaOH} n(OH)_3 - Si - O - Al - O - (OH)_3^{(-)}$$

$$n(OH)_3 - Si - O - Al - O - Si - (OH)_3 \xrightarrow{(-)\ KOH,\ NaOH} (Na,K)(-Si - O - Al - O - Si - O)n + 3nH_2O$$

oligo(sialate-siloxo) (Na,K)-poly(sialate-silioxo)

As the process continues, various monomeric, oligomeric and polymeric units continue growing producing chains that eventually crosslink in gelation phase and form a complex 3D network. This geopolymerization process is similar to methods used in processing organic polymers producing amorphous and semi-crystalline materials comparable to feldspar [6]. GP structure can be described as X-ray amorphous, 3-D framework of corner-sharing $[SiO_4]$ and $[-AlO_2-]^-$ tetrahedra in IV-fold coordination [7] ,

where the IV-coordinated aluminum present in the structure differentiates a geopolymer from other poly-aluminosilicate materials. The negatively charged aluminum ions, $[-AlO_2-]^-$, in the GP framework are balanced by the positively charged metal ions [6, 8-10] positioned in the framework cavities. Some of the water from aqueous solution remains in the tridimensional GP framework as physically and chemically bonded water within framework cavities and pores, or as OH^- groups bonded to Al and Si tetrahedra [11, 12] Figure 1.1 illustrates the geopolymerization process based on a simplified model described in literature and modified here [13, 14]

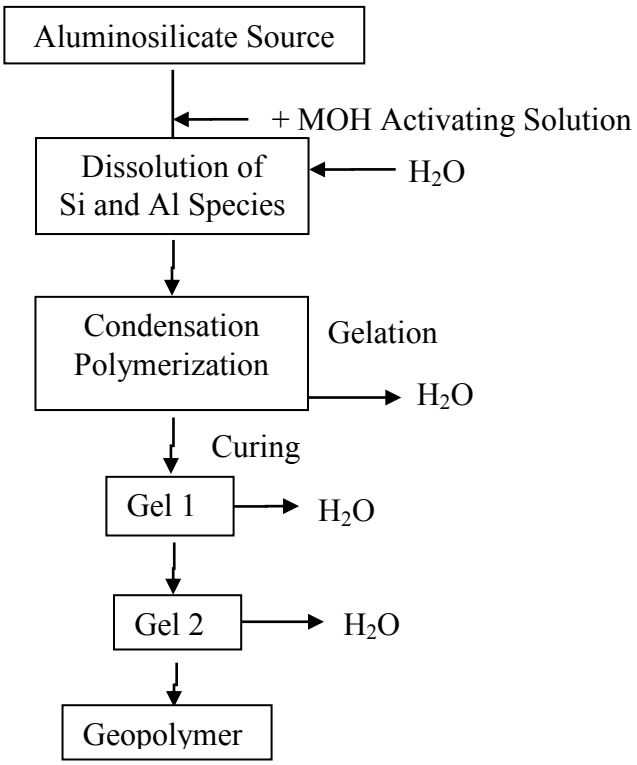

Figure 1.1 Geopolymerization process [13, 14].

Notwithstanding, the simplistic model shown in Figure 1.1, does not begin to convey the geopolymer processing complexities. The several processing mechanisms are still not completely understood. This is mainly due to extremely rapid Si and Al dissolution and polymerization in the initial reaction stages, preventing quantitative measurements [2, 3]. Additionally, many variables such as precursor selection and processing methods greatly affect geopolymerization mechanisms. Consequently, the final product's microstructure and properties are affected as well. Therefore, conclusively identifying the parameters that affect structure and properties of end product is very difficult to determine.

Geopolymers are usually referred to as poly (sialates) [1] as shown in Reaction 1.4, having empirical formula $M_n(-(SiO_2)_z\text{-}AlO_2)_n \cdot wH_2O$, where M is a monovalent cation (K, Na, etc.), z is the atomic ratio Si/Al = 1, 2, 3 or higher, n is a degree of polycondensation and w is water molar amount. A SiO_2/Al_2O_3 = 1, 2, or 3 molar ratios yield poly(sialate) (M-PS) or M(-Si-O-Al-O-), poly(sialate-siloxo) (M-PSS) or M(-Si-O-Al-O-Si-O-), and poly(sialate-disiloxo) (M-PSDS) or M(-Si-O-Al-O-Si-O-Si-O) respectfully. Sialate links between $(-Si\text{-}O\text{-}Si\text{-}O-)_n$ chains occurs for molar ratios $SiO_2/Al_2O_3 > 3$ [15]. A poly (sialate) structure adapted from literature [16] for various SiO_2/Al_2O_3 molar ratios is presented in Figure 1.2a where Si atoms are blue, Al atoms are green, O atoms are red, and yellow atom is the activating cation. Figure 1.2b schematically illustrates the geopolymerization process and resulting 3-D framework structure [17]*. The positively charged ions, positioned within the framework cavities,

are the stabilizing cations balancing the negatively charged aluminum anions in the complex geopolymer structure [6].

1.2 Properties and Application of Geopolymers

The unusual combination of properties and inexpensive processing methods has fueled research endeavors on GPs for many potential engineering applications. Much work has been published on various GPs properties and they are reported to vary significantly with chemical composition (Si/Al atomic ratios), precursor source materials, various processing conditions, alkali activator used, etc. [4, 6, 18, 19]. In general, GPs have been found to have good compressive strength when compared to similar cementations materials, low shrinkage, low thermal conductivity, high abrasion resistance, and strong adhesion to various metallic and ceramic substrates, [13, 20]. They are also chemically inert [14], thermally stable [10], and fire resistant [6] up to 1000-1400 °C.

Low technology geopolymer composite applications are currently being utilized [6, 13] and many more applications have been proposed. There is interest in GPs as construction materials [21], concrete binders [20, 22], adhesives [23, 24], toxic waste encapsulation materials [25-27], and biomaterials [28]. In this age of environmental awareness and social responsibility, GPs have been proposed to offer mitigating solutions to industrial waste disposal [29, 30] and CO_2 emissions reduction from the concrete industry [20, 31]. Considering the various geopolymer properties, together

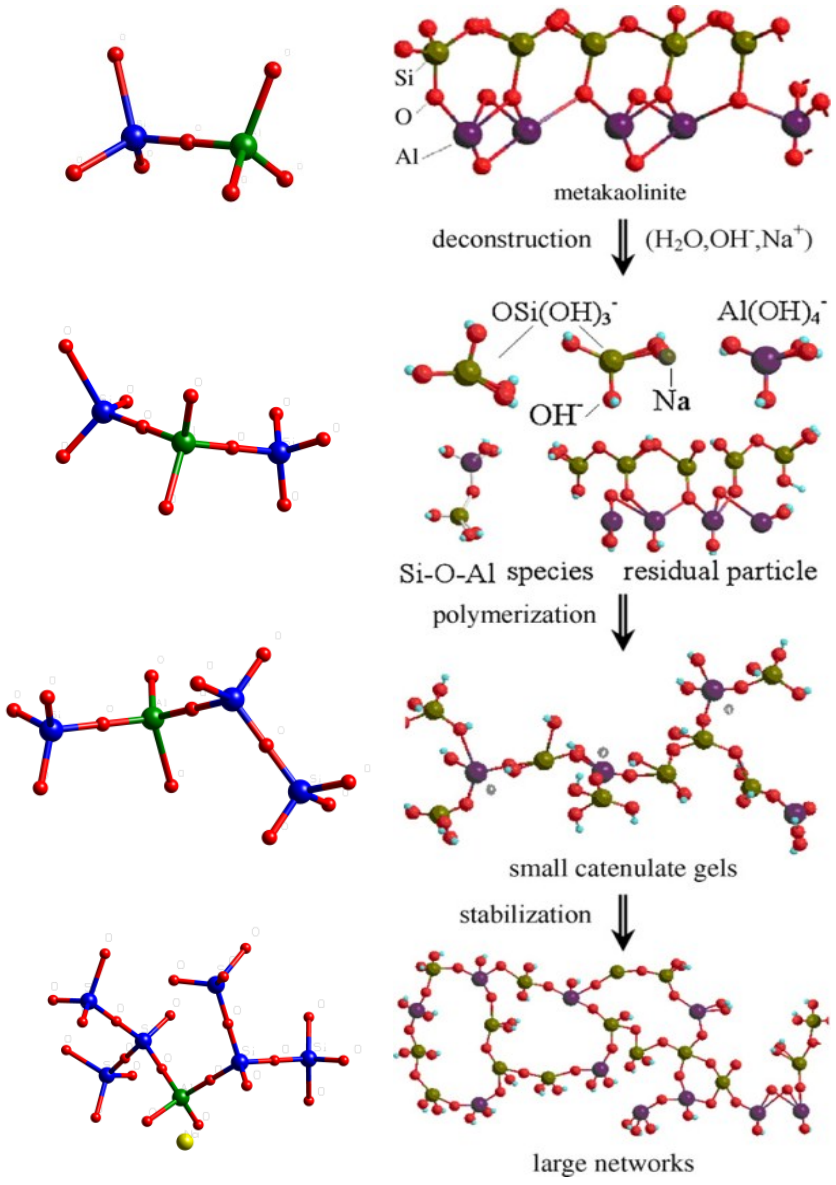

Figure 1.2 a) Polysialate structures from top to bottom, SiO_2/Al_2O_3=1, SiO_2/Al_2O_3=2, SiO_2/Al_2O_3=3 and SiO_2/Al_2O_3 >3, b) illustration of geopolymerization process[17][*].

[*] Reprinted from Thermochimica Acta, Vol. 493/1-2, X. Yao, Z. Zhang, H. Zhu, Y. Chen, Geopolymerization process of alkali-metakaolinite characterized by isothermal calorimetry, page no. 3, copyright (2009), with permission from Elsevier.

with easy and inexpensive processing methods, the possible engineering application fields for GP technology has been only barely opened in the last decade.

1.3 Problem Statement

Better understanding of processing-structure-properties relationship is critical if GPs are to be commercially utilized in many above mentioned applications. Thoroughly understanding the processing-structure-properties relationship is needed in order to tailor the thermal and mechanical properties of GPs for specific applications. The $[SiO_4]$ and $[AlO_4]^-$ monomer polymerization leads to extremely complex structures, illustrated in Figure 1.3. These structures can be quite different and dependent on many processing variables: such as aluminosilicate source (i.e. fly ash, steel slag, variations in kaolin or kaolinite-clays, calcination temperatures, impurity concentration) composition (SiO_2/Al_2O_3 molar ratios), activating cation (Na, K, etc.), water content (H_2O/Al_2O_3 molar ratios), as well as mixing, curing and aging methods, times and conditions.

Accordingly, it has been difficult to determine different effects from processing parameters on the geopolymer structure and properties, as is discussed in more details in subsequent sections of this dissertation. Furthermore, published works impart difficulty in comparing structure and properties of geopolymers due to processing variations. For example, distinctions in reported compressive strength range from as low as 25 MPa [32] to 82 MPa [9], for samples with different Si/Al ratios, water content, and different curing temperatures times and environments. Difficulty comparing properties of MK

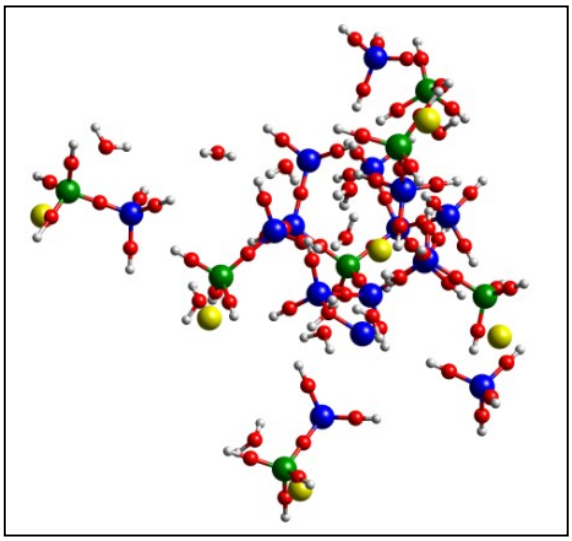

Figure 1.3 Geopolymer 3-D framework.

based geopolymers results from diverse processing parameters and dissimilar metakaolin precursors as well. Moreover, some crucial processing parameters are rarely reported in the corresponding literature. As a result, deciphering which parameter contributes to the observed structure and properties of GPs can be confusing and is more often than not tenuous. In several publications, the attempts have been made to relate observed differences in properties of GPs to the SiO_2/Al_2O_3 ratio and its effect on GPs microstructure. For example, as it is discussed in more details in Section 2 and 4, it has been suggested [4, 9] that higher SiO_2/Al_2O_3 ratios results in higher strength of GPs due to increased density of the final product [1] and stronger Si-O-Si [4] when compared to Si-O-Al linkages [4, 33]. However, that conclusion cannot be applied to explain decrease in compressive strength that is commonly observed in GPs with Si/Al ratios above 2 [4].

It is interesting to note that the geopolymer microstructure, and thus properties have been almost exclusively been related to the SiO_2/Al_2O_3 ratio, and sometimes to metal activator, curing temperature and time, while the initial water quantity in the mixture was varied arbitrarily to provide good workability in the GP paste [32, 34]. On the other hand, a very few studies suggests that the microstructure is also strongly related to the amount of water involved in the initial mixture [12]. Hence, following questions still remain unanswered: What factors affect predominantly the geopolymer microstructure? Is silicon content solely responsible for geopolymers structure as proposed in the literature or does water have a more important role? How does the different microstructure affect geopolymer mechanical and thermal properties?

Ideally, geopolymer research has been focused on industrial waste utilization or inexpensive natural sources as precursor materials due to availability. Thus, affectively mitigating problems with landfill waste disposal and designating geopolymers as environmentally friendly green materials. Alas, the impurities in these aluminosilicate sources are likely affecting the GPs properties. Thus, understanding an already complex geopolymerization process and the resulting product structure becomes even more complicated. A solution may be offered from pure synthetic geopolymer materials in which pure Si and Al species are controlled and utilized for producing pure geopolymeric materials. In this fashion, not only does the process eliminate effects on GPs properties from impurities, it may also provide synthetically pure geopolymers in which impurities may have an adverse effect in certain applications. Additionally, processing synthetically pure GPs may provide further insight into the

geopolymerization process. However, a fundamental problem of processing synthetic, chemically pure GPs obtained using alternative methods and precursors has not been address adequately in the literature.

1.4 Research Objectives

The technological potentials of GPs in many engineering applications cannot be underestimated. Yet, moving forward from research to applications is constrained, as it is pointed out in the previous section, mostly by the lack of deep understanding in the complex processing parameters affecting GP structure, properties and behavior under diverse conditions. The main goal in this research is focused on the initial geopolymer chemical composition and its effects on the thermal conductivity and mechanical strength after curing. The specific objectives are as follows:

Objective 1: To understand the effects of two major factors, namely $H_2O/(SiO_2 + Al_2O_3)$ and SiO_2/Al_2O_3 molar ratios on geopolymer atomic structure, porosity and microstructure with K and Na metal activators for metakaolin based GPs.

Objective 2: Relate the microstructure to the mechanical and thermal properties of the resulting geopolymeric products from Objective 1.

Objective 3: Investigate possible synthesis routes to process chemically pure geopolymers without impurities found in natural sources.

1.5 Dissertation Organization

This dissertation consists of 6 sections. Section 2 reports and discusses preliminary research work on the development of structure and mechanical properties of MK based geopolymers in the early stages of geopolymerization. In Section 3, experimental work and results on the effects that water content, composition, and aging time have on the microstructure of GPs is discussed. These results are then related to experimental work on GPs' thermal and mechanical properties discussed in Section 4. Section 5 covers processing methods, results and challenges regarding synthetically pure geopolymers. Finally, Section 6 provides concluding remarks and addresses future work.

2. EFFECT OF SiO_2/Al_2O_3 RATIO ON MECHANICAL PROPERTIES OF K- AND Na-ACTIVATED GEOPOLYMERS

2.1 Literature Review

The mechanical properties of GPs are critical if they are to be commercially utilized in many of the applications discussed in Section 1. Most of the studies on the mechanical properties of GPs processed from MK have been carried in effort to characterize their compressive strength. As previously mentioned, the maximum compressive strength reported in literature varies from as low as 25 MPa to 22 MPa, for samples with different Si/Al ratios and water content [4, 5, 9, 32, 34-37]. The difficulty in relating the compressive strength of the various metakaolin based GPs reported in literature lays in different processing conditions and metakaolin precursors that used in contrasting studies. Thus, deciphering which parameter contributes to the compressive strength can be confusing and is ultimately elusive, and is discussed in more details in Section 4. In several publications, attempts have been made to relate observed differences in compressive strengths to the Si/Al ratio and its effect on the microstructure of GPs [9, 34, 38]. It was suggested that increasing Si/Al results in increased compressive strength due to increased density of the final product and stronger Si-O-Si bonds [4]. Theoretically, Si-O-Si linkages are stronger than Si-O-Al linkages; suggesting an increase in Si content would improve the compressive strength [4, 33]. Most importantly, at low Si content a microstructure of GPs consisted of large interconnected pores and loosely packed precipitates. Homogeneous and dense

microstructures are observed with higher Si/Al content, thus resulting in increasing compressive strength with increasing Si/Al ratio. However, that is not the case for Si/Al greater than 1.9 when strength actually starts to decrease with increasing Si content. A higher strength in K over Na based GPs is noted in the range $1.4 \leq Si/Al \leq 1.9$, while the strength of Na and K is similar with Si/Al>1.9 [9].

Surprisingly, a smaller number of papers report on fracture toughness and elastic moduli of GPs although those properties are also crucial for their engineering applications. Duxson et al. [9] showed that Young's modulus increases with Si/Al ratio, and levels at ~5.5 GPa for Si/Al in the 1,62 to 2.15 range, for both, Na- and K-based geopolymers. Belena, et al. [39] showed, using nanoindentation tests that Young modulus of Na-activated GPs prepared with ratio of Si/Al=1.75, and N/Al=1, can increase from 7 GPa to 14 GPa by using different curing conditions and processing by injection molding. As to the best of our knowledge, the only reported study on fracture toughness, K_{IC}, of GPs is that of B. A. Latella, et al.[37] for GPs with ratios of Si/Al = 2 and Na/Al = 1 processed using several different precursors. They measured the fracture toughness in the range of 0.25-0.65 $MPa \cdot m^{1/2}$ and concluded that porosity is the crucial microstructural variable controlling the mechanical properties of the GPs, in addition to presence of impurities and unreacted phases.

Based on the briefly reviewed studies in previous paragraphs, it is clear that mechanical properties of geopolymers reported in the literature varies significantly and depends on many variables, including Si/Al molar ratios, type of aluminosilicate source, water content, curing time and temperature, aging time, etc. Thus, results published in

various papers cannot be easily compared because a large number of processing variables differ in those studies. This is the largest obstacle towards better understanding the response in this new class of inorganic polymers under mechanical loads.

The purpose of this study is to further elucidate the mechanical behavior as a result of Si content and type of metal activator on MK based geopolymers. This study investigated the effects of the Si/Al ratio and metal activators (Na and K) on a set of mechanical properties in metakaolin-based GPs, including compressive strength, Young's modulus, hardens and fracture toughness, while keeping all other processing variables the same for all processed samples. The ratios considered were Si/Al= 1.25, 1.5, 2, and 2.5 with H_2O/Al_2O_3= 11 and 13 and atomic ratios at Na/Al and K/Al equal to 1. Moreover, the effects in different curing times on the GPs mechanical properties were investigated.

2.2 Experimental Methods

Metakaolin (MK) was selected as precursor material in this study because it usually contains fewer impurities when compared to other GP precursors. MetaMax® (BASF catalysts LLC, NJ) metakaolin with 53 wt% of SiO_2, 43.8 wt% of Al_2O_3 and 3.2 wt% of impurities (mostly TiO_2) was selected as the purest precursor among several different tested MK. An amorphous fumed silicon (IV) oxide (Alfa Aesar, MA) and 350-410 m^2/g specific surface area, was utilized for modification of Si/Al ratio of MK precursor. Potassium hydroxide (KOH) (Mallinckrodt Chemicals, NJ), sodium

hydroxide (NaOH) (Mallinckrodt Chemicals, NJ) and deionized water were used to process metal alkaline solutions.

Table 2.1 The chemical composition of studied GPs where M = Na or K and Y is curing time in hours (24 or 48).

Sample labels	Si/Al	SiO_2/Al_2O_3	M_2O/ Al_2O_3	M/Al	H_2O/ Al_2O_3	$H_2O/ (Al_2O_3+SiO_2)$
	AR	*MR*	*MR*	*AR*	*MR*	*AR*
M-1.25-Y	1.25	2.5	1.00	1.00	11.0	3.14
M-1.5 -Y	1.50	3.0	1.00	1.00	11.0	2.75
M –2.0-Y	2.00	4.0	1.00	1.00	11.0	2.20
M-2.5 -Y	2.50	5.0	1.00	1.00	13.0	2.16
AR = Atomic Ratio, *MR* = Molar Ratio M = Metal activator						

Potassium and sodium silicate solutions were prepared by dissolving KOH or NaOH pellets in deionized water. SiO_2 was mixed into the alkali solutions. The alkaline silicate solutions were stirred for 24 hours in sealed containers to minimize possible reaction with atmospheric CO_2. Solutions were prepared for Si/Al atomic ratios of 1.25, 1.5, 2.0, and 2.5. The MK precursor is added to alkaline silicate solutions the following day and mixed in a vacuum mixer until homogenous mixtures were obtained. The

atomic and molar ratios used in this study are summarized in Table 2.1**.** For all samples, M/Al (where M is K or Na) was kept constant and equal to 1, i.e. to the stoichiometric ratio required to keep negative charges of Al tetrahedral balanced. H_2O/Al_2O_3 molar ratio was equal to 11 for all samples except for those with Si/Al=2.5. For samples with Si/Al=2.5, H_2O/Al_2O_3=13 was used, because mixture with lower water ratio had very high viscosity for mixing and processing air-bubble free samples with homogeneous structure.

K-based and Na-based samples were mixed for 23 and 3 minutes, respectively, in the vacuum mixer. Na-based samples are mixed for a significantly shorter time, since they start to polycondensate and harden much faster than K-based samples. After mixing, the samples were poured into molds and placed in sealed containers before curing at 80 ºC for 24 and 48 hours. The samples were then aged in air at room temperature for 1 day before testing. All processed samples were labeled M-X-Y, where M represents the alkaline metal, X represents Si/Al atomic ratio and Y represents the curing time in hours.

X-ray Diffraction (XRD) analysis of all samples was carried out using a Bruker-AXS D8 Advanced Bragg-Brentano X-ray Powder Diffractometer (Bruker AXS Inc, WI) with Cu-Kα radiation source generated at 40 mA and 40 kV, in the 2θ range of 10-50° with 2θ step of 0.02°. In addition, ^{27}Al MAS NMR spectra was collected using a WB Avance 400 Bruker (Bruker AXS Inc, WI) spectrometer using a standard 4 mm NMR probe with a spinning rate of 10 KHz. The ^{27}Al chemical shift was referred to an external standard of $[Al(H_2O)_6]^{3+}$.

The Scanning Electron Microscope (SEM), Quanta Q600 FEG-SEM (FEI Corp., OR), with Energy-Dispersive Spectrometer (EDS) was used to study microstructure and chemical composition of the GPs. Samples were slightly polished and sputter coated using platinum/gold to enhance the quality of SEM images. A set of samples were prepared with the same Si/Al ratios mentioned above and aged for 24 hours to calculate apparent density ρ . The mass, *m*, and volume, *v*, of each samples is measured and apparent density, is then calculated (ρ=*m*/*v*). The microstructures and properties are then related to apparent density and Si content. Microindentation measurements were carried out on polished GP samples to determine Young's modulus using Fischerscope HM2000 micro-indenter (Helmut Fisher GMBH, Germany) with standard pyramidal Vickers indenter. Indentations were performed on each sample with a minimum of 9 locations. The indents had depths of up to 0.1 μm with holding time of 20s. The Vickers hardness of prepared samples was ascertained using a Micro-hardness Tester LM 300 AT (LECO, MI) at room temperature using an indentation load of 500 g and a standard Vickers indenter. The length of the corner cracks generated by indentations was measured using SEM. The following equation was used to calculate fracture toughness from the length of the Palmqvist-type corner cracks: [40]

$$K_{IC} = \left(\frac{0.129H\sqrt{a}}{\phi}\right)\left(\frac{E\phi}{H}\right)^{0.4}\left(\frac{c}{a}\right)^{-1.5} \quad \text{.....(2.1)}$$

where H is the hardness, a is the length of the indent diagonal, E is Young's modulus, ϕ is a constant related to the sample's geometry and c is the length of surface crack.

A 810 Material Testing System (MTS Corporation, MN) was utilized to determine sample compressive strength. The constant displacement rate was 0.60 mm/min at room temperature. The Flextest SE Ver. 5.0 program monitored and measured the displacements (mm) and forces (lbs). More than 15 samples were tested for each composition under the same conditions. The results were analyzed using Weibull distribution to determine probability of survival as a function of compressive stress using procedure that is described in more detail elsewhere [41].

2.3 Results and Discussion

2.3.1 Structural Characterization

Typical XRD patterns of the MK precursor and synthesized K- and Na-based GPs with different Si/Al ratios after curing for 24 hours at 80 $^{\circ}$C are shown in Figure 2.1. The MK precursor shows x-ray amorphous structure with broad hump within 15-30° 2θ range and a maximum at $2\theta_{max}$ = 23° that is characteristic of amorphous aluminosilicate phases [32, 42]. A shift in the hump to $2\theta_{max}$=28-30° for both K and Na geopolymers previously reported as a typical feature of MK based GPs [34, 36] can be also seen in Figure 2.1. The decrease of $2\theta_{max}$ by 2° with increasing Si/Al ratio and/or the difference in alkali metal introduced into the matrix may be attributed to structural difference in the geopolymer matrix from environmental bonding changes during geopolymerization [34, 43]. The sharp peak at 2θ =25.36°, and few smaller sharp peaks at higher 2θ, in MK and

all GP samples is due to the presence of crystalline TiO_2 (PDF Number: 01-076-1931) impurity in the MK precursor [44] . Whereas the diffractograms indicate typical hump shifts for geopolymers, XRD does not provide adequate information on the atomic GP structures namely Si and Al tetrahedra [42]. Thus, NMR spectroscopy was carried out in addition to XRD to verify complete geopolymerization of the samples.

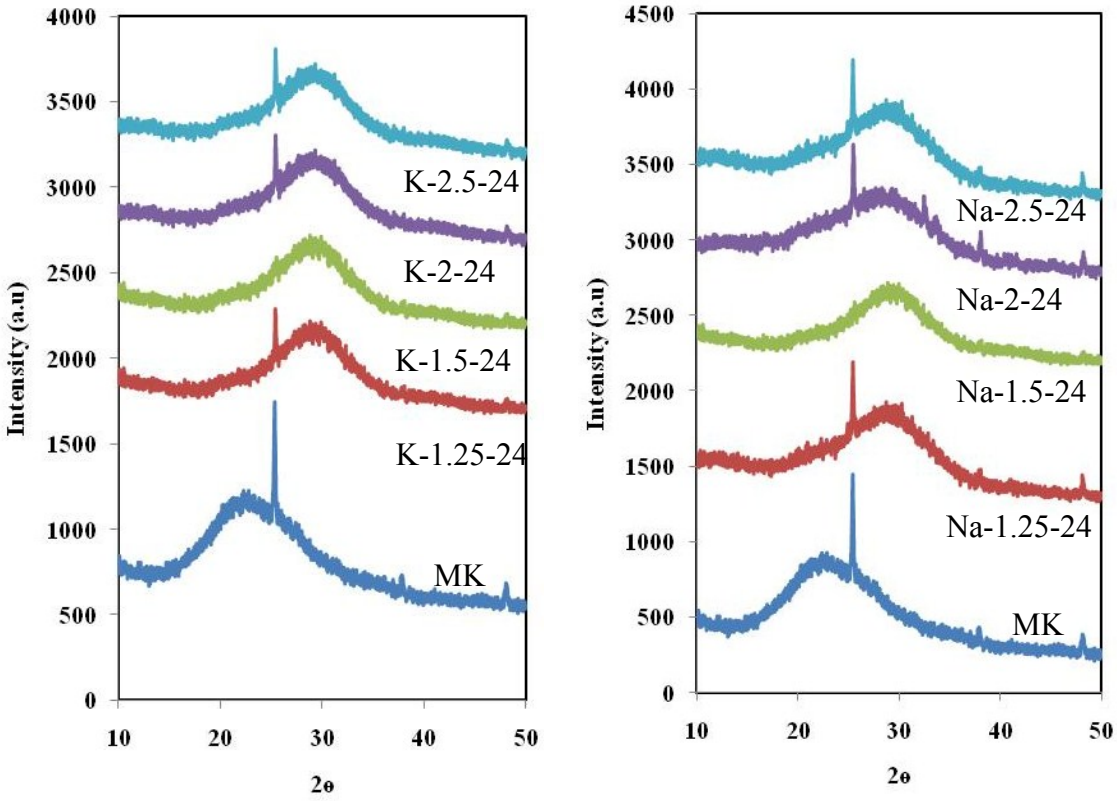

Figure 2.1 XRD diffraction spectra: (a) K-based and (b) Na-based geopolymers after curing for 24 hours.

The selected, but typical ^{27}Al MAS NMR spectra for the MK precursor and both K- and Na-based GP samples after curing for 24 hours at 80 $^{\circ}$C are shown in the Figure 2.2**.** The ^{27}Al spectra in Figure 2.2a indicate presence of IV (Q_4), V (Q_5), and VI (Q_6)-coordinated Al in the MK precursor. In the MK precursor, the amounts of IV and VI coordinated Al with chemical shifts at ~53 ppm and ~ 0 ppm, respectively, are equivalent and are less than the amount of V-coordinated Al with chemical shift at ~23.3 ppm. Although it was first believed that a high concentration of IV coordinated Al in MK was needed to form geopolymers [45], more recent studies and results here indicate the importance of the presence of V-coordinated Al in geopolymer MK precursor. It has been shown that geopolymerization has two exothermic effects. Thermodynamically speaking it is believed that the first effect is a result of the reactivity of –Al=O (V-coordinated Al) while the second exothermic effect is a result of the reactivity of –Al–O–Al–O linkages (IV-coordinated Al) [45]. The ^{27}Al MAS NMR spectra of the K- and Na-based GP samples shown in Figures 2.2b and 2.2c, respectively, for Si/Al=1.25-2.5 show that little or no V and VI coordinated Al remains after curing for 24 hours. The majority of Al is the IV-fold coordination with chemical shift of ~53 ppm. X-ray amorphous nature of the synthesized samples and presence of predominantly IV-coordinated Al are the best evidence of completed geopolymerization even after curing for only 24 hours [1]. Not surprisingly, K- and Na-activated GP samples cured for 48 hours show the same XRD and ^{27}Al MAS NMR features (not shown here).

Cross-sectional SEM images of both K and Na geopolymers with atomic ratios Si/Al = 1.25-2.5 are shown in Figure 2.3. Overall, K- GPs seem to have a more

homogenous microstructure and a less porosity than the Na- GPs within the same Si/Al ratio. Relating K- and Na-based GPs for the different Si/Al ratios, it can be observed that GPs with Si/Al=1.5 and 2 appear to have more dense homogeneous microstructure. The

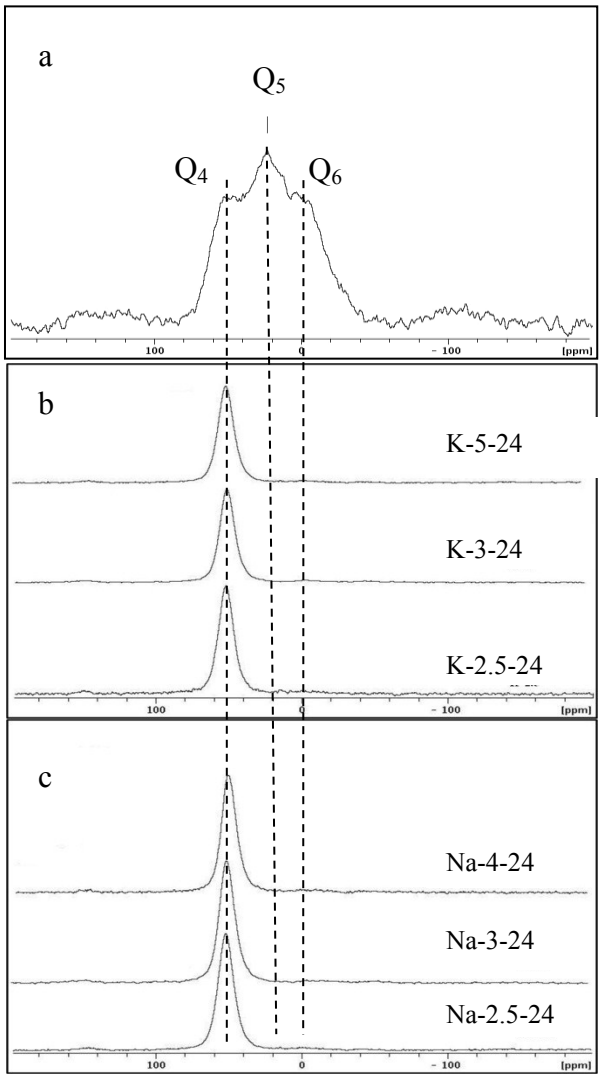

Figure 2.2 ^{27}Al MAS-NMR chemical shifts for a) MK, b) K-based, and c) Na-based geopolymer samples.

microstructure of GPs with Si/Al=1.25 are relatively loosely packed GP particles (precipitates) with large number of interconnected pores in comparison to samples with Si/Al=1.5 and 2. However, Si/Al=2.5 samples are comprised of larger GP particles like those with Si/Al =1.5 and 2, but contains greater number of large pores (~5 μm and up) and even some microcracks. These observations are in good agreement with previous microstructural studies of GPs with different Si/Al ratios [4]. Qualitative EDS analysis (not shown here) confirmed presence of only Al, Si, O and K or Na in all processed samples and overall Si/Al and Na (or K)/Al ratios calculated from EDS analysis were close to that of the initial precursor mixture.

Figure 2.4 shows that apparent density increases monotonically from 1.39 g/cm^3 to 1.82 g/cm^3 for K-based GPs, and from 1.27 g/cm^3 to 1.72 g/cm^3 for Na-based GPs with increasing Si/Al from 1.25 to 2.5. Apparent densities measured in this work are close to those reported by Wang et al. [46] and slightly below those reported by Duxson et al. [4] for Na-based GPs with the same composition. As suggested by Duxon et al. [4], the reason for density increase with increasing Si/Al ratio is the higher portion of solid components due to addition of SiO_2 to activating solutions to increase Si/Al ratio, while keeping H_2O/ Al_2O_3 ratio constant, Table 2.1.

More importantly, results shown in Figure 2.4 are in good agreement with our microstructural observations (Figure 2.3) accordingly in which Na-activated GPs have more porous microstructure when compared to K-activated ones. The reason for higher porosity and lower density of Na-based GPs in this study is not clear at this point.

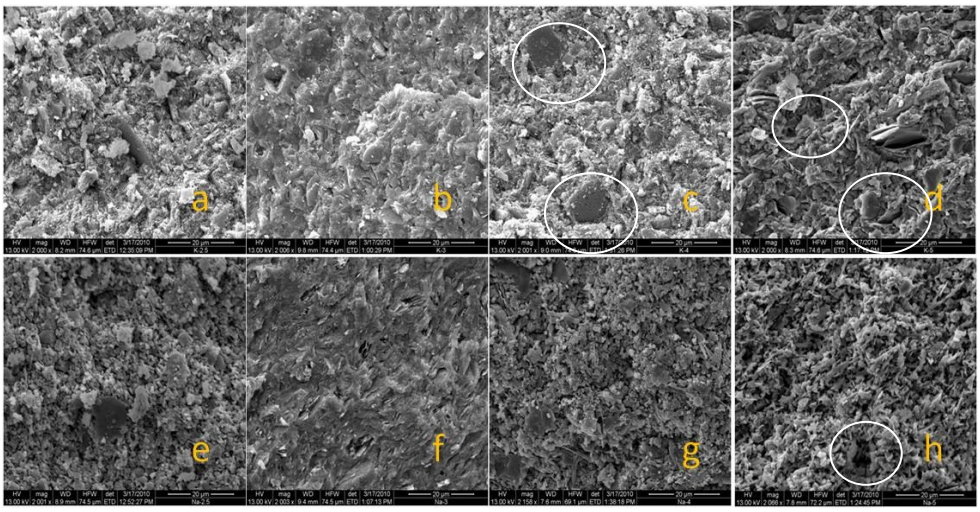

Figure 2.3 Secondary electron SEM images of GPs (a-d) K-1.25, 1.5, 2, and 2.5, respectively, and (e-h) Na-1.25, 1.5, 2, and 2.5 respectively, after curing for 24h.

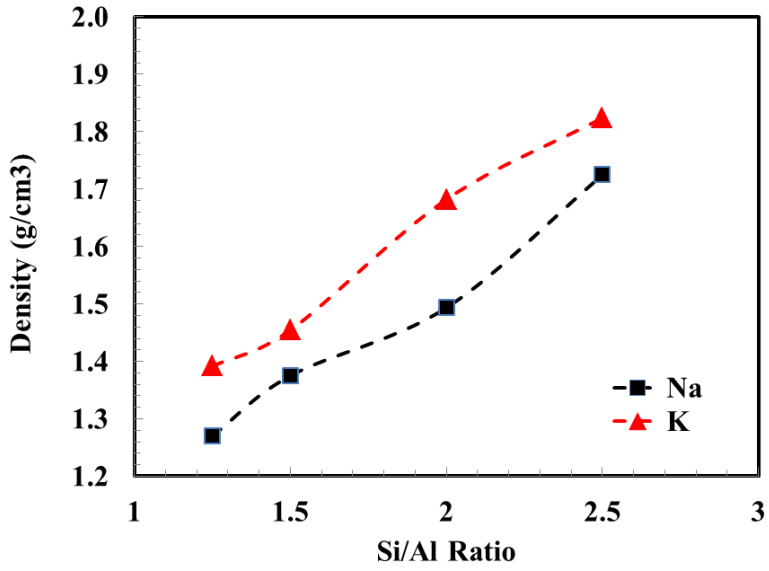

Figure 2.4 The apparent densities calculated in K- and Na-GPs.

However, it could be related to the fact that initial Na-based activating solutions are much more viscous than K-based solutions. Na-GPs polymerize much faster, thus prohibiting long mixing, good homogenization and degassing (removal of entrapped air bubbles). Additionally, it is suggested that smaller silicate monomers and dimers favor ion pairing with the smaller Na cations, whereas K cations favor ion pairing with larger silicate oligomers [14]. This may be a contributing factor not solely on the apparent densities for both K- and Na-based GPs, but also the differences in microstructure seen in Figure 2.3.

The fact that GPs with Si/Al=2.5 have greater number of large pores and less uniform microstructure, when compared to samples with Si/Al=1.5 and Si/Al=2, may appear in contradiction with the density results showing monotonic increase in density with increasing Si/Al ratio, Figure 2.4. The possible reason for this discrepancy lies mainly in presence of larger amount of unreacted MK in the samples with higher Si/Al ratios. GPs usually contain unreacted MK particles weakly bonded to GP, and thus easily pull out from the surface during polishing process [42] leaving surface cavities with the typical layered structure. Those cavities can be observed quite frequently in SEM images of the samples with Si/Al=2.5 (as denoted by circles in Figures 2.3c and 2.3h), giving the impression of higher porosity of those samples. We must take into account that initial mixtures with Si/Al=2.5 are very viscous because of the lower total water/solid ratio (i.e. $H_2O/(MK+SiO_2)$ ratio) as compared to the samples with lower Si/Al ratios (Table 2.1). It is not surprising then that poor mixing and faster hardening of those samples result in a larger amount of unreacted MK particles. During the mixing process in a reactive liquid-

solid system with high viscosity, some parts of material have less water available than other parts, and thus do not react completely [14]. This can also be the reason for the less homogenous structure with numerous large pores and some microcracks that are observed in the samples with Si/Al=2.5.

2.3.2 Mechanical Properties

Young's modulus determined using micro-indentation for Na- and K-based GPs with different Si/Al ratios cured for 24 hours are shown in Figure 2.5**.** Throughout the range of Si/Al ratios K-based GPs have slightly higher Young's modulus than the Na samples with the exception of Si/Al=1.5. Also, the Young's moduli of both Na- and K-based GPs increase with increasing Si/Al ratio up to Si/Al=2, after which they slightly decreases again. These observations can be related to: (a) lower porosity of K-based GPs when compared to Na-based ones and (b) increase in the density of both K- and Na-based GPs with increasing Si content.

The trends shown here, as well as measured values of Young's modulus are very similar to previously published results by Duxson et al. [9]. Duxson et al. reported increasing values of Young's modulus with increasing Si/Al ratios up to Si/Al=1.65, and almost constant modulus for GPs with Si/Al rations between 1.65 and 2.15 attributing these observations to good microstructural homogeneity in the GPs with Si/Al>1.65, having very little unreacted MK and few isolated pores. However, results shown here indicate decrease in elastic moduli for the samples with Si/Al > 2, regardless of

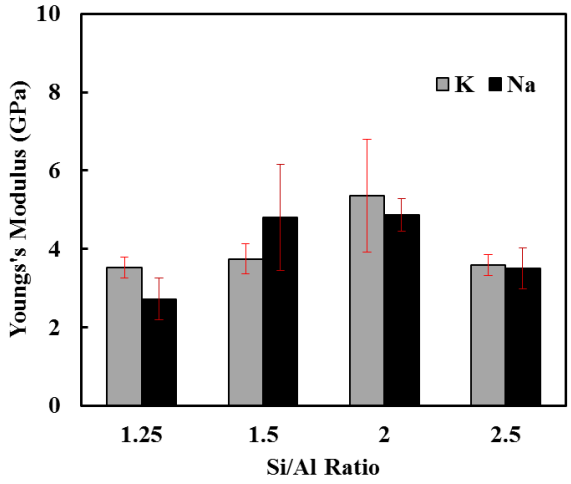

Figure 2.5 Average values of Young's modulus of GPs with different SiO_2/Al_2O_3 ratio determined by microindentation testing. The error bars denote standard deviations.

monotonic increase in the density of the samples with increasing Si/Al ratios (Figure 2.4).This suggests that measured elastic moduli of GPs do not only depend on their apparent densities, but also on their composition and microstructure. Both Na- and K-based GP samples with Si/Al=2.5 show higher microstructural inhomogeneity and larger number of large pores and microcrack when compared to samples with Si/Al=2 (Figure 2.3), resulting in the lower values of elastic moduli.

The changes in Vickers's hardness with increasing Si/Al ratios for both Na- and K-activated GPs cured for 24 hours show almost the same trend as in the case of Young's modulus, Figure 2.6. Once again, K-based GPs have slightly higher hardness than the Na-based GP samples, but in both Na- and K-based GPs, Vickers hardness

increases with increasing Si/Al ratio up to Si/Al=2, after which it slightly decreases. These observations can be again related to the microstructural differences between samples with different Si/Al ratios and alkali activators, as discussed in previous paragraphs. It is worth noting that all Vickers hardness values reported here are higher than 200 MPa published by Lecomte et al. [47] for GPs prepared from different precursors, but in the same range as values published by Belena et al [48].

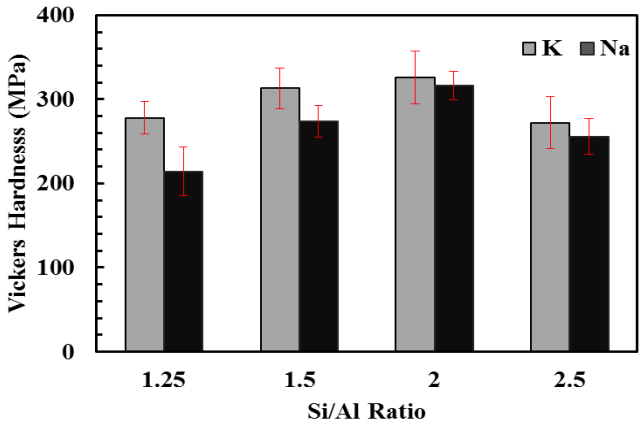

Figure 2.6 The average Vickers hardness values of K- and Na-based GPs. Error bars above columns represent standard deviation.

Results of Vickers indentation were used to determine GPs fracture toughness from the length of corner cracks at the indents using Equation 2.1, and the results are shown in Figure 2.7. While Figure 2.7a shows the fracture toughness of Na- and K-based GPs with different Si/Al ratios, Figures 2.7b and 2.7c show selected but typical

micrographs of the Vickers indents without and with corner cracks, respectively. As it can be seen in Figure 2.7a, fracture toughness of Na-base GPs is lower than that of K-based ones, for all Si/Al ratios.

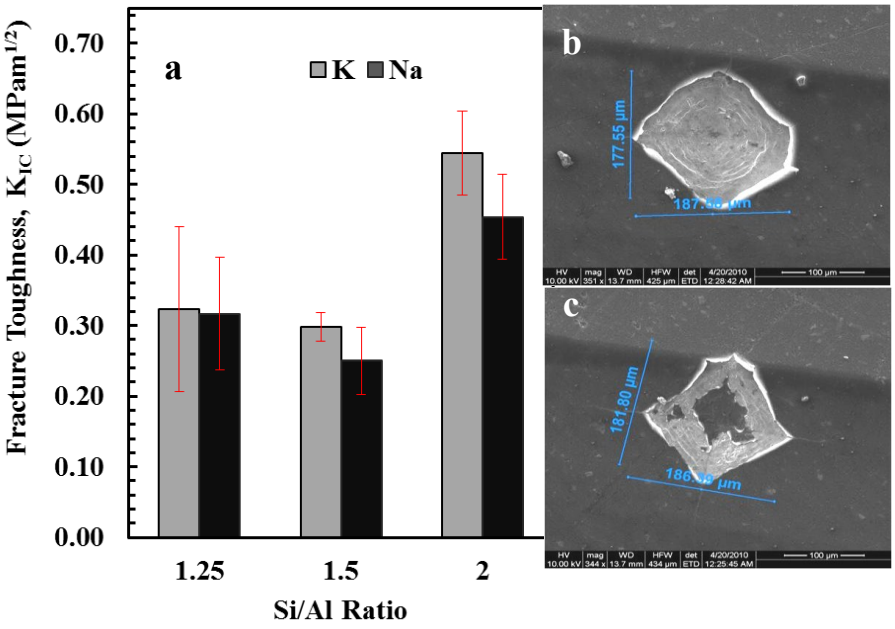

Figure 2.7 (a) Average fracture toughness values for K- and Na-based GPs with different Si/Al ratios. Selected but typical SEM micrographs of Vickers indents (b) without corner cracks (K-1.5-24) and (c) with corner cracks (K-1.25-24). Error bars in (a) represent standard deviation. Blue lines in (b) and (c) denote length of the indent diagonals.

Moreover, it appears that indentation fracture toughness of GPs with both Na and K activators increases with increasing Si/Al ratio up to Si/Al=2. As to best of our knowledge the only study on fracture toughness of GPs has been published in open

literature by Latella et al. [37]. They determined fracture toughness of GPs from three-point bending tests of the notched bars and showed that it increases from 0.25 $MPa \cdot m^{1/2}$ to 0.56 $MPa \cdot m^{1/2}$ as the density of GP samples increases. The results in Figure 2.7 show not only that indentation fracture toughness determined in this study is close to that published by Latella et al. [37], but also that it increases with increasing Si/Al ratio, i.e. density of the samples.

However, we were unable to determine indentation fracture toughness of Na- and K-based GPs with Si/Al=2.5, because no corner cracks were observed in any of the Vickers indents in those samples. In addition, as illustrated in Figure 2.7b, corner cracks were not present even on all Vickers indents in samples with Si/Al ratio below 2.5. The formation of the corner cracks during Vickers indentation occurs only in brittle materials, where mechanical energy stored in the material below indenter cannot be consumed by any of the mechanisms of plastic deformation, but has to be released by formation of corner cracks. Still, the lack of corner cracks in some of the Vickers indents does not mean that GPs are not brittle materials; the low values of their fracture toughness confirm that they are. Thus, the reason for the lack of corner crack must lie in the fact that geopolymer are highly porous and soft materials. Hence, large part of mechanical energy during indentation is consumed for densification of the material below the indent, rather than for the formation of corner cracks. Moreover, Figures 2.7b and 2.7c show that the fracture in the GP samples is conchoidal in nature. For these reasons, applicability of Vickers indentation for determining indentation fracture toughness of geopolymers is questionable, regardless of the fact that results shown here

are in good agreement with previously determined fracture toughness using other methods [37].

The average compressive strength of K- and Na-activated GPs with different Si/Al ratios and cured for 24 and 48 hours are plotted in Figure 2.8. Since GPs are brittle materials with a broad distribution of strengths, Weibull statistic was used to analyze compressive testing data. The results are summarized in Table 2.2. Figure 2.8 and Table 2.2 clearly show that samples with Si/Al ratio of 1.5 in both Na- and K- activated GPs have a higher compressive strength than other samples with different Si/Al ratios. In addition, K-activated specimens were significantly stronger than Na-activated specimens only for Si/Al=1.25. Above Si/Al=1.5, the compressive strengths of both Na- and K -activated GPs are comparable. In most Si/Al compositions, the compressive strength is increased by extending curing time from 24 to 48 hours, Figure 2.8 and Table 2.2.

Although compressive strengths reported here for Si/Al=1.25 are comparable to the strengths reported by Duxson et al. [4, 9], at higher Si/Al ratios compressive strengths determined in this study are significantly lower than previously published values [4, 9]. The reason for this discrepancy is twofold. First, the compressive strength in this study was calculated from the loads at which the first cracking appears, which was in many cases below maximum load on load-displacement curves recorded during compressive testing.

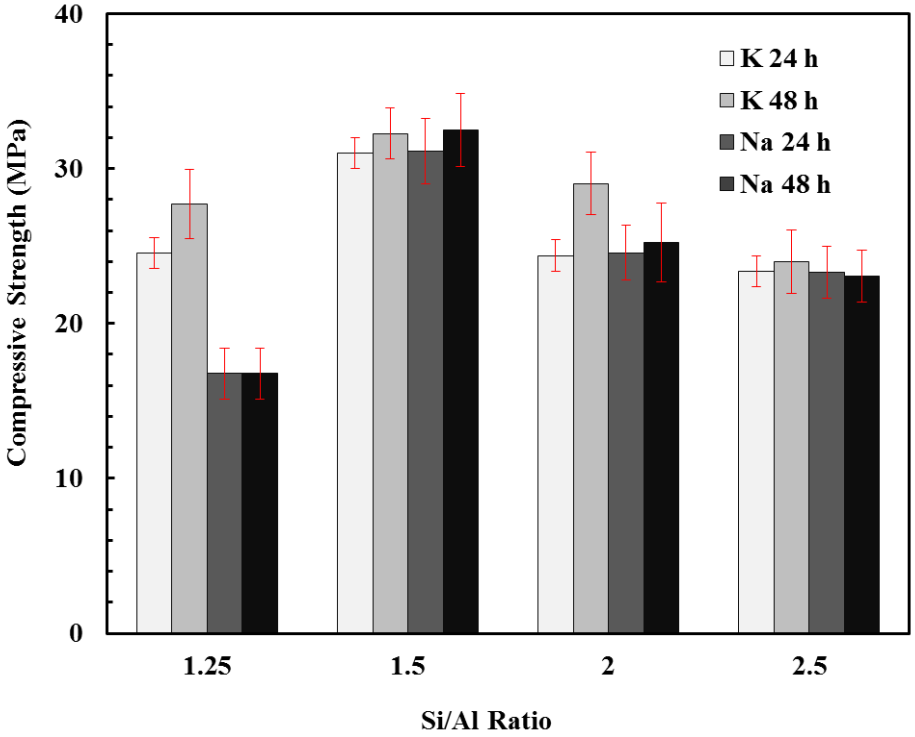

Figure 2.8 Average values of compressive strengths for K- and Na-based GPs with different Si/Al ratios after curing for 24 and 48 hours. Error bars in | represent standard deviation

Table 2.2 Weibull analysis results, where σ_0 is characteristic compressive strength and m is Weibull modulus.

Activator →	K				Na			
Curing time →	24 h		48 h		24 h		48 h	
Si/Al ↓	σ_0, MPa	m	σ_0, MPa	m	σ_0, MPa	m	σ_0, MPa	m
1.25	25.5	2.9	28.7	3.3	17.0	0.6	17.5	0.9
1.5	32.0	5.4	33.3	6.6	32.1	5.2	37.1	5.9
2.0	26.1	3.9	30.1	5.0	26.6	5.7	26.4	0.6
2.5	24.1	5.5	25.0	3.9	24.1	4.7	24.0	3.2

Secondly, the compressive strengths shown in Figure 2.8 and Table 2.2 were determined after curing for 24 and 48 hour and ageing for only 1 day, while compressive strengths reported by Duxson et al. [4, 9] were determined upon aging for 7 and 28 days after processing. Since compressive strength of GPs increases by increasing curing time from 24 to 48 hours due to more complete geopolymerization and gelation (Figure 2.8), it is not surprising that additional aging can result in additional strength development.

The trends observed in geopolymer compressive strengths are in some way different than those of Young's modulus, Vickers hardness and fracture toughness. Although it is expected that compressive strength increases with Si/Al ratio because of higher strength of Si-O-Si linkages when compared to Si-O-Al linkages and higher density in the samples with higher Si/Al ratios, results of this study show that samples with Si/Al=1.5 have the highest strength. To explain observed trend, one has to take into account that strength reported here is not the GPs intrinsic property, but like in other brittle solids, depends mostly on the size and distribution of strength controlling defects, such as cracks, inclusions, macrovoids etc. At lower Si/Al ratios, the activated solutions are less viscous because of higher water/solid ratios ($H_2O/(SiO_2+Al_2O_3)$ ratios in Table 2.1), resulting in better mixing, uniform microstructure and increase in the strength with increasing Si/Al ratios. However, with further addition of SiO_2 in the activating solutions to increase overall Si/Al ratios, they become more viscous, prohibiting good and uniform mixing. This results in more inhomogeneous microstructure when compared to the samples with lower Si/Al ratios, with numerous inclusions of unreacted MK, large pores and some microcracks that can all serve as origins in the failure. Thus, although GPS

density increases monotonically with increasing Si/Al ratio, the strengths of GPs will peak at intermediate Si/Al ratios. Additional evidence for the large differences in the distribution of strength controlling defects can be found in Table 2.2, that shows that Weibull modulus varies from as low as 10.6, suggesting relatively broad size distribution of the strength controlling defects, to as high as 15.7.

3. THE EFFECTS OF $H_2O/(SiO_2 + Al_2O_3)$ AND SiO_2/Al_2O_3 MOLAR RATIOS ON THE STRUCTURE, DENSITY, AND OPEN POROSITY IN K- AND Na-BASED GEOPOLYMERS

3.1 Literature Review

Over the last decades, intensive research on GPs has resulted in large number of publications discussing geopolymerization mechanisms and kinetics [14, 38, 49-51], the role of different alkali activators (Na, K, Ca, etc.) and aluminosilicate sources [8, 52-54], microstructure of GPs [36, 55, 56], and their mechanical [4, 9, 57] and thermal [19, 58-62] properties. However, although water is one of the key ingredients in synthesis of GPs, only a few studies have briefly discussed the effect of water on geopolymerization process, and structure and properties of GPs [63, 64]. Water not only provides the medium for the dissolution of aluminosilicate precursors and speciation, but also aids the transfer of various ions and polycondensation of Al and Si monomeric and oligomeric species [3, 64-66]. It is well established that dissolution of aluminosilicate precursors into Al and Si monomeric and oligomeric species is initiated in the early stages of geopolymerization by addition of alkaline aqueous solutions with pH above 13[6]. During the dissolution, water is consumed to form monomeric, mostly $Si(OH)_4$ and $Al(OH)_4^+$, and various oligomeric species. However, water is also released as these monomeric and oligomeric species polycondensate during polymerization and gelation of the solution [1, 67]. After completed geopolymerization, water remains entrapped in

the pores or bonded to the developed 3-D GP network and/or possibly in silanol and aluminol groups within the structure[45].

Zuhua et al.[64] showed that high liquid/solid ratio in the initial solutions accelerate dissolution and hydrolysis while hindering the polycondensation processes. They have also suggested that non-evaporable water has important role in stabilizing the strength of geopolymers. In another study, Okada et al.[63] indicated that higher H_2O/Al_2O_3 ratios resulted in larger pores and greater pore volume with good water absorption properties but low mechanical strength, while lower H_2O/Al_2O_3 resulted in a denser product with smaller pores and pore volume having better water retention and mechanical strength. Several other recently published studies also suggested that amount of water, i.e. liquid/solid ratio in initial solutions, might have stronger effect on the microstructure as well as the strength of the resulting GPs than their chemical composition [4, 68]. It is important to note that water is sometimes added to improve GP paste workability with little consideration as to the effects the excess water has on the structure and properties in the resulting product. [34, 69-71]

Perera et al.[12] showed in their study that cured geopolymers contain remnants of water in three different forms. Firstly, “free” water exists in cured GPs as a thin nanoscale surface layer and water located in intergranular sites. Secondly, there is interstitial water that may be associated with activating cation. And finally, OH groups can still remain in the cured GPs. Perera et al. [12] reports that around 60% of the initial water is free water and is lost when heating the material to 150 °C. At 300 °C, the interstitial water is almost completely lost while OH groups were nominally still present

in the GPs. They also showed that almost all water is lost at about ~700 °C. Thermal gravimetric analysis of geopolymers reported by Davidovits [11], indicates similar findings referring to Perera's "free" water as physically bonded water, interstitial water as chemically bonded water and further weight loss above 300 °C due to dehydroxylation of OH^- groups resulting in additional polycondensation into -Si-O-Si- linkages.

The reviewed studies mentioned above suggest that water content in the initial solutions, as well as the amount and type of residual water, might have a crucial role in microstructural development of GPs during curing, and consequently their properties. However, most of the studies have related microstructure of GPs to the SiO_2/Al_2O_3 ratios and/or types of alkali in the activating solution used for processing metakaolin-based GPs[4, 9, 34, 37, 38, 56]. In general, GPs with different SiO_2/Al_2O_3 ratios were usually synthesized from metakaolin precursors using constant H_2O/Al_2O_3 (mostly between 10-13 and adding SiO_2 or alkali-silicates to alter SiO_2/Al_2O_3 ratio present in the aluminosilicate precursor). Thus, GPs samples with different SiO_2/Al_2O_3 ratios were at the same time prepared with the different liquid/solid ratios, i.e. $H_2O/(SiO_2+Al_2O_3)$, making it difficult to distinguish effect of SiO_2/Al_2O_3 ratio from that of water content on the structure of GPs. Even more, water content in initial solutions were also commonly altered to adjust their viscosity and workability during their mixing.

In order to further demonstrate the role of water during and after synthesis, geopolymers samples with different SiO_2/Al_2O_3 and $H_2O/(SiO_2+Al_2O_3)$ molar ratios were prepared and structurally characterized in this study. The weight loss due to water

evaporation was studied over extended aging up to 21 days and during heating to 1000 ^{o}C. Observed differences in the water loss during aging and heating in, open porosity, density and microstructure of GPs were related to liquid/solid ratios in their synthesis, their composition, type of alkali (Na or K) and type of remaining water in the structure.

3.2 Experimental Methods

Metakaolin (MK), brand name MetaMax® (BASF catalysts LLC, NJ), with composition of $2.05SiO_2 \cdot Al_2O_3$ and 3.2 wt% of impurities (mostly TiO_2) was used as a precursor for all GP samples in this study. Amorphous fumed silicon (IV)-oxide, SiO_2, (Alfa Aesar, MA) was added to alkaline solution to vary the SiO_2/Al_2O_3 ratio of the geopolymer samples. The activating alkali metals used in making silicate solutions were KOH (Mallinckrodt Chemicals, NJ) and NaOH (Mallinckrodt Chemicals, NJ) pellets.

First, alkaline solutions were made by adding measured amounts of KOH or NaOH pellets to deionized water. Various amounts of SiO_2 was added to KOH or NaOH solutions. The silicate solutions and mixed on magnetic stirrers for 24 hours in sealed beakers at room temperature. Metakaolin was added to the prepared alkali-silicate solutions and mixed in a vacuum for various times, from 1 to 30 minutes depending on composition, until a homogenous mixture was obtained. The mixtures were poured into cylindrical plastic molds, 25.4 mm in diameter and 25.4 mm high. Roughly, half of all molds was sealed with plastic film. Next, all the molds were placed in closed plastic containers and cured at 60 ºC for 24 hours in the laboratory oven. Samples cured in sealed molds are further referred to as sealed samples, while those cured in open molds

are further referred to as unsealed samples. Table 3.1 shows the different molar ratios used to synthesize samples. The labeling protocol of the samples is as follows: *M-SiO_2/Al_2O_3-X* where *M* is the alkaline metal (K or Na), *SiO_2/Al_2O_3* is the SiO_2/Al_2O_3 molar ratio and *X* is the $H_2O/(SiO_2+Al_2O_3)$ molar ratio. The samples had resulting molar ratios SiO_2/Al_2O_3 = 2.5, 3 and 4 and $H_2O/(Al_2O_3+SiO_2)$ = 2, 3 and 4. In addition, samples with $H2O/(Al_2O_3+SiO_2)$ ratios of 2.2, 2.75 and 3.14 were prepared, since they correspond to the H_2O/Al_2O_3=11 a commonly used ratio in GP preparation with SiO_2/Al_2O_3 = 2.5, 3 and 4, respectively. For all samples, M/Al (where M is K or Na) was kept constant and equal to 1, i.e. to the stoichiometric ratio required to keep negative charges of Al tetrahedral balanced.

After curing, GP samples were aged at ambient conditions for 21 days. The weights of the samples were measured before curing (day 0), after curing (day 1) and every day during aging (day 2 – day 22). The wt%'s of residual water in GP samples were calculated from those measurements using following equation:

$$wt\% = \frac{w\prime_{H_20} - \Delta w}{w_{sample}} \cdot 100\% \quad (3.1)$$

where w'_{H_20}, Δw, and w_{sample} are initial weight of the water in the sample, total weight change of the sample during curing and aging, and total weight of the sample at the moment of the measurement.

The structure of the cured samples was characterized after curing for 21 days. X-ray diffraction, XRD, analysis was carried out to determine an X-ray amorphous

structure commonly seen in geopolymers or eventual presence of crystalline phases. More details on XRD characterization was provided in Section 2.2 of this dissertation. In this work, crystalline peak identification in XRD spectra was carried out using the EVA program. The ^{27}Al MAS NMR spectra was also collected and analyzed, while microstructure was studied using Scanning Electron Microscope, SEM. More details on ^{27}Al MAS NMR and SEM can also be found in Section 2.2.

Density and open porosity of samples aged for 21 days was determined using alcohol immersion technique according to the ASTM Standard C20-00[72]. After recording a sample's dry weight, W_{dry}, the samples were submerged in 200 proof ethanol, while sealed in a desiccator under vacuum for 5 minutes. The submerged samples remained at room temperature for approximately 30 min until a no change in temperature was recorded. The ethanol density, $p_{ethanol}$, for each sample was determined using the standard density vs. temperature tables. The apparent mass of the sample was measured by recording the weight of a suspended wire, W_{wire}, submerged in the ethanol and then recording the weight with the sample on the wire, W_{susp}. The sample was then removed from the ethanol. Excess ethanol was removed by patting the samples dry for 60 seconds. The weight was recorded again as W_{wet}. These measurements were used to determine the bulk density and % open porosity as follows:

$$Bulk\ Density = W_{dry} \times \frac{\rho_{ethanol}}{W_{wet} - W_{susp} + W_{wire}} \quad \text{.....} \quad \text{.....(3.2)}$$

$$\%\ Open\ Porosity = \frac{(W_{wet} - W_{dry}) \times 100}{W_{wet} - W_{susp} + W_{wire}} \quad \text{.....} \quad \text{.....(3.3)}$$

Table 3.1 The molar compositions and labels are given below for geopolymers samples with wt% of remaining water after their curing and aging for 21 day at ambient conditions.

Activator	SiO_2/Al_2O_3	$H_2O/(Al_2O_3+SiO_2)$	H_2O/Al_2O_3	Sample Label	wt% of H_2O after aging	
					unsealed	sealed
KOH K/Al=1	2.5	2.0	7.0	K-2.5-2	6.68	7.08
		3.0	10.5	K-2.5-3	9.14	9.56
		3.144	11.0	K-2.5-3.14	6.18	8.53
		4.0	14.0	K-2.5-4	8.29	9.27
	3.0	2.0	80	K-3-2	8.33	8.02
		2.75	11.0	K-3-2.75	7.24	7.16
		3.0	12.0	K-3-3	7.44	8.46
		4.0	16.0	K-3-4	8.41	8.50
	4.0	2.0	10.0	K-4-2	8.44	8.36
		2.2	11.0	K-4-2.2	10.81	8.74
		3.0	15.0	K-4-3	9.18	8.45
		4.0	20.0	K-4-4	9.46	10.44

Table 3.1 Continued.

Activator	SiO_2/Al_2O_3	$H_2O/(Al_2O_3+SiO_2)$	H_2O/Al_2O_3	Sample Label	wt% of H_2O after aging	
					unsealed	sealed
NaOH Na/Al=1	2.5	2.0	7.0	Samples cannot be processed		
		3.0	10.5	Na-2.5-3	17.15	14.29
		3.144	11.0	Na-2.5-3.14	15.61	15.91
		4.0	14.0	Na-2.5-4	15.30	16.26
	3.0	2.0	8.0	Na-3-2	16.70	17.58
		2.75	11.0	Na-3-2.75	17.18	15.28
		3.0	12.0	Na-3-3	17.08	15.55
		4.0	16.0	Na-3-4	15.49	15.25
	4.0	2.0	10.0	Na-4-2	18.93	20.17
		2.2	11.0	Na-4-2.2	19.83	18.38
		3.0	15.0	Na-4-3	18.03	19.71
		4.0	20.0	Na-4-4	18.76	18.40

Thermal Gravimetric Analysis, TGA, and Thermal Mechanical Analysis, TMA, were carried out using TA Instruments (New Castle, DE) TGA Q500 V6.3 and TMA 2940, respectively, to study the kinetics of water loss and dimensional changes of aged samples during heating up to 1000 ^{o}C. A heating rate of 20 ºC/min was used for both TMA and TGA measurements.

3.3 Results

Selected, but typical, XRD results for both K- and Na-activated geopolymers in Figure 3.1 show amorphous halos with the maximum at $2\theta_{max} \sim 22°$ for MK precursor and at $2\theta_{max} = 27\text{-}30°$ for cured geopolymers. The sharp peak at $2\theta = \sim 27.43°$ that corresponds to nonreactive crystalline TiO_2 impurity (PDF number: 00-034-0180) that was present in the MK precursor. The shift of amorphous halo from $2\theta_{max} = 22°$ in MK processor to $2\theta_{max} = 27\text{-}30°$ in cured GP samples has been commonly reported in the literature and explained by structural changes caused in the structure of aluminosilicates during geopolymerization [6, 13, 43].

^{29}Si MAS NMR is often carried out to identify the type of sialates in the GP structures, their coordination number and first neighbor types (Si and/or Al). However, a key feature in confirming a geopolymer matrix is the presence of IV-coordinated Al. (Q_4) Therefore, only selected but typical ^{27}Al MAS NMR are shown here in Figure 3.2. Chemical shifts shown for MK precursor in Figure 3.2 indicate three different coordination of Al: Q_4, at ~53 ppm, Q_5 at 23.3 ppm and Q_6 at 0 ppm. After curing and aging, only Q_4 Al with chemical shifts at ~53 ppm is present in all GP samples, regardless of their composition and $H_2O/(Al_2O_3+SiO_2)$ ratio, as it is illustrated in Figure 3.2.

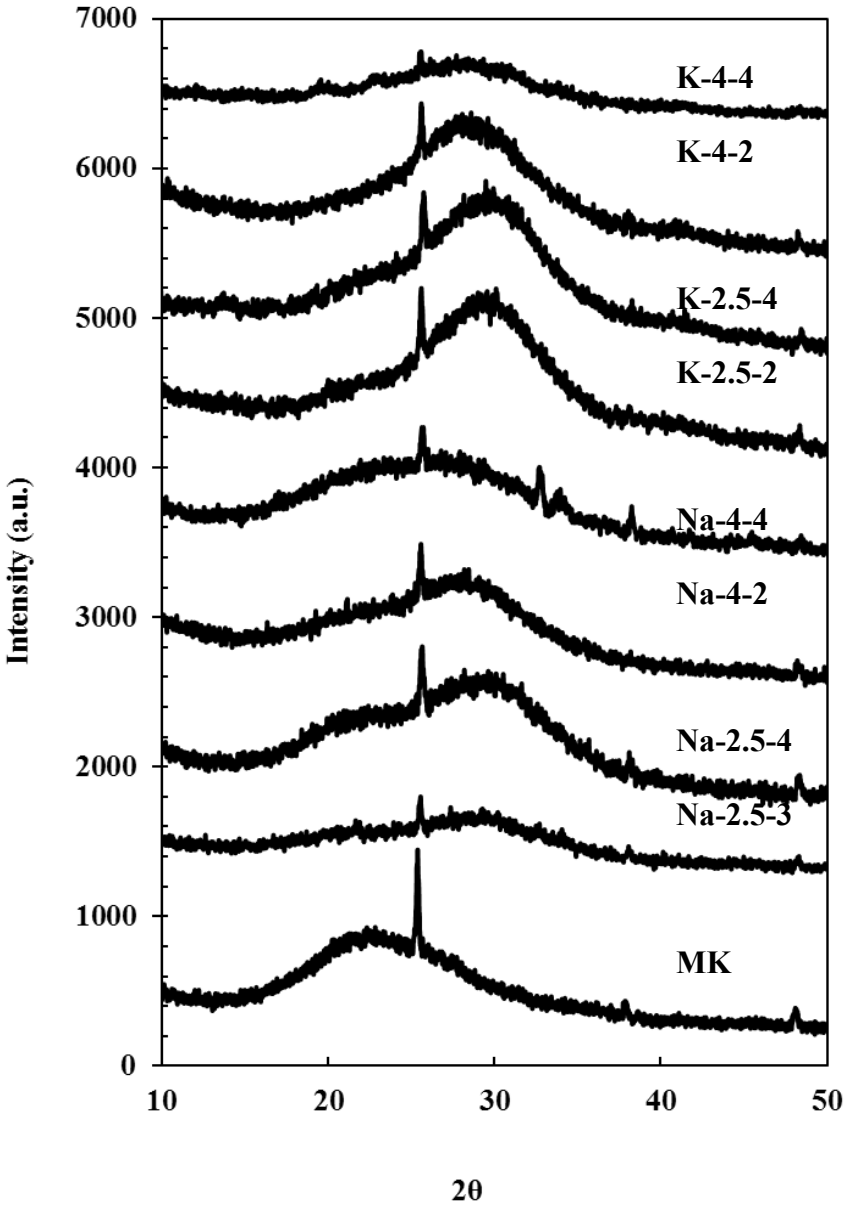

Figure 3.1 XRD of selected K- and Na-based geopolymers after curing and aging for 21 days. For comparison, XRD of the virgin MK is also shown in the figure.

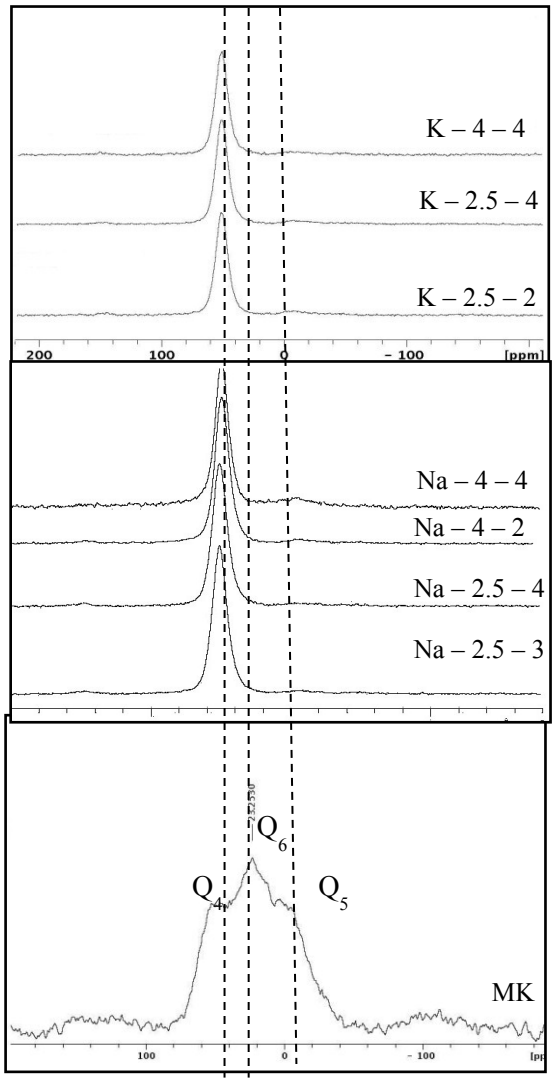

Figure 3.2 ^{27}Al MAS-NMR of virgin MK, and selected K- and Na- activated geopolymer samples after curing and aging for 21 days. Dashed lines mark Q_4, Q_5, and Q_6 - coordinated Al referred to an external standard of $[Al(H_2O)_6]^{3+}$.

A typical but selected changes of the wt% of the remaining water in GP samples determined using Equation 3.1 during curing in sealed and unsealed molds, and

subsequent aging for 21 days are shown in Figure 3.3 for K-activated samples with SiO_2/Al_2O_3=3, and $H_2O/(Al_2O_3+SiO_2)$ ratios of 2, 2.75, 3 and 4. The trend shown in this figure is typical for all examined sealed and unsealed K- and Na- activated geopolymers, showing that larger amount of water evaporates within the first 7 days of aging at ambient conditions.

After aging for 7 days, the rate of water loss is significantly slower. Figure 3.3 also shows that the initial water loss/evaporation during curing (after day 1) is larger in unsealed samples, than in sealed ones. Results of the water loss studies during curing and aging are summarized in Figures 3.4 (page 48) and 3.5 (page 49), and in Table 3.1. While Figures 3.4 and 3.5 show water wt% in GP samples before curing (day 0), after curing (day 1) and after aging for 22 days (day 22) as a function of $H_2O/(Al_2O_3+SiO_2)$ for sealed and unsealed K- and Na-activated GP samples, Table 3.1 only lists the remaining water wt% in all samples after aging for 21 days.

Once again, Figures 3.4 and 3.5 show that water loss during curing is more intensive in unsealed samples, than in sealed ones. More importantly, results shown in Figures 3.4 - 3.5 and Table 3.1, suggests that wt% of water after curing and aging for 21 days is independent of initial $H_2O/(Al_2O_3+SiO_2)$ ratios and sealing conditions during curing. Approximately 6 to 10 wt% of all K-activated samples after aging for 21 days is residual water, while in all Na-activated samples that amount ranges between approximately 15 and 20 wt%. Also, results in Figures 3.3 and 3.4 suggests that amount of non-evaporable water after curing for 21 days at ambient conditions is slightly higher in samples with higher SiO_2/Al_2O_3 ratios.

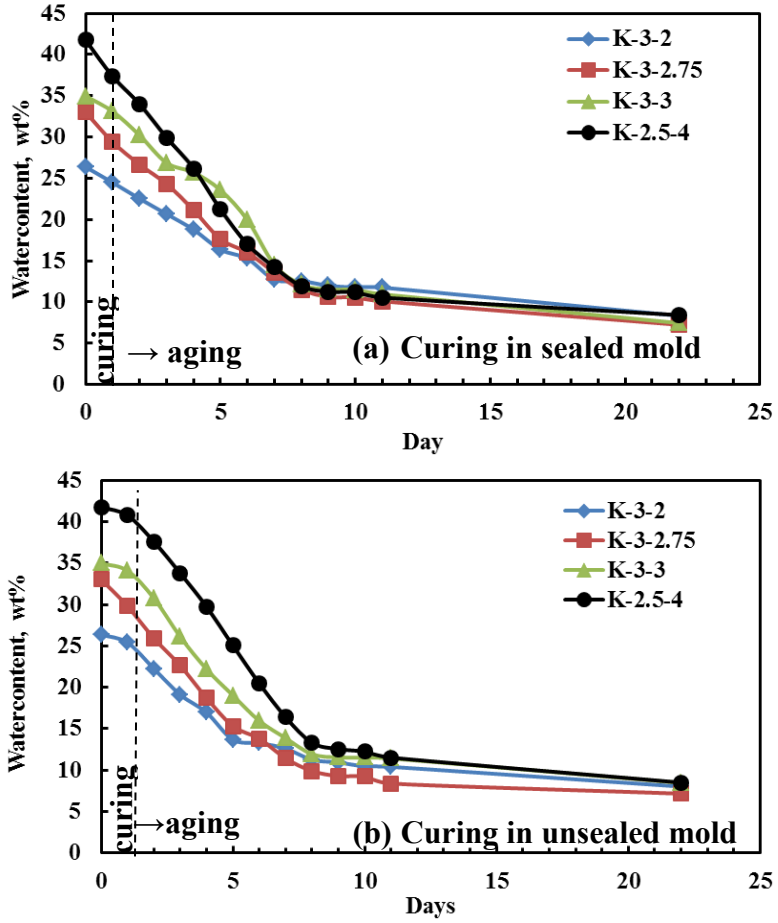

Figure 3.3 The wt% of water remaining in K-3-X samples with $H_2O/(SiO_2/Al_2O_3)$ = 2- 4 during curing in (a) sealed and (b) unsealed molds and aging for 21 days in air.

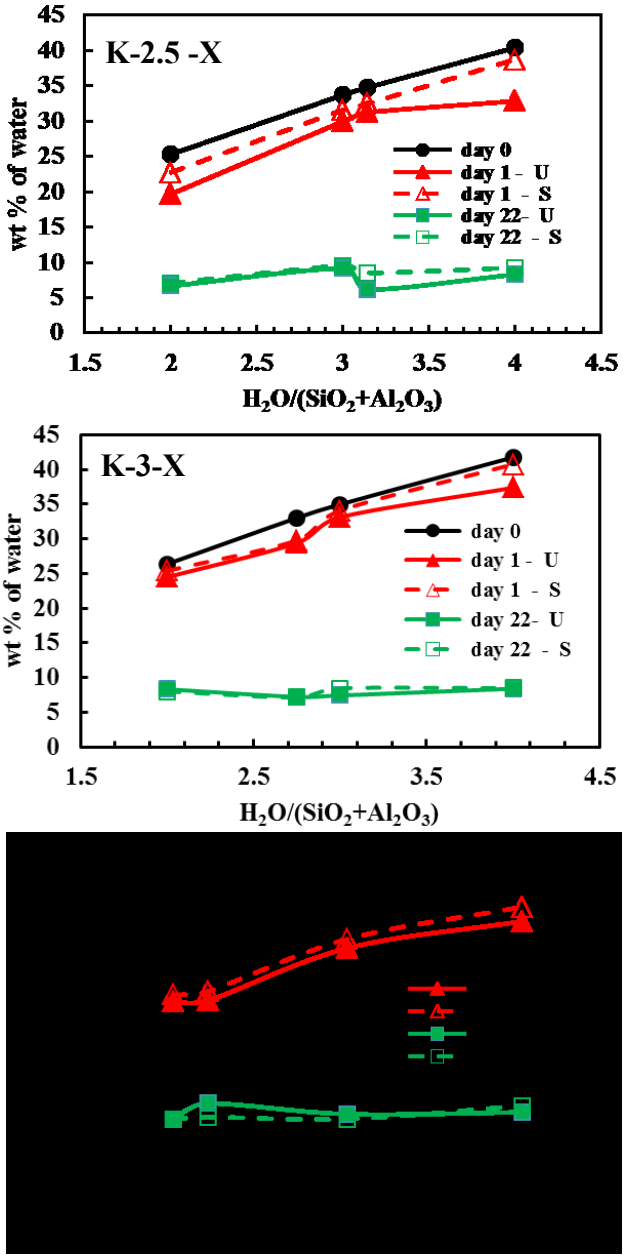

Figure 3.4 The change of wt% of water remaining in K-GPs with SiO_2/Al_2O_3= 2.5- 4 during curing in unsealed (labeled as U) and sealed (labeled as S) molds as a function of initial water content, i.e. $H_2O/(SiO_2 + Al_2O_3)$ ratio. Day-0 denotes samples after mixing, day-1 after curing, and day-22 after aging for 22 days.

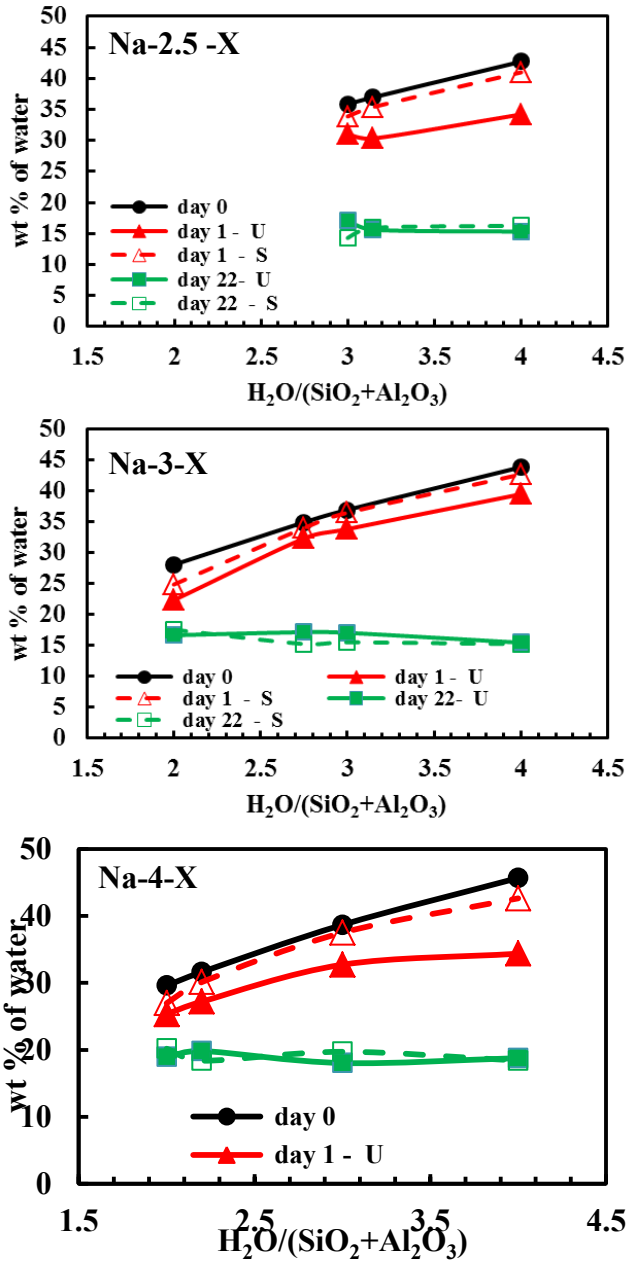

Figure 3.5 The change of wt% of water remaining in Na-GPs with SiO_2/Al_2O_3= 2.5- 4 during curing in unsealed (labeled as U) and sealed (labeled as S) molds as a function of initial water content, i.e. $H_2O/(SiO_2 + Al_2O_3)$ ratio. Day-0 denotes samples after mixing, day-1 after curing, and day-22 after aging for 21 days.

The density and open porosity determined using alcohol immersion method are plotted as a function of $H_2O/(SiO_2 + Al_2O_3)$ ratios in Figures 3.6 and 3.7, respectively, for K- and Na-activated GPs with different SiO_2/Al_2O_3 ratios. Apparent density, Figure 3.6, of both K- and Na-activated GPs decreases with increasing $H_2O/(Al_2O_3+SiO_2)$ molar ratios, and are independent of the SiO_2/Al_2O_3 ratios. However, the apparent density of Na-activated GPs is slightly higher than that of K-activated ones, especially at lower $H_2O/(SiO_2 + Al_2O_3)$ ratios. Not surprisingly, the percent of open porosity (Figure 3.7) increases with increasing $H_2O/(SiO_2 + Al_2O_3)$ ratios and also seems to be independent of SiO_2/Al_2O_3 molar ratios. At lower $H_2O/(SiO_2 + Al_2O_3)$ ratios, K-activated GPs show more open porosity than Na-activated ones.

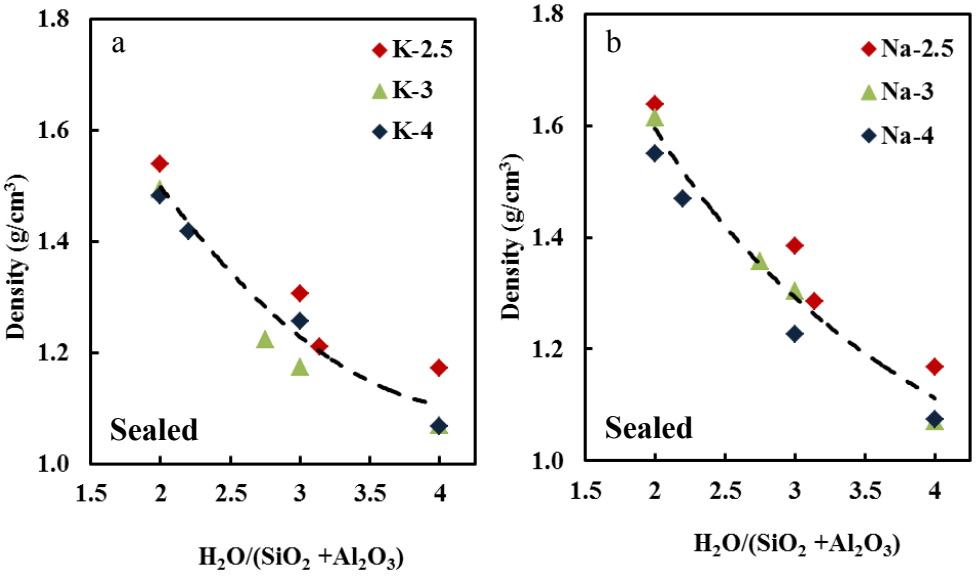

Figure 3.6 Density of (a) K- and (b) Na-GPs with SiO_2/Al_2O_3 =2.5- 4 as a function of initial water content, i.e. $H_2O/(SiO_2 +Al_2O_3)$ after curing and aging for 21 days

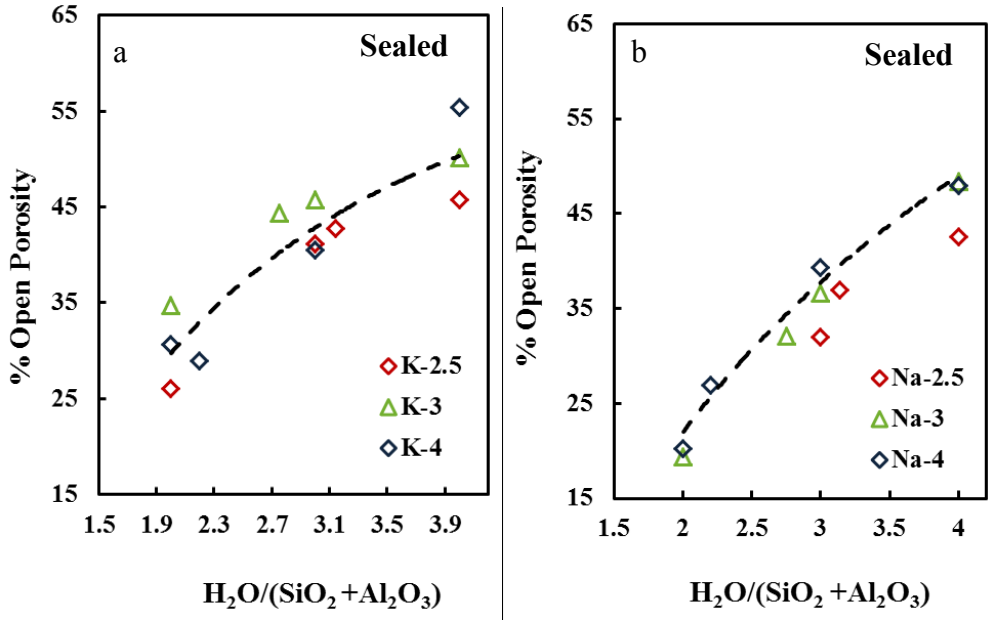

Figure 3.7 % Open porosity of (a) K- and (b) Na-GPs with SiO_2/Al_2O_3 =2.5- 4 as a function of initial water content, i.e. $H_2O/(SiO_2 + Al_2O_3)$ after curing and aging for 21 days.

Comparatively, there is an insignificant variation in density and open porosity between covered and uncovered samples (not shown here) for all values of *X*. Selected, but typical SEM images of K- and Na-activated GPs shown in Figures 3.8 and 3.9 respectively are in the good agreement with the results of density and open porosity measurements. Microstructure of the cured and aged GP looks less homogeneous and dense as the $H_2O/(SiO_2 + Al_2O_3)$ ratios in GP samples increases, Figures 3.8 and 3.9.

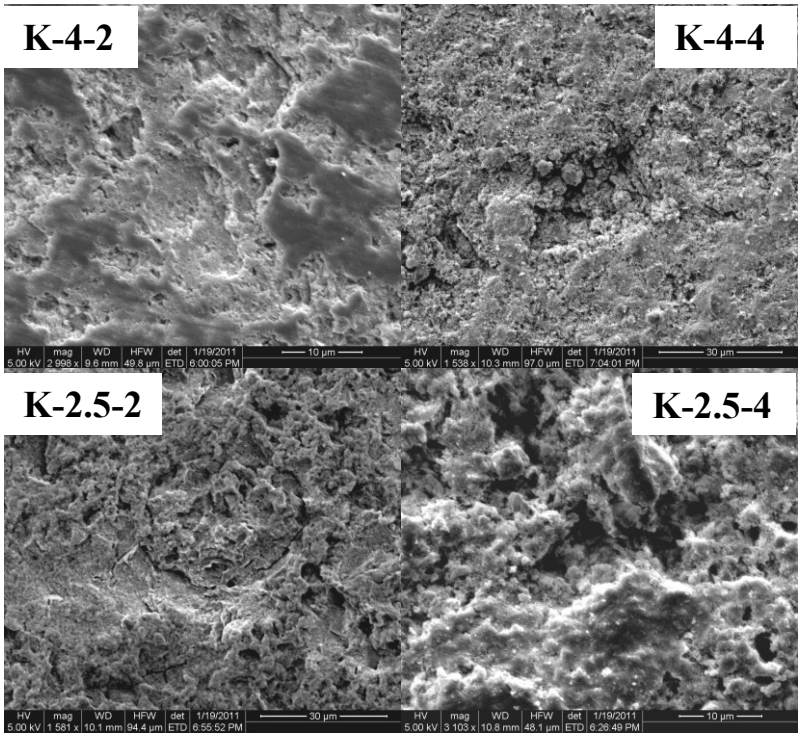

Figure 3.8 SEM micrographs of K-2.5-2, K-2.5-4, K-4-2 and K-4-4 geopolymer samples cured in sealed molds and aged for 21 days.

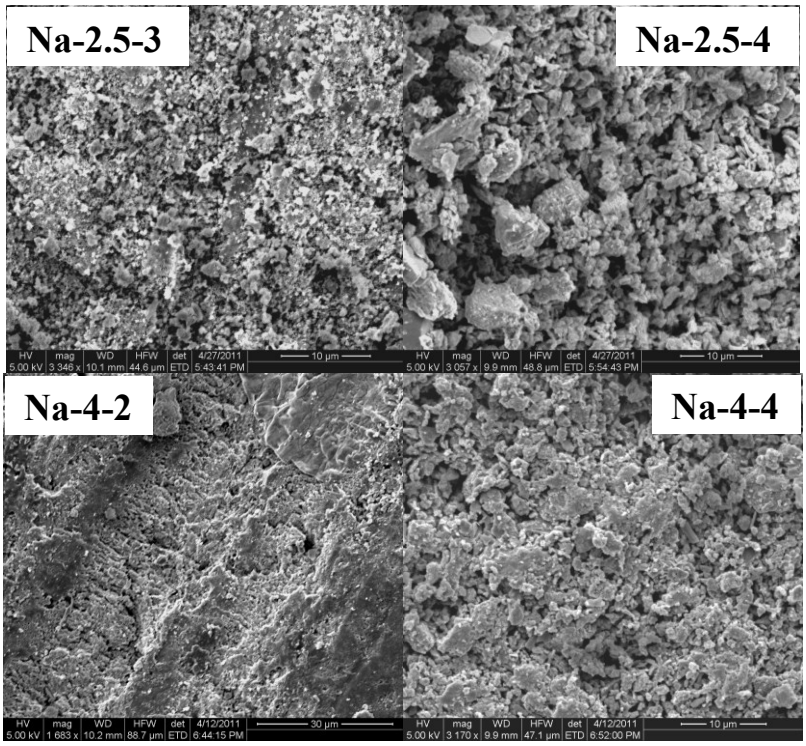

Figure 3.9 SEM micrographs of Na-2.5-3, Na-2.5-4, Na-4-2 and Na-4-4 geopolymer samples cured in sealed molds and aged for 21 days.

TGA results during heating from room temperature to 1000 °C for selected K- and Na- activated GPs with SiO_2/Al_2O_3 =2.5- 4 and $H_2O/(SiO_2 + Al_2O_3)$ = 2.2, 2.75 and 3.14 are summarized in Figure 3.10. As seen in the weight loss (Figures 3.10a and 3.10b) and especially in weight loss derivative (Figures 3.10c and 3.10d) vs. temperature plots, almost all weight loss due to water evaporation occurs at temperatures ≤ 200 ° C, and no weight loss was detected above ~ 300 ° C. In addition, results in Figure 3.10 indicate that weight loss is more significant in samples with higher SiO_2/Al_2O_3 ratios, and in Na-activated GPs when compared to K-activated ones.

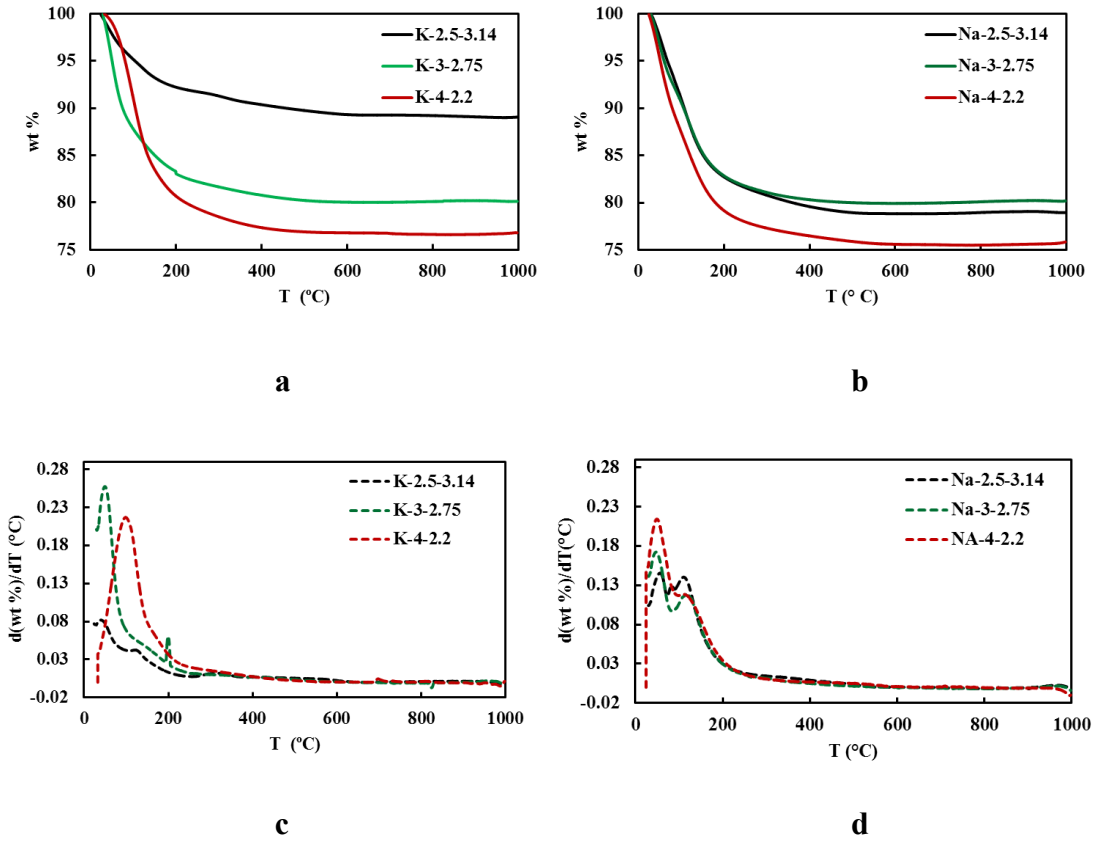

Figure 3.10 The weight loss as a function of temperature for (a) K- and (b) Na-based geopolymers determined by TGA. Figure (c) and d) show derivative of weight loss with respect to temperature for K- and Na-activated samples, respectively. Water ratio for all samples correspond to H_2O/Al_2O_3 =11.

Figure 3.11 shows the percent dimensional changes with respect to temperature for selected aged K- and Na- activated GPs with SiO_2/Al_2O_3 =2.5- 4 and $H_2O/(SiO_2 + Al_2O_3)$ = 2.2, 2.75 and 3.144. All the samples show no dimensional changes below 200 °C, and expansion of less than 0.02 % expansion at ~250 °C. Above 250 °C, GP samples show additional contractions that are small, and do not exceed 0.16 % even after exposure at 1000 ^{o}C. The increase in dimensional changes of Na-activated samples at

temperatures above 800 ^{o}C is most likely because of their crystallization[19, 73] and cracking.

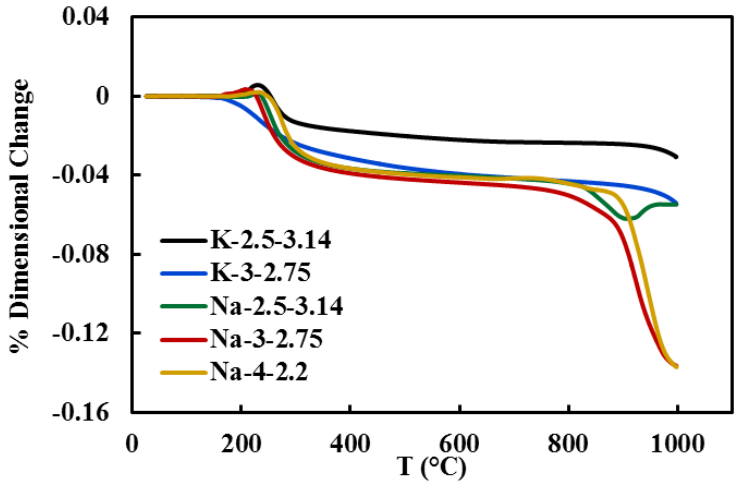

Figure 3.11 TMA results for selected K- and Na- activated geopolymers with H_2O/Al_2O_3 = 11, indicating less than 0.16% dimensional changes.

3.4 Discussion

This investigation shows conclusively that: (a) regardless of the amount of water and SiO_2/Al_2O_3 ratios used to process samples, all K- and Na-activated samples have almost the same amount of residual water after aging for 21 days at ambient conditions. (b) the amount of water used in processing GPs is the most dominant factor affecting their density and open porosity after curing and extended aging, while SiO_2/Al_2O_3 molar ratio does not play any significant role.

As shown in Figures 3.1 and 3.2, all samples prepared with $H_2O/(SiO_2 + Al_2O_3)$ ratio ranging from 2 to 4, corresponding to H_2O/Al_2O_3 = 7 - 20 (Table 3.1), and SiO_2/Al_2O_3 = 2.5- 4 shows typical structural characteristics of geopolymers even after aging for 21 days at ambient conditions; they are all XRD amorphous, with all Al being IV-coordinated [43]. The importance of this finding, in conjunction with the effect of water content on the density and porosity of the GPs (Figure 3.6 and 3.7), cannot be overestimated since it indicates that water can be used as one of the processing parameter to synthesize stable geopolymers with different structural properties, and thus mechanical and thermal properties [4, 68, 74, 75]. Results of the water loss measurements during curing and aging at ambient conditions summarized in Figures 3.3-3.6 and Table 3.1 clearly show that:

(a) most of the water is lost/evaporated during initial 7 days of aging; and

(b) regardless of the amount of water and SiO_2/Al_2O_3 ratios used to process samples, ~6 to ~10 wt% of all K-activated and ~15 to ~20 wt% of all Na-activated GP samples is residual water after aging for 21 days.

Most of the water that evaporates during aging is "free' water, as referred to by Perera et al.[31] or physically bonded water, as referred to by Davidovits[32], that exists in cured GPs as a thin nanoscale surface layer or water physically entrapped in intergranular sites. We have shown here, that most of the "free" water can evaporate from GP samples during extended aging at ambient temperatures, and not only during

additional heating up to 150 ^{o}C, as it has been previously shown in the literature [11, 19, 76].

The residual water after extended aging, which amount does not depend on initial $H_2O/(SiO_2 + Al_2O_3)$, is chemically bonded water, i.e. interstitial water most likely associated with activated cation [12]. Therefore, the lager amount of the water remains in the Na-activated samples when compared to K-activated one, since Na^+ anion is smaller and more electropositive than K^+ anion, thus keeping larger amount of chemically bonded water entrapped in GP skeletal pores. It is worth nothing here that additional aging of Na-activated samples for 145 days at ambient conditions (not shown) did not result in any significant water loss when compared to samples aged for 21 days. In addition, amount of residual water increases slightly with increasing SiO_2/Al_2O_3, as seen in Figures 3.4, 3.5 and 3.10. This can be explained by higher water affinity of (-SiO_2-) group when compared to (-AlO_2-) [77]. During heating of aged GP samples, all residual chemically bonded water is gone at 200 °C, as shown in Figure 3.10. This is in good agreement with previously published findings [11, 12]. However, unlike in the case of previously published TGA data, no weight loss above 300 ^{o}C associated with dehydroxylation of OH was detected in this study. This suggests that extended aging not only results in evaporation of "free" water, but also in more complete polycondensation and formation of 3-D GP network without non-bridging hydroxyl groups remaining in the structure.

The deference between the wt% of residual (chemically bonded) water after aging determined by weight loss (Figures 3.5 and 3.6) and TGA measurements (Figure

3.10) needs to be discussed in more detail. While calculated residual water after aging for 21 days is 6-10 wt% for all K-activated and 15 -20 wt% of all Na-activated GP samples, TGA results show water loss of 10-22 wt% for K- and 19-25 wt% for Na-activated samples. The reason for this discrepancy is multifold. First, the wt% of the residual water during aging was calculated assuming that only water present in the structure was the water that is initially added to the mixture, as shown in Equation 3 1. However, due to incomplete dehydroxylation of MK during calcining, it usually contains remaining OH groups that release water during polycondensation into -Si-O-Si- or -Si-O-Al- linkages. Second, KOH, NaOH and SiO_2 are all hydrophobic, and thus actual initial water content in the prepared GPs could be slightly here than reported in Table 3.1. Third, GPs can absorbs a large quantity of water [63], thus some of the moisture from air was most likely absorbed by samples after their aging, but before TGA testing.

The result shown in this study with the most important practical implication is certainly that on the effect of the initial water content on the density and open porosity of GP samples. Figures 3.6 and 3.7 clearly show that density and open porosity of GPs is vastly affected by $H_2O/(SiO_2 + Al_2O_3)$, not by Si_2O/Al_2O_3 ratios. Although densities and porosities of the GPs may be affected by differences in geopolymerization mechanism due to different H_2O/Al_2O_3 and Si_2O/Al_2O_3 ratios, as suggested in the literature [4, 63, 68, 76], results shown here indicate that amount of “free” water, entrapped in intergranular space, have the dominant effect on density and porosity of GPs. Since the amount of the interstitial chemically bonded water in the GP’s skeletal cavities is the same after extended aging and independent of the initial water content, addition of more

water results in lager amount of “free” water that stays entrapped in intergranular space after geopolymerization and evaporates during extended aging, leaving larger amount of intergranular pores in the structure. SEM images in Figures 3.8 and 3.9 confirm this conclusion. While microstructure of the samples prepared with the smaller amount of water is homogenous and dense, the microstructures of the samples prepared with large amount of water consist of loosely packed GP precipitates with large intergranular pores. In addition, observed differences in density and porosity between K- and Na-activated GP samples, Figures 3.6 and 3.7, can be explained by different amounts of residual chemically bonded water present in those samples after aging for 21 days. For the reasons discussed above, Na-activated GP samples contain larger amount of residual chemically boded water that is entrapped in interstitial sites after aging, and thus those samples appear to have higher apparent densities and lower amount of open porosity when compared to K-activated GP samples.

Last but not the least, the TMA results in Figure 3.11 suggests that the fully developed GP matrix during extended aging with most of the “free” water evaporated is not susceptible to thermal shrinkage, regardless of their chemical composition, initial water content and porosity. These results are significantly different from shrinkage up to 20 % that was reported for samples tested after only 20 hour of curing [11, 19, 78, 79]. Such a large dimensional changes associated with water release during heating previously reported in literature can lead to intensive cracking of GPs, that in turn limits significantly their applications at elevated temperatures. However, results shown here

suggest that by simply removing the “free” water during extended aging, this problem can be solved for GPs with different initial water contents.

4. EFFECT OF WATER CONTENT USED IN PROCESSING GEOPOLYMERS ON THEIR THERMAL CONDUCTIVITY AND COMPRESSIVE STRENGTH

4.1 Literature Review

As discussed in more details in Section 2, it is believed that the governing factor controlling strength of GPs is SiO_2/Al_2O_3 molar ratio, and to a lesser degree, the metal cation used for their processing [9, 32]. Many studies have shown that increasing SiO_2/Al_2O_3 molar ratios to approximately 2 increases the compressive strength of GPs [4, 33, 68]. The reason for this observation is twofold. First, Si-O-Si bonds are stronger than Si-O-Al bonds and are believed to account for the increased strength with increasing Si content [4, 33]. Second, in most of those studies, as shown in Table 4.1, GPs with various SiO_2/Al_2O_3 ratios were prepared using constant or only slightly different H_2O/Al_2O_3 ratios. Therefore, a total liquid/solid ratio of initial solutions was lower for higher SiO_2/Al_2O_3 ratios, resulting in the higher densities of GPs, and thus higher mechanical strengths [4, 33, 68]. On the other hand, decrease in compressive strengths observed in some studies for GPs with $SiO_2/Al_2O_3>2$ is commonly attributed to the larger amount of unreacted material that was found in those samples, and possibly differences in GP 's microstructure and pores size distribution [4, 9, 33, 68].

Results from studies reporting on the compressive strengths of GPs summarized in Table 4.1 have yet another important implication - maximum compressive strengths

Table 4.1 Summary of the published compositions, processing parameters and maximum compressive strengths of metakaolin (MK) based GP. NS- not specified in the reference.

SiO_2/Al_2O_3 ratio	Alkali activator ratio	Water Ratio	MK calcination temperature (°C)	Curing temperature (°C) / curing time (hr) / Aging (days)	Maximum compressive strength, (MPa)	Reference
1.08 - 3	Na/Al=0.5 - 2	H_2O/SiO_2=2.8	750	75 /24 / 7	62 ±3	[34]
2.5 - 5	Na/Al=0.8 – 1.6	H_2O/Na_2O=13.6	750	40/ ≤72/ NS	~25	[32]
4	Na/Al=1.1	H_2O/Al_2O_3=11	NS	85/ 2/NS	74	[5]
2.5 - 3.8	Na/Al=0.7 - 1.2	H_2O/Al_2O_3=12-16	NS	85/2 / NS	48	[36]
2.5 - 4.3	Na/Al=1	H_2O/Na_2O=11	NS	40/20/ 7	~82	[9]
2.5 - 4.3	K/Al=1	H_2O/Na_2O=11	NS	40/20/ 7	~82	[9]
2.3 - 4	Na/Al=1	H_2O/Al_2O_3=11	NS	40/20/NS	~75	[4]
2	Na/Al=1	H_2O/Al_2O_3=9.4	750	60/24/10	70	[37]
2.5-5	Na/Al=1	H_2O/Al_2O_3=11-13	750	80/48/1	37	[68]
2.5-5	K/Al=1	H_2O/Al_2O_3=11-13	750	80/48/1	33	[68]

of geopolymers published in different studies vary in the wide range from <25 to 82 MPa. Even more, the compositions, i.e. SiO_2/Al_2O_3 and Na(or K)/Al ratios, of GPs having maximum compressive strength in those studies were quite different. Taking this into account, as well as the fact that samples tested in different studies were

prepared using different MK sources, and curing and aging conditions (Table 4.1), suggest that the strength of geopolymer is more likely a complex function of several variables affecting their microstructure and cannot be related only to their chemical composition. The additional evidence for this can be also found in several studies[9, 68] that show that strength of GPs develops over the extended curing and edging time.

Although, GPs have been considered as good refractory materials [78, 80, 81] for thermal coatings and insulators [79, 82, 83], surprisingly, a small number of studies discuss their thermal conductivity. Low thermal conductivities have been reported for GP foams. These type of GPs are reported to have thermal conductivities of 0.03 W/m·K [84], ≥0.036 W/m·K [85] and 0.16 W/m·K) [86]. Duxson et. al. [87] reported on thermal conductivities measured within a temperature range from 40 º C to 100 º C. under various relative humidifies (R.H.) They report a thermal conductivity of ~0.80 W/m·K ($2.3 \leq SiO_2/Al_2O_3 \leq 4.3$) for both K- and Na-based GPs in "as cured" conditions at 100% R.H. Samples tested at 45% R.H. have thermal conductivities of 0.38 W/m·K for both K- and Na-activated GPs with SiO_2/Al_2O_3 =2.3, and 0.55 W/m·K for Na-activated and 0.48 W/m·K K-activated GPs with SiO_2/Al_2O_3 =4.3. Although the thermal conductivities decreased with decreasing R.H., an increase was noted with increasing SiO_2/Al_2O_3 ratios. The decrease in thermal conductivity was attributed to reductions in specific heat from dehydration of the pores, which correlate to residual water previously reported [88].

The conflicting results briefly reviewed above suggests that processing-structure-properties relationship in GPs is still very elusive and more work is needed to

distinguish effect that different processing variable have on the microstructure and properties of GPs. In Section 3 [88] we have shown that amount of the residual water in GPs after ageing for 21 days in ambient conditions is independent of initial content of the water in activated solutions for GPs prepared with $SiO_2/Al_2O_3 = 2 – 4$, $H_2O/(SiO_2 + Al_2O_3) = 2.5 – 4$ and Na(or K)/Al=1. However, amount of excess or "free" water that evaporates during aging was shown to have dramatic effect on density and porosity of GPs. In Section 2, we also conclusively showed[88] that water/solid ration, not SiO_2/Al_2O_3 as previously reported in literature; plays dominant role in the density and open porosity. This finding, when put together in conjunction with results that indicate that density and porosity might have the most important effect on properties of GPs [4, 68], raises the question to what extent the water content in the initial activated solution affect mechanical and thermal properties of GPs. This is especially important because water is also often arbitrary added to activation solutions to enhance their workability [32, 34]. In this study a comprehensive characterization of aged and fully stabilized GPs with $H_2O/(SiO_2 +Al_2O_3)$=2-4, SiO_2/Al_2O_3=2.5-4 and K(or Na)/Al=1 where carried out to gain further insight in the effects of water and chemical composition on the thermal conductivity and compressive strength of metakaolin based geopolymers.

4.2 Experimental Methods

Geopolymer for this study were synthesized using the procedure similar to that previously described in Section 3.2.. Metakaolin, K and Na activators, and different $H_2O/(SiO_2 + Al_2O_3)$ and SiO_2/Al_2O_3 ratios. MetaMax ® (BASF catalysts LLC, NJ)

metakaolin with SiO_2/Al_2O_3=2.05, was selected among several different metakaolins as a model aluminosilicate source or precursor because it contains relatively low amount of impurities in this metakaolin (~3.2 wt %). A potassium hydroxide (KOH Mallinckrodt Chemicals, NJ) and sodium hydroxide (NaOH Mallinckrodt Chemicals, NJ) palettes were used to prepare aqueous activating solutions. Amorphous fumed SiO_2 (Alfa Aesar, MA) having surface area of 350-410 m^2/g is used to prepare alkaline silicate solutions to alter SiO_2/Al_2O_3 ratios in final products.

Alkaline solutions were prepared by adding KOH or NaOH to deionized water. The ratio of K/Al and Na/Al was kept with a stoichiometric value of 1 to balance the negatively charged IV-coordinated $[-AlO_2-]^-$ in the cured GPs with the positively charged cations namely Na^+ and K^+. Various amounts of SiO_2 was added to KOH or NaOH solutions then sealed and placed on magnetic stirrer for 24 hours. Metakaolin was added to the prepared alkaline silicate solutions and mixed in a vacuum mixer for various times depending on composition until a homogenous mixture is obtained. Table 3.1 shows the different molar ratios used to synthesize samples. The labeling protocol of the samples is the same as in Section 3, i.e. as follows: *M-SiO_2/Al_2O_3-X* where *M* is the alkaline metal (K or Na), SiO_2/Al_2O_3 is the SiO_2/Al_2O_3 molar ratio and *X* is the $H_2O/(SiO_2+Al_2O_3)$ molar ratio. The samples had resulting molar ratios SiO_2/Al_2O_3 = 2.5, 3 and 4 and $H_2O/(Al_2O_3+SiO_2)$ = 2, 3 and 4. In addition, samples with $H_2O/(Al_2O_3+SiO_2)$ ratios of 2.2, 2.75 and 3.14 were prepared, since they correspond to the H_2O/Al_2O_3=11 that is commonly used to prepare GPs with SiO_2/Al_2O_3 = 2.5, 3 and 4, respectively. It is worth noting here, that Na-activated samples with samples low

liquid to solid ratio, namely samples Na-2.5-2 and Na-3-2 could not be prepared in large quantity required for mechanical testing because very fast curing and thickening prevented good mixing and homogenization of those activating solutions.

The homogenous mixtures were then poured into cylindrical plastic molds 25.4 mm in diameter and 25.4 mm high for compression testing and 38.1 mm in diameter and 25.4 mm high for thermal conductivity measurements. The individual molds were sealed with a thin plastic foil, placed in the sealed container and in cured oven at 80 ºC for 24 hours. Samples were additionally aged in the molds under sealed conditions for 7 days at ambient temperature. The samples were then removed from the molds and to base surfaces were made flat and parallel for thermal and mechanical testing using a send paper. Furthermore, the samples were dried for 3 additional days at ambient conditions before testing.

Density and open porosity of samples were determined using alcohol immersion technique according to the ASTM Standard C20-00[72]. After recording dry weight of the samples, $W_{dry,}$ samples were submerged in 200 proof ethanol with known density; $\rho_{ethanol}$ sealed in desiccator, and kept in vacuum for 5 minutes. The apparent mass of the sample was measured by recording the weight of a suspended wire, W_{wire}, submerged in the ethanol and then recording the weight with the sample on the wire, W_{susp}. The sample was then removed from the ethanol. Excess ethanol was removed by patting the samples dry for 60 seconds. The weight was recorded again as W_{wet}. These measurements were used to determine the bulk density and % open porosity as follows:

$$Bulk\ Density = W_{dry} \times \frac{\rho_{ethanol}}{W_{wet} - W_{susp} + W_{wire}} \quad \text{..... (4.1)}$$

$$\%\ Open\ Porosity = \frac{(W_{wet} - W_{dry}) \times 100}{W_{wet} - W_{susp} + W_{wire}} \quad \text{.....(4.2)}$$

Thermal Constant Analyzer (Hot Disk TPS 2500S, Thermal Test Inc.) was used to determine the thermal conductivity of geopolymers at near room temperature. Polished samples had dimensions 25.4 mm height and 38.1 mm in diameter. Two samples were vertically stacked with a kapton sensor placed in between the two stacked samples. The sensor is a double spiral nickel coil in a polyimide kapton coating. Each sample was tested 3 times and an average value calculated.

The 810 Material Universal Testing Machine (MTS Corporation, MN), was used carry on compressive strength measurements. Minimum 12 samples of each composition where loaded until failure. The compressive strength in this study was calculated by dividing the loads at which the first cracking appears with cross section area of the sample. It is worth noting here that load at which was first cracking appeared was in many cases below maximum load on load-displacement curves recorded during compressive testing. Since GP are brittle solids with wide distribution of strength. Weibull statistic (probability of survival vs. strength) was used to analyze results and determine the characteristic compressive strength, σ_o, and Weibull modulus, m . The σ_o and m were determined from –lnln(1/S) vs. ln σ plots, where S and σ are probability of survival and compressive strength of n-th sample, respectively, using procedure described elsewhere [41].

4.3 Results

The results of XRD examination and ^{27}Al MAS NMR (not shown here) of fully cured and aged GPs resulted in completely XRD amorphous structures with all Al being IV-coordinated. More detailed structural and microstructural analysis of GP samples prepared with $H_2O/(SiO_2 + Al_2O_3)$=2-4, SiO_2/Al_2O_3=2.5-4 and K(or Na)/Al=1 can be found in Section 3 [88].

The density and open porosity of examined GP samples determined using alcohol immersion method are plotted as a function of $H_2O/(SiO_2 + Al_2O_3)$ summarized in Figure 4.1, respectively, for K- and Na-activated GPs with different SiO_2/Al_2O_3 ratios. For both K- and Na-activated GPs, apparent density decreases and vol% of open porosity increases with increasing $H_2O/(Al_2O_3+SiO_2)$ molar ratios, as previously shown in Section 3 [88]. In addition, observed differences in density and porosity between K- and Na-activated GP samples, Figure 4.1, has been previously explained by different amounts of residual chemically bonded water present in those samples after aging[88]. It has been shown that, Na-activated GP samples contain larger amount of residual chemically boded water that is entrapped in interstitial sites even after extended aging, and thus, those samples appear to have higher apparent densities and lower amount of open porosity when compared to K-activated GP samples [88].

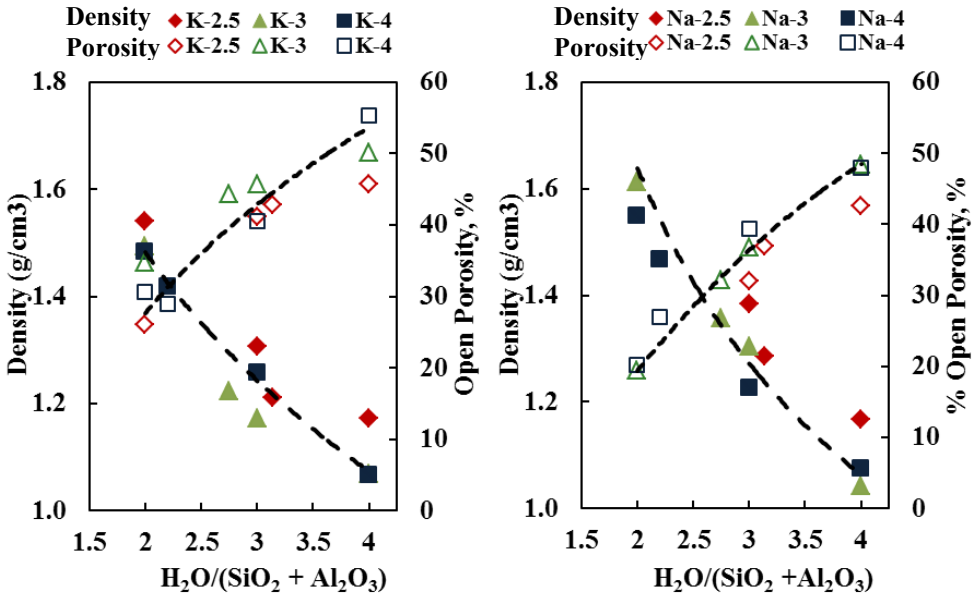

Figure 4.1 Density and open porosity as a funtion of $H_2O/(SiO_2 + Al_2O_3)$ for K- and Na-activated geopolymers.

Thermal conductivities of both K- and Na-activated GP samples determined by Thermal Constant Analyzer were plotted in Figure 4.2 as a function of $H_2O/(SiO_2 + Al_2O_3)$. The results conclusively show that the thermal conductivity decreases from ~0.35 W/m·K to ~0.17 W/m·K for K-activated GPs, and from ~0.43 W/m·K to ~0.20 W/m·K for Na-activated ones, as $H_2O/(SiO_2 + Al_2O_3)$ increases from 2-4. More importantly, results shown in Figure 4.2 suggest that thermal conductivity is independent on SiO_2/Al_2O_3 ratio. Moreover, Figure 4.2 shows that Na-activated GPs have a slightly higher thermal conductivity than Na-activated ones. This differences in thermal conductivity is more significant at low $H_2O/(SiO_2 + Al_2O_3)$ molar ratios.

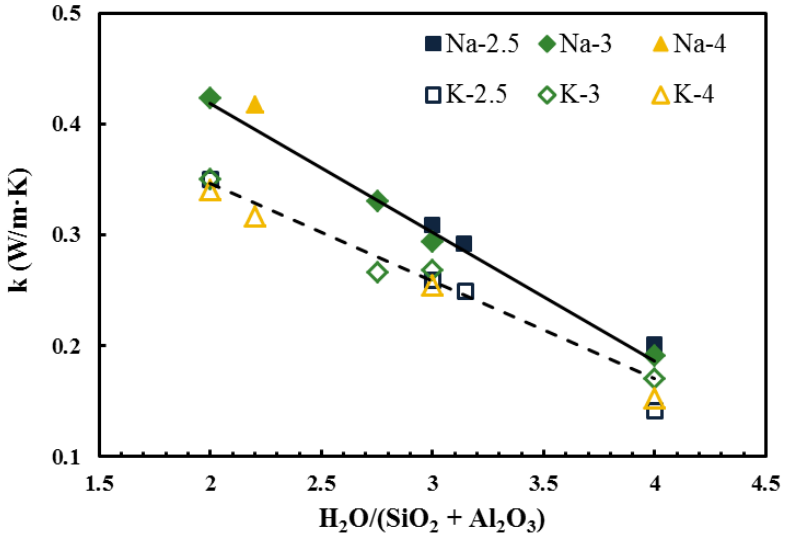

Figure 4.2 Thermal conductivities of K-(dashed line) and Na-(solid line) activated GPs versus $H_2O/(SiO_2 + Al_2O_3)$ molar ratios for different SiO_2/Al_2O_3 ratios.

Selected but typical Weibull plots, i.e. –lnln(1/*S*) vs. ln σ plots, are illustrated in Figure 4.3 for K-activated GPs with $SiO_2/Al_2O_3 = 4$ and $H_2O/(SiO_2 + Al_2O_3) = 2$, 2.2, 3 and 4. The results of mechanical testing in compression are summarized in Table 4.2. Table 1 lists average compressive strengths and standard deviations, as well as results of the Weibull statistical analysis (characteristic strength and Weibull modulus) for both K- and Na-activated geopolymers. Last column in Table 4.2 contains densities of corresponding samples as plotted in Figure 4.1 for easy comparison

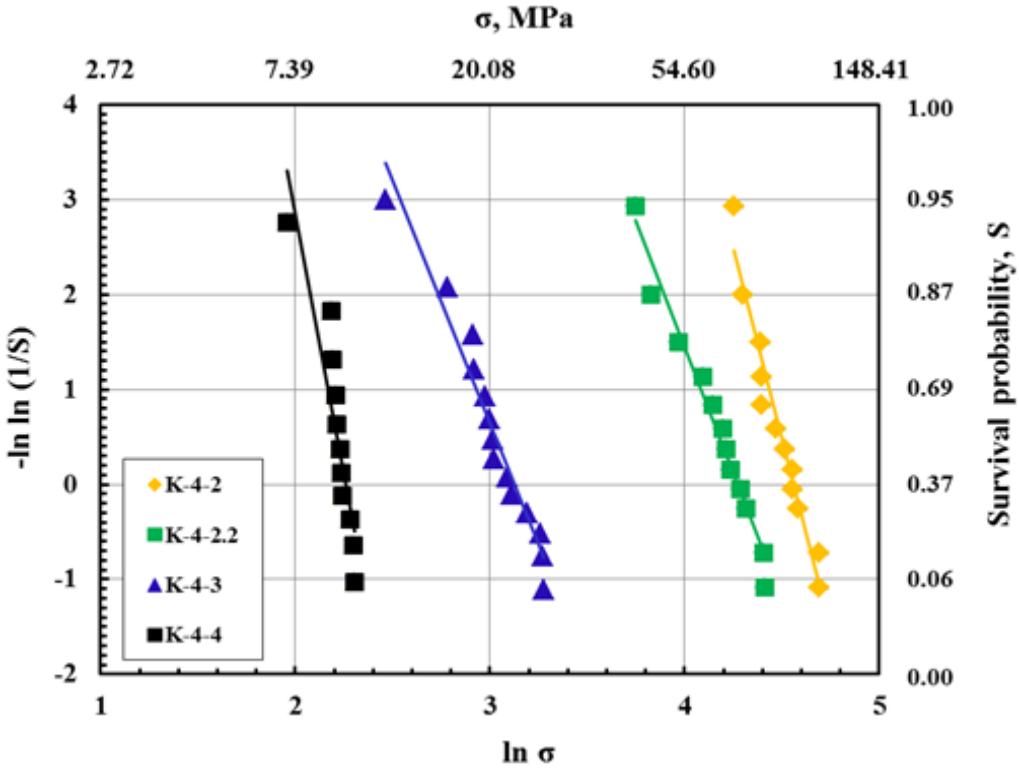

Figure 4.3 Selected, but typical Weibull plots for K-activated GP samples with SiO_2/Al_2O_3 = 4 and $H_2O/(SiO_2/Al_2O_3)$ = 2, 2.2, 3 and 4.

Table 4.2 Average strengths and results of the Weibull statistical analysis for both K- and Na-activated geopolymers. Last column contains densities of corresponding samples as plotted in Figure 4.1.

Activator	Sample	Average ± Standard Deviation, (MPa)	Weibull Strength (MPa)	Weibull Modulus	Density (g/cm^3)
Potassium	K-2.5-2	45.26 ± 4.50	47.11	8.14	1.54
	K-2.5-3	23.15 ± 4.46	25.19	5.11	1.31
	K-2.5-3.14	21.94 ± 1.96	22.56	10.52	1.21
	K-2.5-4	10.28 ± 2.23	11.22	4.74	1.17
	K-3-2	57.76 ± 8.52	61.24	6.58	1.49
	K-3-2.75	36.36 ± 12.91	40.85	3.00	1.22
	K-3-3	24.14 ± 3.61	28.33	4.04	1.17
	K-3-4	15.91 ± 1.84	17.38	6.73	1.07
	K-4-2	89.26 ± 12.51	95.80	7.98	1.48
	K-4-2.2	64.94 ± 12.90	71.49	5.31	1.42
	k-4-3	20.96 ± 4.05	22.75	5.11	1.26
	K-4-4	9.26 ± 0.86	9.60	10.97	1.07

Table 4.2 continued.

Activator	Sample	Average ± Standard Deviation, (MPa)	Weibull Strength (MPa)	Weibull Modulus	Density (g/cm^3)
Sodium	Na-2.5-2	-	-	-	-
	Na-2.5-3	45.16 ± 3.16	46.66	14.80	1.38
	Na-2.5-3.144	40.19 ± 3.18	41.64	13.56	1.29
	Na-2.5-4	13.54 ± 1.97	14.38	7.55	1.17
	Na-3-2	-	-	-	-
	Na-3-2.75	41.47 ± 4.68	43.38	7.84	1.36
	Na-3-3	37.68 ± 6.08	40.36	6.43	1.30
	Na-3-4	23.57 ± 2.75	23.57	10.96	1.07
	Na-4-2	74.64 ± 13.80	80.48	5.65	1.55
	Na-4-2.2	63.06 ± 7.88	66.08	8.63	1.47
	Na-4-3	29.16 ± 4.32	29.78	5.40	1.23
	Na-4-4	6.03 ± 1.01	6.55	6.11	1.07

The characteristic Weibull strengths plotted as a function of $H_2O/(SiO_2 + Al_2O_3)$ molar ratios in Figure 4.4 clearly show that compressive strength decreases significantly with increasing $H_2O/(SiO_2 + Al_2O_3)$ molar ratio for both K- and Na-activated samples. For $H_2O/(SiO_2 + Al_2O_3)$ above approximately 2.75, SiO_2/Al_2O_3 seems to have a little effect on compressive strength of both Na- and K-activated GPs. This conclusion is especially true if we take into account a very broad distribution of compressive strengths reported here with large standard deviation and relatively low Weibull moduli, Table 4.1. For $H_2O/(SiO_2 + Al_2O_3)$ ratio below approximately 2.75, SiO_2/Al_2O_3 have

significant effect on the compressive strength of K-activated GPs, with strengths going up as SiO_2/Al_2O_3 increases, Figure 4.4 . Unfortunately, the same occlusion cannot be made for Na-activated samples, since they could not be processed with lowest $H_2O/(SiO_2 + Al_2O_3)$ ratio for SiO_2/Al_2O_3 of 2.5 and 3. When comparing strengths of Na- and K-activated GPs with SiO_2/Al_2O_3=4 in Figure 4.4, it is clear that K-activated samples are stronger at all $H_2O/(SiO_2 + Al_2O_3)$ ratios. However, it cannot be derived for samples prepared with SiO_2/Al_2O_3 ratios of 2.5 and 3, especially at higher $H_2O/(SiO_2 + Al_2O_3)$ ratios.

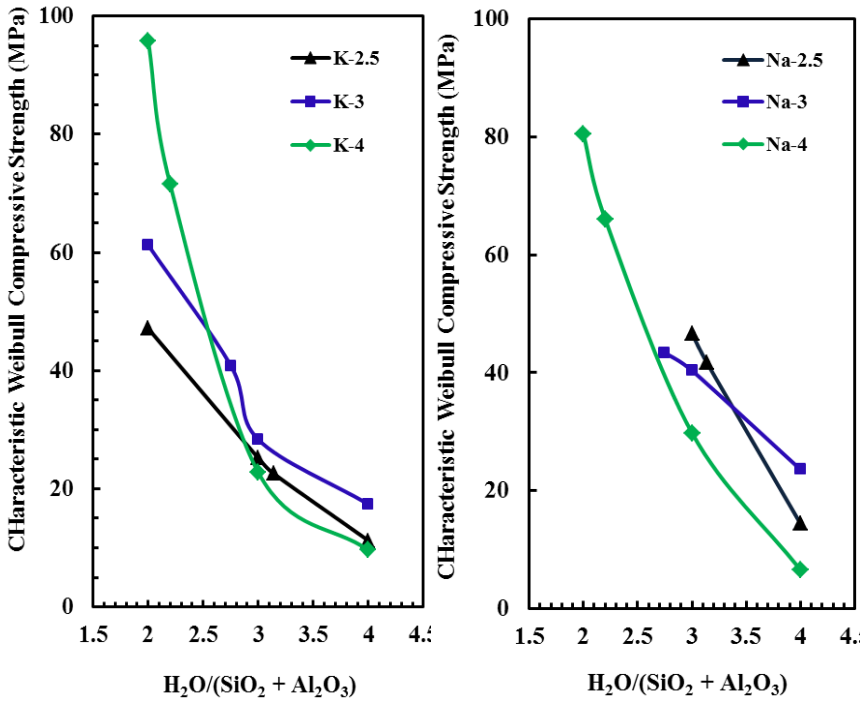

Figure 4.4 Characteristic Weibull compressive strength of K- and Na-activated GPs with different SiO_2/Al_2O_3 ratios as a function $H_2O/(SiO_2/Al_2O_3)$ molar ratios.

4.4 Discussion

The results presented in this section clearly show that amount of water used in processing GPs is: (a) the most dominant factor affecting their thermal conductivity, and (b) is crucial, but not the only factor influencing compressive strengths of GPs. When these findings are put in conjunction with our results that demonstrate a strong effect of water content on density and open porosity of GPs shown in Figure 4.1, we can conclude that it is porosity of GPs that plays crucial role in thermal and mechanical behavior of GPs, rather than water ratio per se.

Previously published results clearly showed that[88], regardless of the amount of water and SiO_2/Al_2O_3 ratios used to process samples, most of the "free" or excess water is lost/evaporated during initial 7 days of aging. Furthermore, only ~6 to ~10 wt% of all K-activated and ~15 to ~20 wt% of all Na-activated GP samples is residual or chemically bonded water after extended aging. Since the amount of the residual or chemically bonded water in the GP's skeletal cavities is the same after extended aging and is independent of the initial water content, the addition of more water during processing results in lager amount of "free" water. This additional water stays entrapped in intergranular space after geopolymerization and evaporates during extended aging, leaving larger amount of intergranular pores in the structure.

As shown in Figure 4.2, for GPs prepared with $H_2O/(SiO_2 + Al_2O_3)$ ratio ranging from 2 to 4, corresponding to H_2O/Al_2O_3 = 7 - 20 (Table 3.1), and SiO_2/Al_2O_3 = 2.5- 4, thermal conductivity is almost exclusively determined by $H_2O/(SiO_2 + Al_2O_3)$ ratio in activated solutions, hence by porosity and density of the samples. This concussion is not

surprising, since GPs are highly porous structures, in which air entrapped in numerous pores and probably residual water effects thermal conductivity more than composition, i.e. the SiO_2/Al_2O_3 ratio of 3-D structural network. Additional indirect evidence that support this conclusion lays in the fact that Na-activated GPs have higher thermal conductivity than K-activated ones, especially at lower H_2O/Al_2O_3 ratios. As it can be seen in Figure 4.1, Na-activated GPs have higher density than K-activated ones for the reason that is discussed in more details elsewhere[88]; therefore, they have at the same time higher thermal conductivities.

Thermal conductivities reported here are in good agreement with previously published values by Duxson et. al[87] that range 0.38 W/m·K to 0.48 W/m·K for Na-activated GPs with SiO_2/Al_2O_3 =2.3-4.3 prepared with constant SiO_2/Al_2O_3 ratio and tested at 45% R.H., but significantly lower than ~0.80 W/m·K measured for as cured samples at 100% R.H. This also confirms that amount of the "free" water entrapped in the pores can affect significantly thermal conductivity of GP. Thus, to lower thermal conductivities, not only should GPs be processed with a high level of porosity, but also all "free" water should be removed from pores during extended aging or drying. Not surprisingly, thermal conductivity values reported here are significantly higher than those reported for highly porous GP foams[84, 85], once again, demonstrating the important effect of porosity on the thermal conductivity of GPs. More importantly, results from this study replotted in Figure 4.5 for samples with constant H_2O/Al_2O_3= 11 illustrate, that when samples are prepared keeping constant H_2O/Al_2O_3 ratios, but

varying only SiO_2/Al_2O_3 ratio, misleading conclusion [87] can be drawn that thermal conductivity of GPs increases with increasing SiO_2/Al_2O_3 ratio.

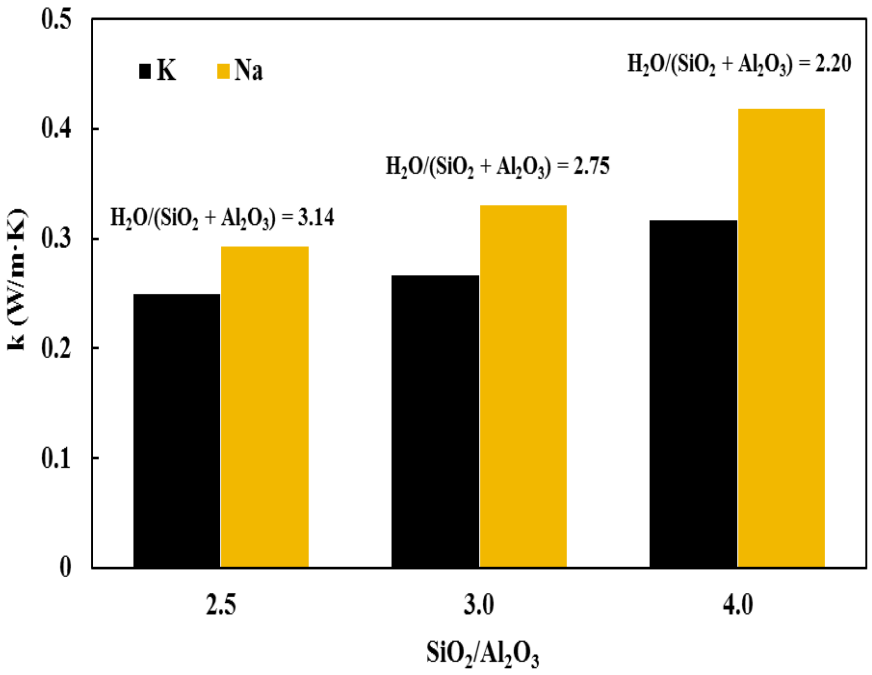

Figure 4.5 Thermal conductivity as a funtion of SiO_2/Al_2O_3 molar ratio for K- and Na-activated GPs with H_2O/Al_2O_3= 11 corresponding to $H_2O/(SiO_2 + Al_2O_3)$ = 3.14, 2.75 and 2.2 molar ratios.

As shown in Figure 4.4 and Table 4.2, relation between $H_2O/(SiO_2 + Al_2O_3)$ ratio in activating solutions, and hence density and porosity of GPs and their compressive strength is not so simple as in the case of thermal conductivity, suggesting that other structural factors also play important role in mechanical behavior of GP.

Although strength decreases strongly with increasing $H_2O/(SiO_2 + Al_2O_3)$ ratio and porosity of the samples as shown in Figure 4.4, it have only a dominant effect on the compressive strengths at higher $H_2O/(SiO_2 + Al_2O_3)$ ratios and hence higher porosity of the samples, Figure 4.4. However, in the case of higher density samples prepared with lower $H_2O/(SiO_2 + Al_2O_3)$ ratios, samples with higher SiO_2/Al_2O_3 ratios have at the same time the higher compressive strengths. Importance of this observation cannot be overestimated, since it suggests that strength of the GP skeleton becomes more important factor determining their overall strength, as the density of GPs increases. Thus, at higher densities, samples with greater SiO_2/Al_2O_3 ratios show higher compressive strengths because the higher GP strength samples contain a larger amount of Si-O-Si which are stronger than Si-O-Al bonds [4, 33].

Results present here however do not imply that strength of GPs is only the function of their porosity and SiO_2/Al_2O_3 ratios. Previously published results suggested that the amount of unreacted MK in GPs have important effect on compressive strengths of GP, since it is usually very weakly bonded to the GP matrix and can serve as an origin of the failure when GPs are loaded [56, 68]. On the other hand, the amount of unreacted MK is usually higher in samples in which dissolution and good mixing of activated solutions is prevented by low $H_2O/(SiO_2 + Al_2O_3)$ ratios, and high viscosity of activating solutions. Although more work is needed to fully understand why Na-activated GP have lower strength than K-activated ones with the same $H_2O/(SiO_2 + Al_2O_3)$ ratios, as it is demonstrated in Figure 4.4. The possible reason may lay in the higher amount of unreacted MK present in Na-activate GPs. Na-activated solutions have very high

viscosity, especially at low $H_2O/(SiO_2 + Al_2O_3)$ ratios due to fast polycondensation[14]. This prevents a good mixing and homogenization of Na-activated solutions leading to the higher amount of unreached MK. Even more, Na-activated solutions with $H_2O/(SiO_2 + Al_2O_3)$=2 and SiO_2/Al_2O_3=2.5 and 3 could not be mixed in this study, as mentioned earlier because of the high viscosity of the activated solutions.

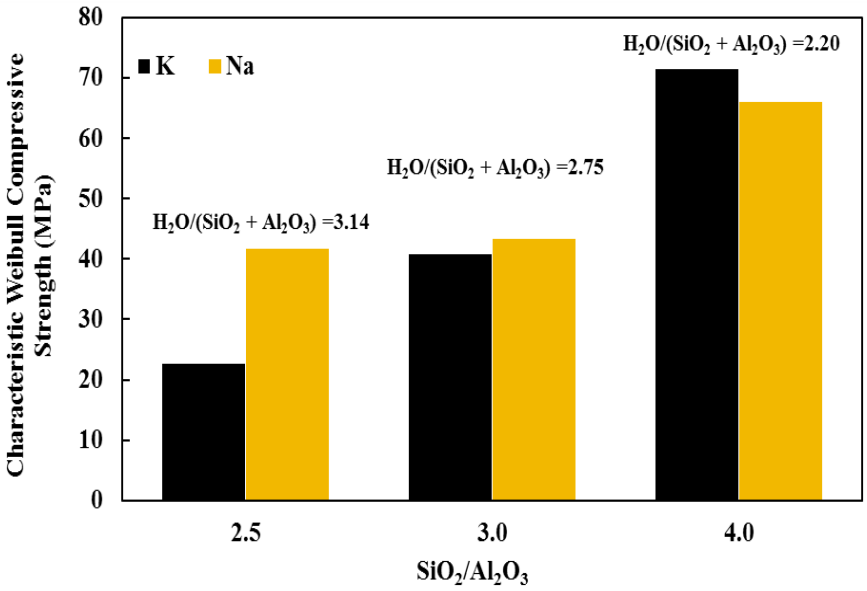

Figure 4.6 Characteristic Weibull compressive strength as a funtionof SiO_2/Al_2O_3 molar raitos for K- and Na-based GPs with H_2O/Al_2O_3= 11 corresponding to $H_2O/(SiO_2 + Al_2O_3)$ molar ratios shown above each column.

It is worth noting that maximum compressive strength of 95 MPa reported here for K-activated GPs with $H_2O/(SiO_2 + Al_2O_3)$=2 and SiO_2/Al_2O_3=4 is the highest ever

reported for unreinforced pure GPs prepared using MK and pure K or Na activators, Table 4.2. Also, results given in Figure 4.4 and Table 4.2 clearly show that strength of GPs with the same SiO_2/Al_2O_3 can vary from as low as 9 MPa to as high as 95 MPa, only by varying $H_2O/(SiO_2 + Al_2O_3)$ ratio from 4 to 2. This finding can shed more light on high variation of compressive strengths reported earlier for GPs in different studies, Table 4.1, since the samples in different studies were prepared using deferent amounts of water in activated solutions. More importantly, results from this study reported in Figure 4.6 for samples with constant H_2O/Al_2O_3= 11 illustrate, that when samples are prepared keeping constant H_2O/Al_2O_3 ratios, but varying only SiO_2/Al_2O_3 ratio, the might lead to misleading conclusion[4, 68] that SiO_2/Al_2O_3 ratio is the most important factor controlling compressive strengths of GPs.

The effect of aging or drying on the strength development in GPs needs to be discussed in more details here. Previously shown results in Section 2 results suggest that extended aging and drying of geopolymers at ambient conditions after their curing for usually 24 to 48 hours at elevated temperatures, not only results in evaporation of "free" water, but also in more complete polycondensation and formation of 3-D GP network without non-bridging hydroxyl groups remaining in the structure. When compressive strengths of aged samples reported here are compared to the strengths of the samples that were only cured for 24 and 48 hours [68], but prepared using the same procedure and precursors as in this study, Figure 4.7, noticeable increase in compressive strength can be observed after aging for 10 days. This is especially true in samples with higher SiO_2/Al_2O_3 ratios. The reason for this observation, thus, must lay in additional

polycondensation and development of stronger, more cross-linked GP skeleton during additional aging in ambient conditions.

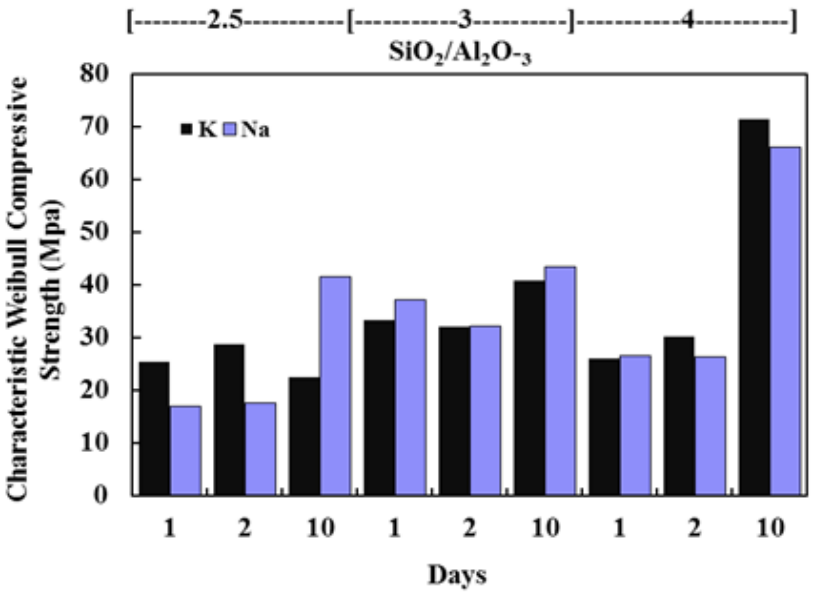

Figure 4.7: Comparison of characteristic Weibull compressive strengths for K- and Na-activated geopolymers with H2O/Al2O3= 11 (corresponding to H2O/(SiO2 +Al2O3) = 3.14, 2.75, and 2.2) for SiO2/(Al2O3) = 2.5, 3 and 4 after curing for 1 and 2 days [68, 74]

Last but not the least, the practical implications, of the results presented here, has to be discussed. If GPs are to be used as thermal insulators, their thermal conductivity could be easily lowered simply by preparing activated solutions with higher $H_2O/(SiO_2 + Al_2O_3)$ ratio. However, that price paid for decreasing thermal conductivity is a lower GPs compressive strength. An additional implication of the results presented here is that

common practice of adding water to activation solutions to enhance their workability and mixing [32, 34] can result in GPs with significantly lower thermal conductivities and mechanical strengths.

5. PROCESSING OF GEOPOLYMERS BY COPOLYMERIZATION OF SiO_2 AND $Al(OH)_3$ IN K-ACTIVATED AQUEOUS SOLUTIONS

5.1 Literature Review

Alkaline activated aluminosilicate inorganic polymers, commonly referred to as Geopolymers (GPs), are usually processed from natural aluminosilicate sources (clays), and industrial waste (furnace slag and fly ash) in highly alkaline aqueous solutions at temperatures ranging from 20 °C to 120 °C [13, 89]. The purest aluminosilicate precursor for GPs is metakaolin and metakaolinite that is produced by dehydroxylation of kaolin or kaolinite at 750 °C for up to 6 hours. During alkaline activation of the precursors, the OH^- ions acts as catalyst for simultaneous dissolution, hydrolysis and condensation of Si and Al species [6, 13, 14, 90] in aqueous solutions. The evolution of three major monomeric species during geopolymerization have been predicted using the Partial Charge Model (PCM): $[SiO_2(OH)_2]^{2-}$, $[SiO(OH)_3]^-$ and $[Al(OH)_4]^-$ [2, 3]. The monomeric species begin to polycondensate in alkaline aqueous solutions simultaneously with dissolution and hydrolysis. This reaction mechanism and condensation process is presented in Figure 5.1.

PCM studies also indicated rapid consumption and condensation of $[Al(OH)_4]^-$ species and showed that the dissolution and hydrolysis process cannot be separated from the condensation process[3]. After completed polycondensation during curing of activated aluminosilicate solutions, the final product is solid geopolymeric material with the structure that consist of 3-D framework of interchanging tetrahedral monomers of

SiO_4 and AlO_4 coupled by a shared oxygen atom [6, 13, 73]. As mentioned in previous sections, the negatively charged 4-coordinate Al monomers in the GP framework are balanced by positively charged alkaline metal ions providing structural neutrality in the final product [13]. Generally, Na^+, K^+, Ca^{2+} are frequently used as the metal activators. However others may also be used [1, 91]. Figure 1.1 shows a simplified model of the geopolymerization process described in literature and adapted here [13, 14].

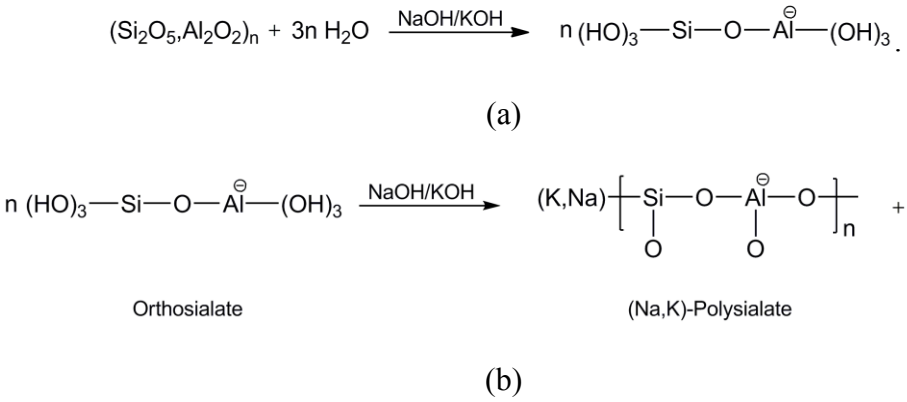

Figure 5.1: Reaction mechanism[1, 91]: (a) Dissolution and hydrolysis of Si and Al species and (b) Condensation polymerization

Geopolymers, made from kaolin clays, steel slag and fly-ash, are filled with impurities from precursor materials. The presence of the reactive or non-reactive impurities affects polymerization process, and thus hinders a clear understanding of the reaction mechanisms. More importantly, impurities commonly present in natural or industrial waste precursors affect structure and properties of the final geopolymer

products. Therefore, new versatile processing methods from chemically pure precursors are required to process geopolymers free of different impurities. Several attempts of processing GPs using pure source materials have been previously reported. Starting materials for synthesis of pure polymeric aluminosilicate included alumina powders and crystalline silica [92], aluminum nitrate in polyvinyl alcohol and colloidal silica [93], aluminum nitrate and tetraethoxysilane [94], and aluminum nitrate solution and potassium metasiicate [52]. Although these novel methods produced successfully geopolymeric materials, they usually required lengthy and complex preparation. In some cases, removal of precipitated byproducts such as metal nitrates was required to process pure GPs [52]. In other cases, high temperature treatments (800-1500 ^{o}C) had to be used [92, 93], thus retreating from low temperature processing as one of the most attractive features of tradition geopolymers.

$Al(OH)_3$ is good candidate precursor, together with SiO_2 [95] because of its good solubility in alkaline solutions at low temperature [96]. Under highly alkaline conditions, $Al(OH)_3$ (pH > 8) [96] readily provides the desired $Al(OH)_4^-$ monomeric species needed to synthesize a geopolymer product according to the following reaction:

$$Al(OH)_3 + OH^- \leftrightarrow Al(OH)_4^- \quad (5.1)$$

In a previous study [97], partial geopolymer synthesis was reported using different $Al(OH)_3$ sources and SiO_2 as a precursor material. The samples in that study were synthesized by dry-mixing the solid silica and aluminum sources, and their

subsequent dissolution and polycondensation in alkaline aqueous solutions. The most complete geopolymerization reactions were reported [97] for Si/Al ratios above ~1.4 and more reactive aluminas such as gibbsite and ρ-alumina with small particle size.

As mentioned above, the key mechanisms in geopolymer synthesis are the simultaneous dissolution, hydrolysis and condensation polymerization processes of precursor material. In this study, pure XRD amorphous SiO_2 and $Al(OH)_3$ have been selected as the precursor material. To further understand polymerization mechanisms of $Al(OH)_3$ and SiO_2 in alkaline solutions, three processing methods that result in copolymerization of Al and Si species have been investigated. An important aspect in achieving a geopolymer product is determined by the amount of available tetrahedrally coordinated Al species consumed by the Si species. A series of samples were prepared using KOH activation for two curing environments and various curing times. Material characterization was carried out using X-ray Diffraction (XRD) and Nuclear Magnetic Resonance (NMR).

5.2 Experimental Methods

Amorphous silicon(IV)oxide and $Al(OH)_3$ (Alfa Aesar, Ward Hill, MA) were used as a precursor material in this study, while activating alkaline aqueous solutions were prepared using KOH (Mallinckrodt Chemicals, NJ) and deionized water. Three mixing methods were carried to prepare samples.

In method A, potassium silicate solutions were prepared by dissolving first KOH, than SiO_2 in deionized water at a temperature of 50 °C. The dry $Al(OH)_3$ powder was

then added slowly to prepared potassium silicate solutions yielding SiO_2 /$Al(OH)_3$ ratios of 1 and 2, and liquid/solid, i.e. H_2O/(SiO_2 +$Al(OH)_3$) ratios of 7.5 and 10, respectively. Samples were mixed in a vacuum mixer, molded and kept sealed in the oven at 80°C until they cured and set satisfactorily (minimum 24 hours). For methods B and C, two alkaline solutions were prepared. In one solution, $Al(OH)_3$ powder was dissolved in previously prepared KOH solutions in deionized water, to produce potassium aluminate solution. The second solution was prepared by dissolving SiO_2 powder in the KOH aqueous solution to produce potassium silicate solution. In method B and C, the potassium aluminate solutions were mixed for 1 ½and 24 hours, respectively, on a magnetic stirrer at 50 °C. Potassium silicate solutions prepared at room temperature where then added to potassium aluminates solutions and mixed in a vacuum mixer. The samples were then cured at 80 °C in sealed molds until they set satisfactorily. In addition, a set of samples mixed using method C were cured in unsealed mold at room temperature in air conditions. The curing times varied from 24 to 96 hours depending on the time required to produce a solid product. Table 5.1 summarizes chemical compositions and processing conditions used in this study. Sample used in this study are labeled as XY where X is mixing method, namely A, B or C, and Y is SiO_2 /$Al(OH)_3$ ratio. Samples having the additional label RT denote samples cured at room temperature. In addition, to aluminosilicate activated solutions, pure potassium silicate and potassium aluminates activated solutions were also separately cured. Alkaline solutions of potassium aluminate and potassium silicates were prepared

as described above and poured into molds. The samples were then placed in the oven at 80 ^{o}C and cured until a monolithic structure was obtained.

Table 5.1 Chemical compositions and molar ratios of prepared samples. All samples were prepared with $KOH/Al(OH)_3$=1. AlQ_4/AlQ_6 ratio as determined by ^{27}Al NMR is given in the last column. RT denotes room temperature.

Sample Name	Mixing Method	$\frac{SiO_2}{Al(OH)_3}$	$\frac{H_2O}{Al(OH)_3}$	Curing			AlQ_4/AlQ_6
				Conditions	T (°C)	t (hrs)	
A2	A	2	30	Sealed	80	24	0.970
A1	A	1	13	Sealed	80	24	0.703
B2	B	2	30	Sealed	80	58	0.403
B1	B	1	13	Sealed	80	58	0.093
C2	C	2	30	Sealed	80	24/72	0.200/0.372
C1	C	1	13	Sealed	80	24/72	0.057/0.064
C2-RT	C	2	30	Air	25	24/72	0.043/ -
C1-RT	C	1	13	Air	25	48/96	0.028/ -

The processed samples were characterized using X-ray diffraction (XRD) and Nuclear Magnetic Resonance (NMR) since geopolymers demonstrate the following distinct structural characterisics [43, 98]:

(a) the material is X-ray amorphous with the halo at 2θ=27-30 ;

(b) the ^{27}Al MAS NMR spectrum indicates tetrahedral aluminum co-ordination.

XRD analysis was carried out using a Bruker-AXS D8 Advanced Bragg-Brentano X-ray Powder Diffractometer (Madison, WI). The samples were crushed into fine powder, and analyzed using a quartz ground disk (GM Associates, Inc., Oakland, CA) for XRD analysis. Scans were performed using a 0.0148 step size, 0.2 step time, and a 2θ range of 7-50. Nuclear Magnetic Resonance (NMR) was carried out on a WB Avance 400 Bruker spectrometer using a standard 4 mm NMR probe. Spinning rates were carried out between 3 and 5 KHz. The ^{27}Al chemical shift wre referred to an external standard and $[Al(H_2O)_6]^{3+}$. The amount of geoplymerised material in the cured sampels was estimated from the AlQ_4/AlQ_6 ratio, where AlQ_4 and AlQ_6 are fractions of IV and VI coodrinated Al, respectively, as determined in ^{27}Al MAS NMR spectrum.

5.3 Results

X-ray diffraction of precursor materials as well as potassium silicate and potassium aluminate are presented in Figure 5.2. $Al(OH)_3$ exhibited featureless x-ray amorphous spectrum, while SiO_2 shows typical amorphous halo at $2\theta = 17$ °[43]. The potassium silicate also exhibits an amorphous halo at $2\theta = 24°$ that corresponds to halo commonly seen XRD of glasses[43]. The potassium aluminate has a few small XRD amorphous halos at $2\theta \sim 13^{o}$ and $2\theta \sim 38^{o}$ that most likely correspond to amorphous potassium aluminates, and large peaks that corresponds to two potassium aluminates, namely bayerite (α-$Al(OH)_3$) and pseudo-boehmite[99, 100]

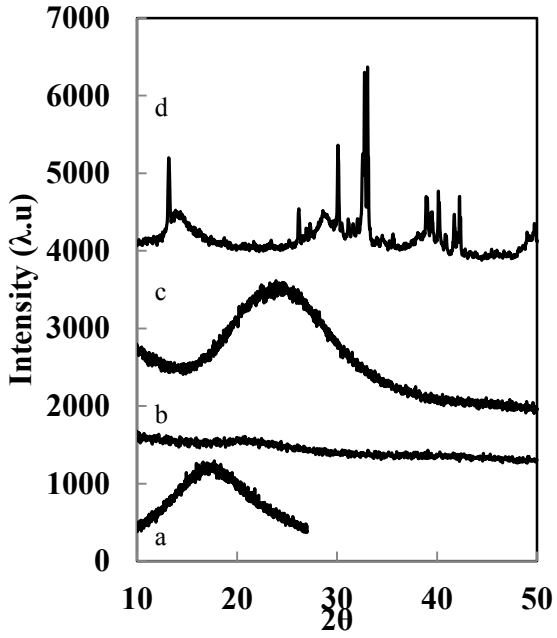

Figure 5.2 XRD of precursor material and prepared monomeric solutions for a) SiO_2 precursor, b) $Al(OH)_3$ precursor c) cured potassium silicate and d) cured potassium aluminate.

XRD spectra of prepared samples using method A and B are presented in Figure 5.3. For samples prepared using method A, X-ray amorphous halos are seen at 2θ around 28° for molar ratios SiO_2 /$Al(OH)_3$ 1 and 2 cured for 24 and 48 hours as typically seen in geopolymer. Similar results are seen for method B samples, however; it is worth noting that these samples required a longer curing time of 58 hours. For both set of samples prepared using method A and B, smaller amorphous halos can also observed at 2θ~13° and 2θ~38° in Figure 5.3, that are at the same position as halos present in potassium aluminate XRD spectra in Figure 5.2d.

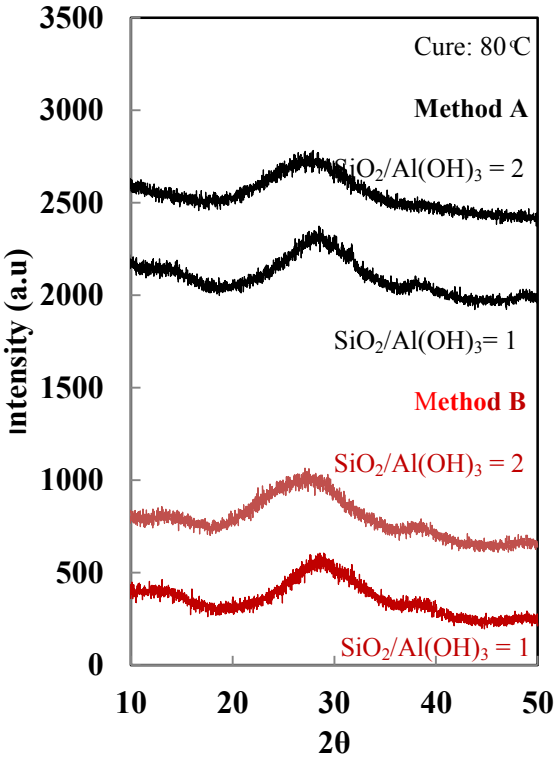

Figure 5.3 XRD of samples prepared using method A and B with $SiO_2/Al(OH)_3$= 1 and 2.

XRD spectra of the samples mixed using method C a cured at 80°C and room temperature are presented in Figures 5.4 and 5.5, respectively. Diffraction patterns for samples cured at 80°C in Figure 5.4 show similar amorphous halos at 2θ~13° and 2θ~38° as seen for the potassium aluminate sample in Figure 5.2, with a more dominant halos in samples with SiO_2 /$Al(OH)_3$=2. Samples with SiO_2 /$Al(OH)_3$=1 display two larger amorphous halos between 2θ of 20° and 30°. The halo at 2θ ~22° is similar to amorphous halos seen in unreacted metakaolin or glasses. The secondary halo at 2θ ~28° is usually indicative of structural changes often associated with geopolymerization[43].

XRD of the samples mixed using method C and cured at room temperature for only 24 or 48 hours, Figure 5.6, show only amorphous halos at 2θ~13° and 2θ~38° similar to those observed in potassium aluminate, Figure 5.2d, and two large amorphous halos between 2θ of 20° and 30°, similar to those in Figure 5.4. However, these samples show some crystalline features after extended curing of 72 and 96 hours for both SiO_2 /$Al(OH)_3$ ratios, Figure 5.5. Crystalline peaks are identified either as $Al(OH)_3$ precipitates (gibbsite), bayerite or pseudo-boehmite, as in the potassium aluminate samples cured for 4 days at 80°C shown Figure 5.3d.

The ^{27}Al NMR chemical shifts for the various samples are presented in the Figures 5.6-5.10. In Figure 5.6, chemical shift for pure $Al(OH)_3$ powders is seen at 0 ppm for 6-coordinated Al Q_6, while asterisks over smaller shifts on both sides of the main chemical shift are side bands resulting from Al quadrupoles. No presence of IV or V coordinated Al can be seen in Figure 5.6. Although Al Q_5 can be hidden in the side band with chemical shifts at 35 ppm, it is unlikely that Al Q_5 exists in $Al(OH)_3$ precursor.

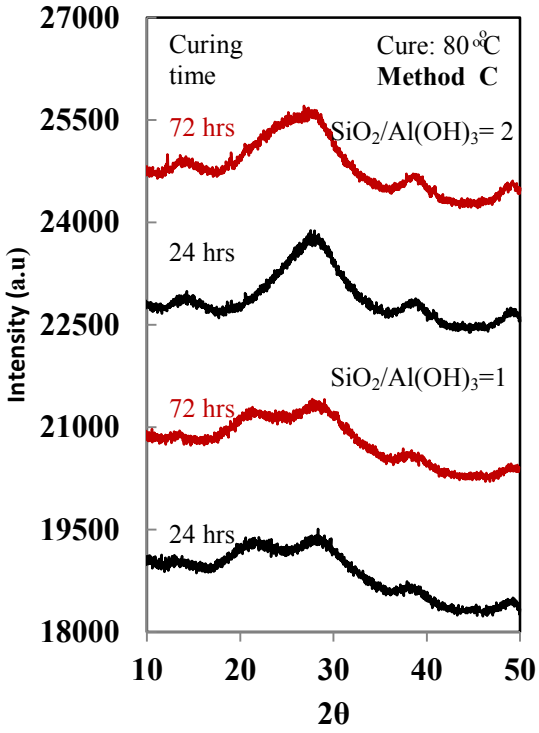

Figure 5.4 XRD of samples prepared using method C with $SiO_2/Al(OH)_3$ = 1 and 2 and cured at 80°C. Curing times for each sample are indicted above XRD spectra.

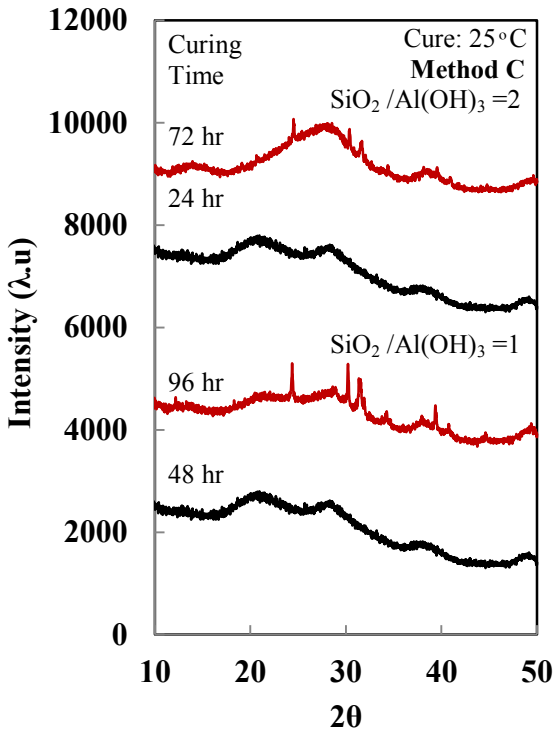

Figure 5.5 XRD of samples prepared using method C with SiO_2 /$Al(OH)_3$ =1 and 2 and cured at room temperature. Curing times for each sample are above each curve.

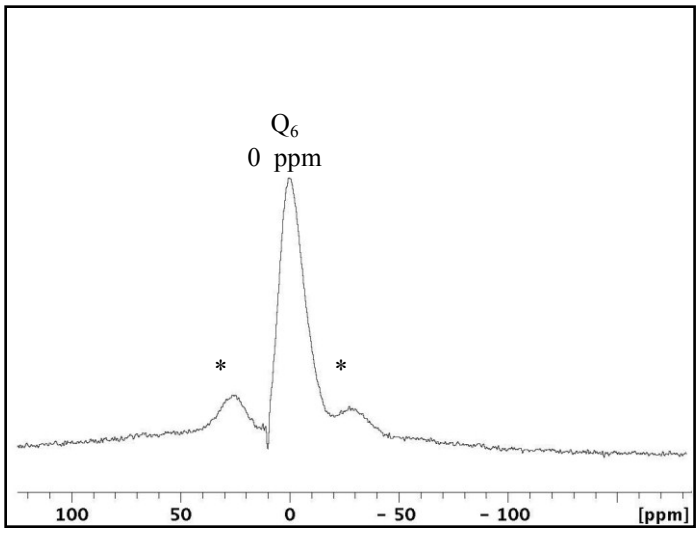

Figure 5.6 ^{27}Al MAS-NMR chemical shift of pure $Al(OH)_3$, asterisks represent quadrupole side bands.

Chemical shifts for the samples mixed using method A and cured for 24 hours are presented in Figure 5.7. The sample with SiO_2 /$Al(OH)_3$=2 has a Q_4/Q_6 = 0.97 indicating roughly a 50% of Al Q_6 from the precursor was converted to Al Q_4. In other words, ~ 50% of Al was incorporated in geopolymer and 50% in potassium alumino-silicates compound. The sample with SiO_2 /$Al(OH)_3$=1 has a Q_4/Q_6 = 0.70 with a lesser degree of Al Q_6 conversion to Al Q_4, indicating conversion to ~ 42% geopolymer and 58 % potassium alumino-silicates.

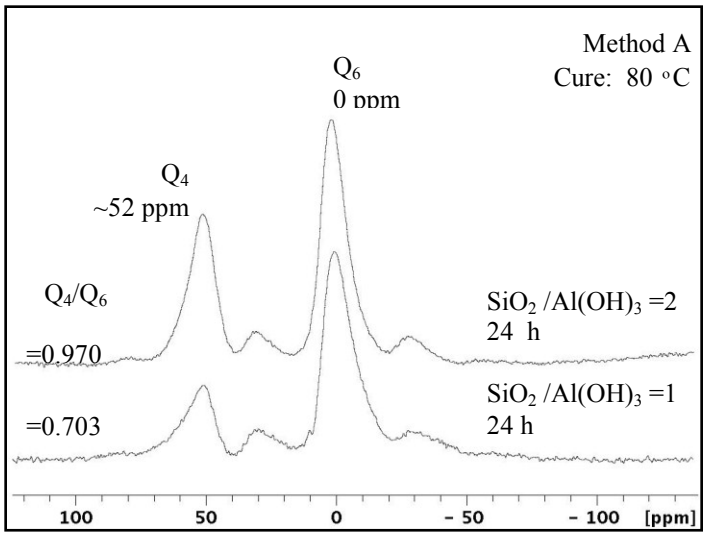

Figure 5.7 ^{27}Al MAS-NMR of the samples prepared using method **A** with 50% of Al Q_4 for Si/Ai =4 and 30 % Al Q_4 for Si/Al = 2.

The ^{27}Al NMR chemical shifts for samples prepared by method B with SiO_2 /$Al(OH)_3$ molar ratios of 1 and 2 are presented in Figure 5.8. In method B, the potassium aluminate is mixed on a magnetic stirrer for only 1 ½ hours, and added to potassium silicate to make samples with SiO_2 /$Al(OH)_3$ ratios 1and 2. As shown in Figure 5.8, sample with SiO_2 /$Al(OH)_3$=2 has approximately a 28.7% conversion of Al Q_6 to Al Q_4, whereas SiO_2 /$Al(OH)_3$=1 sample has conversion of only 8.5 %. The chemical shifts in samples synthesized using method C and cured at 80° C and room temperature is given in Figures 5.9 and 5.10, respectively. In method C, the potassium aluminate is mixed on a magnetic stirrer for 24 hours before adding to potassium silicate solutions. In the case curing at 80° C in sealed molds, Figure 5.9, sample mixed using method C with SiO_2 /$Al(OH)_3$=2 contains about 27% of Al Q_4, while sample with SiO_2

/$Al(OH)_3$=2 contains only 6% Al Q_4. Samples cured in air, Figure 5.11, did not show any significant Al Q_6 conversion to Al Q_4.

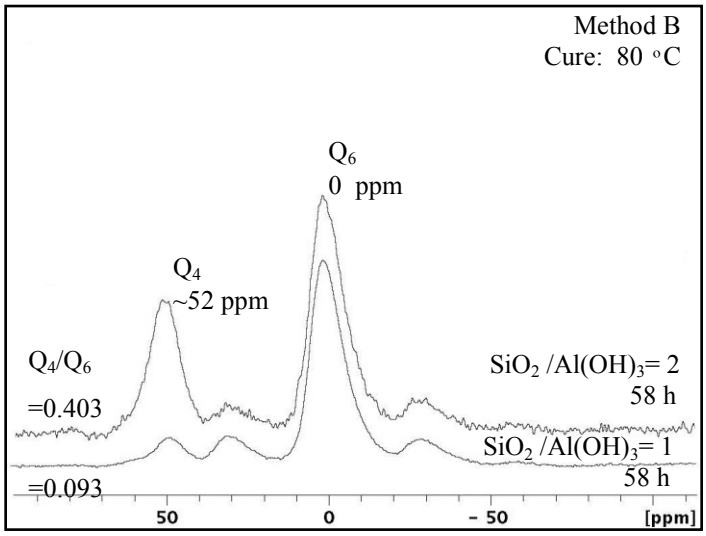

Figure 5.8 ^{27}Al MAS-NMR for the samples prepared using method B with 28.7% conversion of Al Q_6 to Al Q_4 for SiO_2 /$Al(OH)_3$= 2 and 8.5% conversion for SiO_2 /$Al(OH)_3$= 1.

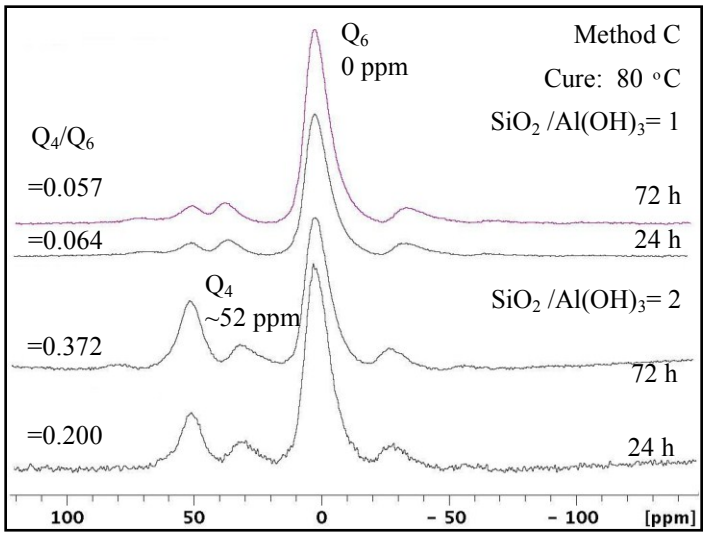

Figure 5.9 ^{27}Al MAS-NMR chemical shifts for the samples prepared using method C, two curing times (24 and 72 hours) and two Si/Al molar ratios. SiO_2 /$Al(OH)_3$= 2 has maximum 27% conversion of Al Q_6 to Al Q_4, whereas SiO_2 /$Al(OH)_3$= 1 has less than 6% conversion.

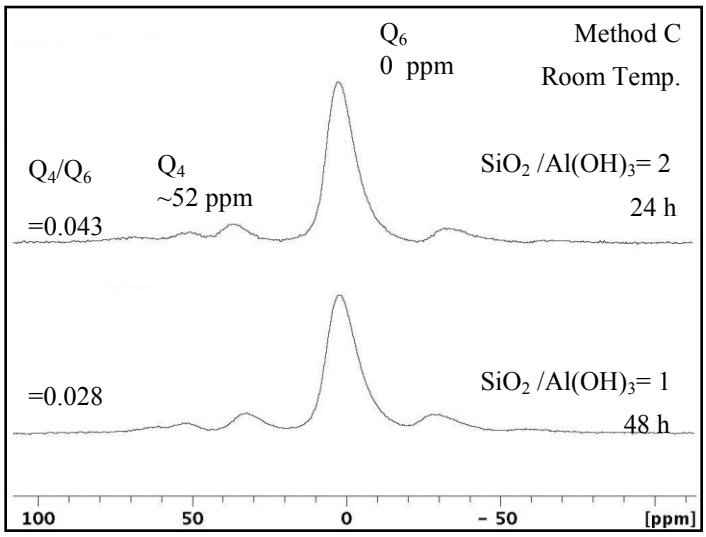

Figure 5.10 ^{27}Al NMR chemical shifts for samples prepared using Method C cured at room temperaure in air. Less than 4% conversion of Al Q_6 to Al Q_4 is seen for both SiO_2 /$Al(OH)_3$ = 1 and 2.

5.4 Discussion

Three different mixing methods have been utilized to synthesize geopolymer structures by copolymerization of Al and Si monomeric species obtained by dissolution of pure SiO_2 and $Al(OH)_3$ precursors in KOH aqueous solutions. The polycondensation process used in this study is illustrated in Figure 5.11. Unlike in the case of the geopolymerization using aluminosilicate precursors such as metakaolin, flay ash, furnace slag, etc. that is illustrated in Figure 1.1, in this study the simultaneous dissolution and condensation polymerization process of both Si and Al species were separated by:

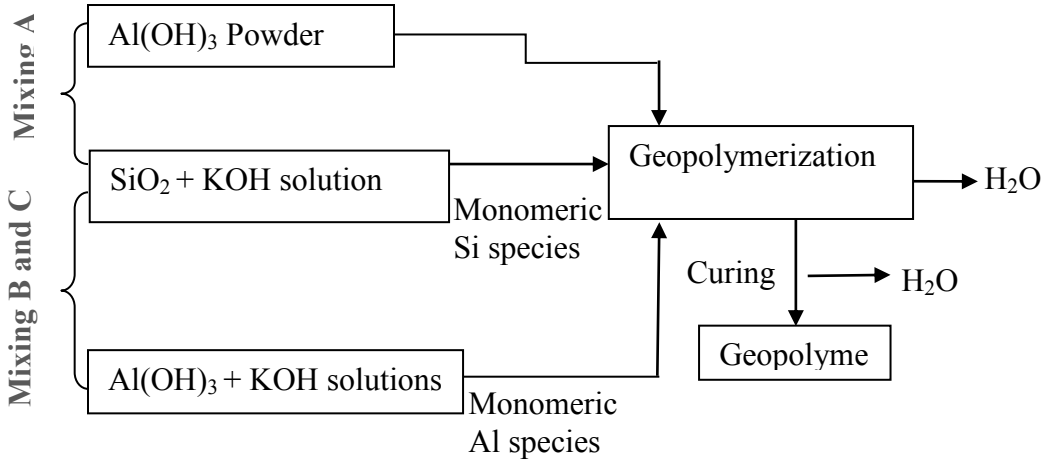

Figure 5.11 Schematic presentation of mixing procedure and geopolymerization used in this study.

1. Dissolution and hydrolysis of SiO_2 and $Al(OH)_3$ in alkaline medium separately to Al and Si monomeric species (mixing methods B and C). The polycondensation process is later initiated when prepared monomeric solutions are mixed together.
2. Dissolution and hydrolysis of SiO_2 in alkaline medium to Si monomeric species and subsequently adding $Al(OH)_3$ (method A). In this case dissolution and polycondensation $Al(OH)_3$ was simultaneous.

XRD results in Figures 5.2-5.5 show that all samples, with exception of pure potassium silicate samples (Figure 5.2d) and those prepared by using mixing method C and cured for longer times at room temperature (Figure 5.5), are completely x-ray amorphous. The results of ^{27}Al NMR shown in Figures 5.6-5.10 and summarized in Table 5.1, suggest that the amount of IV coordinated Al in the samples depends on SiO_2 /$Al(OH)_3$ ratio and mixing methods used to prepare samples. Comparison of ^{27}Al NMR results, Figures 5.7-5.11 and Table 5.1, for the samples prepared using the same mixing and curing procedure clearly indicate that samples with $SiO_2/Al(OH)_3$=2 always have larger amount of IV coordinated Al than those with $SiO_2/Al(OH)_3$=1. This conclusion is in good agreement with results published by O'Connor and MacKenzie [97] who demonstrated that the most complete geopolymerization reactions from SiO_2 and $Al(OH)_3$ precursors occurs at Si/Al ratios above ~1.4. As they explained in their study, the insufficient amount of Si species are available in the activated solutions with Si/Al ratio below optimum 1.4 to react with all available Al spices during polycondensation and form inorganic aluminosilicate polymer with all species being in IV-fold coordination. This conclusion can be also be strengthened by results published in

numerous studies [2, 101] that clearly show that –Al-O-Al- linkages with tetrahedrally coordinated Al cannot form in aluminosilicate polymers (Loewenstein's rule) [102] . Thus, at lower Si amounts in activated solutions, it is less likely that all tetrahedrally coordinated Al will form bonds with Si neighbors during copolymerization. In addition, this also explains why large crystalline peaks are observed in the cured potassium aluminates, Figure 5.3d, when compared to all other aluminosilicate samples in this study. In the absences of Si species in activated solution, Al species tends to precipitate as crystalline phases during curing, with all Al in VI-fold coordination, as it is discussed in more detail below.

Another possible reason for incomplete geopolymerization from pure SiO_2 and $Al(OH)_3$ precursors shown in this study, as well as in previously published papers[97] may be related to different reactivates of the IV-, V-, and VI-coordinated Al that could be present in aluminosilicate source materials. As shown in Figure 5.5, $Al(OH)_3$ powders used in this study as precursor contained only VI-coordinated Al. It has been previously reported that in geopolymerization process using natural sources, V-coordinated aluminum ions have higher reactivity than IV-coordinated ones, and definitely much higher reactivity than VI-coordinated ones [45]. As noted before by O'Connor and MacKenzie [97] in their study on geopolymerization of SiO_2 and different $Al(OH)_3$ precursors, utilization of $Al(OH)_3$ precursors with higher reactivity also resulted in higher yields of IV-coordinated Al in the cured samples.

Although lower Si/Al ratios and use of low reactivity $Al(OH)_3$ precursor can, in general, explain incomplete formation of geopolymers observed in this study, they

cannot explained significant differences in the amount of IV-coordinated Al observed in the samples prepared using different mixing methods, Figures 5.5-5.10 and Table 5.1. The amount of geopolymer matrix is much higher in samples prepared using mixing method A, than methods B and C, since samples processed using method A results in XRD amorphous material with largest conversion of VI coordinated Al to IV coordinated one. These results clearly demonstrate the importance of simultaneous dissolution and polycondensation for processing pure geopolymers as illustrated in Figure 5.1, since in simultaneous dissolution and polycondensation the rates of those two processes for both Si and Al species are more or less balanced resulting in copolymerization of both species. However, as discussed above, the two processes were completely or partially separated, in this study, allowing dissolution and polycondensation of Si and Al species at different rates.

It has been well established that SiO_2 can dissolve and hydrolyze by itself in highly alkaline aqueous solutions, forming monomeric and different oligomeric species, that can further polymerize in the X-ray amorphous structures [103]. Also, numerous studies showed that [96, 104-108] dissolution, hydrolysis, oligomerization, polymerization and eventfully precipitation of crystalline phases in $Al(OH)_3$ alkaline solutions are complex processes that are strongly dependent on molar concretions, pH, time and temperature, among other factors. First, dissolution and hydroxyls of $Al(OH)_3$ in aqueous solutions to $Al(OH)_4^-$ monomeric species needed for geopolymerization is reversible process as it is shown in Reaction 5.1. Changes in concretions of $Al(OH)_3$, OH^-, and $Al(OH)_4^-$ over time and with temperature can easily shift direction of this

reaction. Second, even more complex Al monomeric or oligomeric species can form [105] in $Al(OH)_3$ aqueous solutions at alkaline pH values, including Keggen-13[104] molecule that contains one IV-coordinated Al surrounded by twelve VI-coordinated Al with AlQ_4/AlQ_6 ratio of 0.076. Hence, it is not surprising that different amounts of IV-coordinated Al where observed here in the samples processed using different mixing methods.

When $Al(OH)_3$ powder were added slowly with constant stirring to the prepared highly alkaline potassium silicate solutions, $Al(OH)_4^-$ formed and large amount of them were gradually consumed in copolymerization process by Si species to form geopolymer matrix. Thus, the highest amount of IV coordinated alumina was determined in the samples prepared using mixing method A. When two separate solutions of potassium silicate and potassium aluminate were prepared, as in mixing method B and C, and then mixed together, smaller amount of IV-coordinated Al species formed during copolymerization process. Even more, the amount of IV-coordinated Al decreases as the mixing time of potassium aluminate was longer (compare mixing method B an C). This suggests that more complex Al species, possible even Kiggen 13, forms during extended aging of potassium aluminate solution, leaving smaller amount of $Al(OH)_4^-$ monomeric species with IV-coordinated Al to copolymerize with Si species when potassium silicate solutions were added. On the other hand, possible reason for smaller amount of IV-coordinated Al observed in samples prepared using methods B and C, could be the higher degree of polymerization of Si species in prepared potassium silicate solution, leaving smaller amount of highly active Si monomers and small oligomers to

copolymerize with Al species when they are added. The latter is less likely to have dominate effect on the smaller amount of IV-coordinated Al in the cured samples, since potassium silicate solutions were prepared in the same way using all three mixing methods, but mixing method A produced higher amount of IV-coordinated Al than mixing methods B and C.

Although more work is needed to further optimize processing route and conditions to achieve complete copolymerization of Al and Si species in SiO_2 and $Al(OH)_3$ alkaline solutions and thus process pure geopolymers, results shown here indicate that geopolymerization does occur in these solutions. The importance of the latter cannot be overestimated, because the processing routes discussed here allows to extend the range of inorganic polymers beyond the aluminosilicates , by using other metal hydroxides soluble in aqueous solutions to process inorganic polymers[95].

6. CONCLUSIONS AND FUTURE WORK

This study first investigated the effects of Si/Al and alkaline activator (K or Na) on the microstructure and mechanical properties of metakaolin based geopolymers prepared with H_2O/Al_2O_3=11 or 13 and cured for 24 and 48 hours. The results given in Section 2, clearly demonstrate that he density of GPs increased with increasing Si/Al ratios for both Na- and K-activated GPs, although density of Na-activated GPs was lower than that of K-activated ones for all Si/Al ratios. Increasing density of GPs with increasing Si/Al ratios was found to have significant effect on observed increase in Young's modulus, Vickers hardness, fracture toughness and strengths only at lower Si/Al ratios (below Si/Al=1.5-2). At higher Si/Al ratios, all mechanical properties decrease regardless of increasing density of GPs. With addition of SiO_2 to the activated solutions to increase overall Si/Al ratios, the activated solutions become more viscous because of the higher portion of solid in it, prohibiting good and uniform mixing. This, results in more inhomogeneous microstructure when compared to the samples with lower Si/Al ratios, with numerous inclusions of unreacted MK, large pores and some microcracks that all results in lower mechanical properties.

Results resented in Section 2 indicated that amount of water in the activated solutions, among other processing parameters, might have important role in structure and properties of GP. Therefore, more detailed study on the effects that initial water content, SiO_2/Al_2O_3 ratio, and type of alkaline activator (Na or K) on the microstructure development and amount and type of residual water in geopolymers during extended

aging and heating up to 1000 ^{o}C was carried out. Results of this study (Section 3) clearly indicate that:

- Regardless of the amount of $H_2O/(SiO_2 + Al_2O_3)$ and SiO_2/Al_2O_3 used to process samples, all samples show XRD and NMR features typical for geopolymers.
- Regardless of the amount of $H_2O/(SiO_2 + Al_2O_3)$ and SiO_2/Al_2O_3 all K- and Na-activated samples have almost the same amount of residual water after aging for 21 days at ambient conditions.
- Na-activated samples contain more chemically bonded interstitial water after aging for 21 days than K-activates GP samples.
- Amount of water used in processing GPs is the most dominant factor affecting their density and open porosity after curing and extended aging, while SiO_2/Al_2O_3 molar ratio does not play any significant role.

In addition, the study on the effects of the initial water content, SiO_2/Al_2O_3 ratio, and alkaline activator (Na or K) on the thermal and mechanical properties of geopolymers, Section 4, clearly indicate that:

- Dominant factor controlling thermal conductivity of GPs is $H_2O/(SiO_2 + Al_2O_3)$ ratio used to process activated solutions, and to a lesser degree, the type of activation ion (Na or K). SiO_2/Al_2O_3 was found to have no effect on thermal conductivity.

- Compressive strengths of GPs, although complex function of their composition, and curing and ageing conditions, are strongly affected by $H_2O/(SiO_2 + Al_2O_3)$ ratio used in activated solutions, especially at higher $H_2O/(SiO_2 + Al_2O_3)$ ratio. Evermore, at high and intermediate $H_2O/(SiO_2 + Al_2O_3)$ ratios, it is the most important factor controlling the strength of GPs. At low $H_2O/(SiO_2 + Al_2O_3)$ ratios,). SiO_2/Al_2O_3 ratio has also important role.
- Additional polycondensation during extended ageing and drying of GPs at ambient conditions after their curing at elevated temperatures, results in noticeable increase of compressive strength.
- Thermal and mechanical properties of GPs can be easily altered simply by using different amounts of water in preparing activated solutions.

Lastly in Section 5, partial geopolymerization has been achieved using pure SiO_2 and $Al(OH)_3$ precursors as an alternative to natural or industrial waste sources filled with impurities employed in traditional geopolymer synthesis. The samples were process using three different mixing methods and characterized by XRD and NMR to verify the distinct features of geopolymers in synthesized samples, i,e, their amorphous nature and presence of IV-coordinated Al. It was found that amount of IV-coordinated Al depends strongly on Si/Al ratios and methods used to prepare activated solutions. The latter clearly demonstrated the importance of simultaneous dissolution and polycondensation of both Al and Si species in processing pure geopolymers

A good deal of work was done casting and preparing geopolymers in this investigation. In some cases, the material was difficult to cast due to low workability. Future work on developing better casting methods may prevent some surface defects that were usually observed in processed geopolymers, such as entrapped air bubbles. There is a possibility that the samples will exhibit greater compressive strengths, if defects and better mixing can be obtained . Furthermore, geopolymers may be exploited in many applications. Investigations into other properties such as electrical conductivity have not been carried out extensively at this point. It may be possible to use electrically conductive particles to achieve an electrically conductive geopolymer. There is a great demand for multifunction materials. For example, it may be possible to use good adhesive properties of geopolymers to fabricate multifunctional composite materials. However, in order to achieve advanced applications, rigouts fundamental research is still required if we are to explore different avenues in geopolymer technology.

REFERENCES

[1] J. Davidovits, The Mineral Polymer Concept: Silicones and geopolymers, in: Geopolymer Chemistry and Applications Institut Geopolymere Saint-Quentin, France, 2008, pp. 19-35.

[2] L. Weng, K. Sagoe-Crentsil, Journal of Materials Science, 42 (2007) 2997-3006.

[3] K. Sagoe-Crenstil, L. Weng, Journal of Materials Science, 42 (2007) 3007-3014.

[4] P. Duxson, J.L. Provis, G.C. Lukey, S.W. Mallicoat, W.M. Kriven, J.S.J. van Deventer, Colloids and Surfaces a-Physicochemical and Engineering Aspects, 269 (2005) 47-58.

[5] L.Q. Weng, K. Sagoe-Crentsil, T. Brown, S.H. Song, Materials Science and Engineering B-Solid State Materials for Advanced Technology, 117 (2005) 163-168.

[6] J. Davidovits, Journal of Thermal Analysis, 37 (1991) 1633-1656.

[7] J. Davidovits, Structural Characterization of Goepolymeric Materials with X-Ray Diffractometry and MAS-NMR Spectroscopyin: J. Davidovits, J. Orlinski (Eds.) Geopolymer ’88, Proceedings of the First European Conference on Soft Mineralulgy, Geopolymer Institute, Compiègne, France, 1988. pp.149-166.

[8] P. Duxson, G.C. Lukey, F. Separovic, J.S.J. van Deventer, Industrial & Engineering Chemistry Research, 44 (2005) 832-839.

[9] P. Duxson, S.W. Mallicoat, G.C. Lukey, W.M. Kriven, J.S.J. van Deventer, Colloids and Surfaces a-Physicochemical and Engineering Aspects, 292 (2007) 8-20.

[10] K. Komnitsas, D. Zaharaki, Minerals Engineering, 20 (2007) 1261-1277.

[11] J. Davidovits, Physical Properties of Condensed Geopolymers, in: Geopolymer Chemistry and Applications, Institut Geopolymere, Saint-Quentin, France, 2008, pp. 335-351.

[12] D.S. Perera, E.R. Vance, K.S. Finnie, M.G. Blackford, J.V. Hanna, D.J. Cassidy, C.L. Nicholson, Disposition of Water in Metakaolinite-Based Geopolymers, in: N. Bansal, J.P. Singh, W.M. kriven (Eds.) Advances in Ceramic Matrix Composites XI: Proceedings of the 107th Annual Meeting of the American Ceramic Society : Baltimore, Maryland, USA (2005), American Ceramic Society, Westerville, OH, 2005, pp. 225-236.

[13] P. Duxson, A. Fernandez-Jimenez, J.L. Provis, G.C. Lukey, A. Palomo, J.S.J. van Deventer, Journal of Materials Science, 42 (2007) 2917-2933.

[14] J.L. Provis, J.S.J. van Deventer, Chemical Engineering Science, 62 (2007) 2309-2317.

[15] D. Khale, R. Chaudhary, Journal of Materials Science, 42 (2007) 729-746.

[16] J. Davidovits, 30 Years of Successes and Failures in Geopolymer Applications. Market Trends and Potential Breakthroughs. in: Geopolymer 2002 Conference, Melbourne, Australia, 2002, pp. 1-16.

[17] X. Yao, Z.H. Zhang, H.J. Zhu, Y. Chen, Thermochim Acta, 493 (2009) 49-54.

[18] W.K.W. Lee, J.S.J. van Deventer, Industrial & Engineering Chemistry Research, 41 (2002) 4550-4558.

[19] V.F.F. Barbosa, K.J.D. MacKenzie, Materials Research Bulletin, 38 (2003) 319-331.

[20] P. Duxson, J.L. Provis, G.C. Lukey, J.S.J. Van Deventer, Cement and Concrete Research, 37 (2007) 1590-1597.

[21] W.K.W. Lee, J.S.J. van Deventer, Colloids and Surfaces a-Physicochemical and Engineering Aspects, 211 (2002) 115-126.

[22] M. Sofi, J.S.J. van Deventer, P.A. Mendis, G.C. Lukey, Journal of Materials Science, 42 (2007) 3107-3116.

[23] J. Bell, M. Gordon, W. Kriven, Ceramic Engineering and Science Proceedings 26 (2005) 407-413

[24] S.L. Yong, D.W. Feng, G.C. Lukey, J.S.J. van Deventer, Colloids and Surfaces a-Physicochemical and Engineering Aspects, 302 (2007) 411-423.

[25] M.G. Blackford, J.V. Hanna, K.J. Pike, E.R. Vance, D.S. Perera, Journal of the American Ceramic Society, 90 (2007) 1193-1199.

[26] J.G.S. van Jaarsveld, J.S.J. van Deventer, G.C. Lukey, Chemical Engineering Communications, 191 (2004) 531-549.

[27] Z. Yunsheng, S. Wei, C. Qianli, C. Lin, Journal of Hazardous Materials, 143 (2007) 206-213.

[28] H. Oudadesse, A.C. Derrien, M. Lefloch, J. Davidovits, Journal of Materials Science, 42 (2007) 3092-3098.

[29] S.G. Hu, H.X. Wang, G.Z. Zhang, Q.J. Ding, Cement & Concrete Composites, 30 (2008) 239-244.

[30] S. Andini, R. Cioffi, F. Colangelo, T. Grieco, F. Montagnaro, L. Santoro, Waste Management, 28 (2008) 416-423.

[31] E. Gartner, Cement and Concrete Research, 34 (2004) 1489–1498.

[32] P. De Silva, K. Sagoe-Crenstil, Journal of Australian Ceramics Society, 44 (2008) 39-46.

[33] B.H.W.S. de Jong, G.E. Brown Jr, Geochimica Et Cosmochimica Acta, 44 (1980) 491-511.

[34] M. Rowles, B. O'Connor, Journal of Materials Chemistry, 13 (2003) 1161-1165.

[35] E. Rodriguez, R.M. de Gutierrez, S. Bernal, M. Gordillo, Revista Facultad De Ingenieria-Universidad De Antioquia, (2009) 30-41.

[36] M. Steveson, K. Sagoe-Crentsil, Journal of Materials Science, 40 (2005) 2023-2036.

[37] B.A. Latella, D.S. Perera, D. Durce, E.G. Mehrtens, J. Davis, Journal of Materials Science, 43 (2008) 2693-2699.

[38] P. De Silva, K. Sagoe-Crenstil, V. Sirivivatnanon, Cement and Concrete Research, 37 (2007) 512-518.

[39] I. Belena, W. Zhu, Nanoindentation Study of Na-Geopolymers Exposed to High Temperatures, in: Z. Bittnar, P.J.M. Bartos, J. Nemecek, V. Smilauer, J.

Zeman (Eds.) Nanotechnology in Construction 3, Proceedings of the NICOM3, Springer-Verlag, Berlin Heidelberg, 2009, pp. 169-174.

[40] K. Nihara, Nippon Seram Kyo Gak, 99 (1991) 974-982.

[41] M.W. Barsoum, Mechanical Properties: Fast Fracture, in: Fundamentals of Ceramics, Taylor & Francis Group LLC, New York, 2003, pp. 356-399.

[42] V.F.F. Barbosa, K.J.D. MacKenzie, C. Thaumaturgo, Int J Inorg Mater, 2 (2000) 309-317.

[43] J. Davidovits, Scientific Tools, X-rays, FTIR, NMR, in: Geopolymer Chemistry and Applications, Saint-Quentin, France, 2008, pp. 61-75.

[44] J.L. Bell, P. Sarin, P.E. Driemeyer, R.P. Haggerty, P.J. Chupas, W.M. Kriven, J Mater Chem, 18 (2008) 5974-5981.

[45] J. Davidovits, Metakaolin MK-750 based geopolymer, poly(sialate-siloxo) Si:Al-2:1, in: Geopolymer Chemistry and Applications, Saint-Quentin, France, 2008, pp. 145-192.

[46] H.L. Wang, H.H. Li, F.Y. Yan, Colloids and Surfaces a-Physicochemical and Engineering Aspects, 268 (2005) 1-6.

[47] I. Lecomte, M. Liegeois, A. Rulmont, R. Cloots, F. Maseri, Journal of Materials Research, 18 (2003) 2571-2579.

[48] I. Belena, M.J.L. Tendero, E.M. Tamayo, D. Vie, Boletin De La Sociedad Espanola De Ceramica Y Vidrio, 43 (2004) 569-572.

[49] J.L. Provis, J.S.J. van Deventer, Chemical Engineering Science, 62 (2007) 2318-2329.

[50] H. Rahier, J. Wastiels, M. Biesemans, R. Willlem, G. Van Assche, B. Van Mele, Journal of Materials Science, 42 (2007) 2982-2996.

[51] J.L. Provis, J.S.J. van Deventer, Journal of Materials Science, 42 (2007) 2974-2981.

[52] A. Fernandez-Jimenez, R. Vallepu, T. Terai, A. Palomo, K. Ikeda, Journal of Non-Crystalline Solids, 352 (2006) 2061-2066.

[53] J.G.S. van Jaarsveld, J.S.J. van Deventer, G.C. Lukey, Materials Letters, 57 (2003) 1272-1280.

[54] H. Xu, J.S.J. Van Deventer, International Journal of Mineral Processing, 59 (2000) 247-266.

[55] M.-R. Wang, D.-C. Jia, P.-G. He, Y. Zhou, Ceramics International, 37 1661-1666.

[56] P. Duxson, S.W. Mallicoat, G.C. Lukey, W.M. Kriven, J.S.J. van Deventer, Microstructural characterization of metakaolin-based geopolymers, in: J.P. Singh, N.P. Bansal, W.M. Kriven (Eds.) Advances in Ceramic Matrix Composites X, American Ceramic Society, Westerville, OH, 2005, pp. 71-85.

[57] M. Komljenovic, Z. Bascarevic, V. Bradic, Journal of Hazardous Materials, 181 35-42.

[58] S. Alonso, A. Palomo, Cement and Concrete Research, 31 (2001) 25-30.

[59] V.F.F. Barbosa, Mackenzie, K.J.D., Materials Letters, 57 (2003) 1477-1482.

[60] M. Hussain, R. Varely, Y.B. Cheng, Z. Mathys, G.P. Simon, Journal of Applied Polymer Science, 96 (2005) 112-121.

[61] M. Hussain, R.J. Varley, Y.B. Cheng, G.P. Simon, Journal of Materials Science, 39 (2004) 4721-4726.

[62] J.L. Provis, C.Z. Yong, P. Duxson, J.S.J. van Deventer, Colloids and Surfaces A: Physicochemical and Engineering Aspects, 336 (2009) 57-63.

[63] K. Okada, A. Ooyama, T. Isobe, Y. Kameshima, A. Nakajima, K.J.D. MacKenzie, Journal of the European Ceramic Society, 29 (2009) 1917-1923.

[64] Z. Zuhua, Y. Xiao, Z. Huajun, C. Yue, Applied Clay Science, 43 (2009) 218-223.

[65] W.M. Kriven, J.L. Bell, M. Gordon, Microstructure and microchemistry of fully-reacted geopolymers and geopolymer matrix composites, in: N.P. Bansal, J.P. Singh, W.M. Kriven, H. Schneider (Eds.) Advances in Ceramic Matrix Composites Ix, 2003, pp. 227-250.

[66] T. Hanzlicek, M. Steinerova-Vondrakova, Ceramics-Silikaty, 46 (2002) 97-103.

[67] D.S. Perera, O. Uchida, E.R. Vance, K.S. Finnie, Journal of Materials Science, 42 (2007) 3099-3106.

[68] M. Lizcano, K. Hyunsoo, S. Basu, M. Radovic, submitted to Materials Science and Engineering A (2011).

[69] Z. Aly, E.R. Vance, D.S. Perera, J.V. Hanna, C.S. Griffith, J. Davis, D. Durce, Journal of Nuclear Materials, 378 (2008) 172-179.

[70] A. Buchwald, H. Hilbig, C. Kaps, Journal of Materials Science, 42 (2007) 3024-3032.

[71] P. Rovnaník, Construction and Building Materials, 24 1176-1183.

[72] ASTM C20-00(2010) Standard Test Methods for Apparent Porosity, Water Absorption, Apparent Specific Gravity, and Bulk Density of Burned Refractory Brick and Shapes by Boiling Water, in: ASTM, 2010.

[73] M. Schmucker, K.J.D. MacKenzie, Ceramics International, 31 (2005) 433-437.

[74] M. Lizcano, A.G. Elizondo, R. Benitz, S. Basu, M. Radovic, submitted to Acta Materialia, (2011).

[75] Y.S. Zhang, W. Su, Z.J. Li, Aci Materials Journal, 106 (2009) 96-97.

[76] Y.J. Zhang, Y.C. Wang, D.L. Xu, S. Li, Materials Science and Engineering: A, 527 6574-6580.

[77] N.N. Casillas-Ituarte, H.C. Allen, Chemical Physics Letters, 483 (2009) 84-89.

[78] P. Duxson, G.C. Lukey, J.S.J. van Deventer, Journal of Non-Crystalline Solids, 352 (2006) 5541-5555.

[79] J. Temuujin, W. Rickard, M. Lee, A. van Riessen, Journal of Non-Crystalline Solids, 357 1399-1404.

[80] J.L. Bell, M. Gordon, W.M. Kriven, Use of Geopolymeric Cements as a Refractory Adhesive for Metal and Ceramic Joints in: The 29th International Conference on Advanced Ceramics and Composites, Ceramic Engineering and Science Proceedings, Cocoa Beach, FL, 2005, pp. 497-413.

[81] D.S. Perera, R.L.Trautman., Geopolymers with the potential for use as refractory castables in: AZojomo, accessed: June 2, 2007, AD-TECH, 2006.

[82] J. Temuujin, A. Minjigmaa, W. Rickard, M. Lee, I. Williams, A. van Riessen, Journal of Hazardous Materials, 180 748-752.

[83] J. Temuujin, A. Minjigmaa, W. Rickard, M. Lee, I. Williams, A. van Riessen, Applied Clay Science, 46 (2009) 265-270.

[84] V. Vaou, D. Panias, Minerals Engineering, 23 1146-1151.

[85] F. Liefke, Industrial Applications of Foamed Inorganic Polymers in: Geopolymer '99 Proceedings, Geopolymer Institute, Saint-Quentin, France, 1999, pp. 189.

[86] J. Davidovits, Foamed Geopolymers, in: Geopolymer Chemistry and Applications, Saint-Quentin, France, 2008, pp. 471- 478.

[87] P. Duxson, G.C. Lukey, J.S.J. van Deventer, Industrial & Engineering Chemistry Research, 45 (2006) 7781-7788.

[88] M. Lizcano, A.G. Elizondo, S. Basu, K. Lozano, M. Radovic, submitted to Acta Materialia, (2011).

[89] D.L. Kong, J.G. Sanjayan, K. Sagoe-Crentsil, Cement and Concrete Research, 37 (2007) 1583-1589.

[90] C. Panagiotopoulou, E. Kontori, T. Perraki, G. Kakali, Journal of Materials Science, 42 (2007) 2967-2973.

[91] H. Xu, Geopolymerization of Aluminosilicate Mineralsin: Dissertation, Doctor of Philosophy, Department of Chemical Engineering, Univeristy of Melbourne, 2002, pp. 287.

[92] S. Astutiningsih, Y. Liu, Synthetic alumina silica glass for geopolymer precursor in: International Conference on Pozzolan, Concrete and Geopolymer, Khon Kaen, Thailand, 2006, pp. 81-92.

[93] M. Gordon, J.L Bell, W.M. Kriven, Ceramic Transactions, 165 (2005) 95-106.

[94] X.-M. Cui, G.-J. Zheng, Y.-C. Han, F. Su, J. Zhou, Journal of Power Sources, 184 (2008) 652-656.

[95] E. Wiberg, N. Wiberg, A.F. Holleman, [Lehrbuch der anorganische Chemie. English] Inorganic chemistry / founded by A.F. Holleman ; continued by Egon Wiberg ; translated by Mary Eagleson, William Brewer ; revised by Bernhard J. Aylett., 1st English edition ed., Academic Press, San Diego.

[96] A.B.S. Poleo, Aquatic Toxicology, 31 (1995) 347-356.

[97] S. O'Connor, K. MacKenzie, Journal of Materials Science, 45 3284-3288.

[98] D. Brew, K. MacKenzie, Journal of Materials Science, 42 (2007) 3990-3993.

[99] H.A. van Straten, B.T.W. Holtkamp, P.L. de Bruyn, Journal of Colloid and Interface Science, 98 (1984) 342-362.

[100] J. Temuujin, K. Okada, K.J. MacKenzie, J. Amgalan, British Ceramic Transactions, 99 (2000) 23-25.

[101] E. Yildirim, R. Dupree, Bulletin of Materials Science, 27 (2004) 269-272.

[102] W. Loewenstein, M. Lowenstein., American Mineralogist, 39 (1954) 92-96.

[103] C.J. Brinker, G.W. Scherer, Sol-Gel Science: The Physics and Chemistry of Sol-Gel Processing Academic Press, Boston, 1990.

[104] H. Li, J. Addai-Mensah, J.C. Thomas, A.R. Gerson, Journal of Crystal Growth, 279 (2005) 508-520.

[105] N.D. Tzoupanos, A.I. Zouboulis, C.A. Tsoleridis, Colloids and Surfaces A: Physicochemical and Engineering Aspects, 342 (2009) 30-39.

[106] K.P. Prodromou, A.S. Pavlatou-V_E, Clays and Clay Minerals, 43 (1995) 111-115.

[107] R. Schoen, C.E. Robertson, American Mineralogist, 55 (1970) 43-77.

[108] H. Feng, L. Hu, D. Shan, C. Fang, Y. He, D. Shen, Journal of Environmental Sciences, 20 (2008) 690-695.

VITA

Maricela Lizcano received her B.S. (2004) and M.S. (2006) degrees in mechanical engineering from The University of Texas-Pan American in Edinburg, TX. She entered the doctoral program in the Department of Mechanical Engineering at Texas A&M University in August 2006 and received her Doctor of Philosophy degree in August 2011. Her research interests include nano-reinforced polymeric materials, electrorheologial fluids and low temperature processing inorganic polymers.

Dr. Lizcano may be reached at Texas A&M University, Department of Mechanical Engineering, 3123 TAMU College Station TX 77843-3123 Her email is marcilizcano@yahoo.com.